Measurements and Modelling of Low-Frequency Disturbances in Induction Machines

by

Torbjörn Thiringer

Public defence: 11 November 1996 at 10.15

Opponent: Professor Stephen Williamson, University of Cambridge, England

ABSTRACT

The thesis deals with the dynamic response of the induction machine to low-frequency perturbations in the shaft torque, supply voltage and supply frequency. Also the response of a two-machine group connected to a weak grid is investigated. The results predicted by various induction machine models are compared with measurements performed on a laboratory set-up. Furthermore, the influence of machine and grid parameters, machine temperature, phase-compensating capacitors, skin effect, saturation level and operating points is studied.

The results predicted by the fifth-order non-linear Park model agree well with the measured induction machine responses to shaft torque, supply frequency and voltage magnitude perturbations. To determine the electric power response to very low-frequency perturbations in the magnitude of the supply voltage, the Park model must be modified to take varying iron losses into account. The temperature and supply frequency affect the low-frequency dynamics of the induction machine significantly while the influence of saturation, phase-compensating capacitors, skin effect and static shaft torque is of less importance to an ordinary industrial machine. The static shaft torque is, however, of importance for determining the responses to voltage magnitude perturbations.

The performance of reduced-order induction machine models depends on the type of induction machine investigated. Best suited to be represented by reduced-order models are high-slip machines as well as machines that have a low ratio between the stator resistance and leakage reactances. A first-order model can predict the rotor speed, electrodynamic torque and electric power responses to shaft torque and supply frequency perturbations up to a perturbation frequency of at least 1 Hz. A second-order model can determine the same responses also for higher perturbation frequencies, at least up to 3 Hz. Using a third-order model, all the responses to torque and frequency perturbations as well as the reactive power response to voltage magnitude perturbations can be determined up to at least 10 Hz.

PREFACE

This work was carried out as a part of the wind energy project at the Department of Electric Power Engineering, Chalmers University of Technology. The task given was to investigate the modelling of induction machines as wind turbine generators, i.e., to investigate the suitability and restrictions of different induction machine models. The financial support given by the Swedish National Board for Industrial and Technical Development (NUTEK) is gratefully acknowledged.

I would like to express my deep gratitude to my supervisor during the second part of the work, professor Jorma Luomi, for valuable advice and encouraging guidance. Further, I would like to thank Dr Jonny Hylander, who was my supervisor during the first part, for starting me up in the field of electric energy research. I would also like to thank my project leader, Dr Ola Carlsson, for encouragement and support throughout the work and Margot Bolinder for linguistic help. Finally, I would like to thank colleagues at the department who have assisted me during the work on this thesis. Especially, I would like to thank Robert Karlsson, for assisting me with the experimental equipment.

Last but not least, I would like to thank my wife Susanna for love and support and for patiently putting up with a husband spending late evenings and weekends away.

CONTENTS

LIST OF SYMBOLS

Symbol	Meaning	Unit
B	equivalent damping coefficient	Nms/rad
f	frequency	Hz
f_s	supply frequency	Hz
$H\,(\mathrm{s})$	transfer function	
$H_\mathrm{p}\,(\mathrm{s})$	transfer function for the Park model	
i_dm	magnetizing current in d-direction	A
i_dr	rotor current in d-direction	A
i_ds	stator current in d-direction	A
i_m	magnetizing current	A
i_qm	magnetizing current in q-direction	A
i_qr	rotor current in q-direction	A
i_qs	stator current in q-direction	A
$\underline{i}_\mathrm{Rm}$	iron loss equivalent current vector	A
$\underline{i}_\mathrm{r}$	rotor current vector	A
$\underline{i}_\mathrm{r1}$	current vector of rotor cage one	A
$\underline{i}_\mathrm{r2}$	current vector of rotor cage two	A
$\underline{i}_\mathrm{s}$	stator current vector	A
J	inertia	kgm^2
J_m	machine inertia	kgm^2
J_l	load inertia	kgm^2
J_t	wind turbine rotor inertia	kgm^2
K	equivalent torsional stiffness	Nm/rad
k_1	constant	H
k_2	constant	H/A
k_3	constant	H/°C
k_r	rotor coupling factor	
k_s	stator coupling factor	
L_dr	rotor inductance in d-direction	H
L_ds	stator inductance in d-direction	H
L_l	line inductance	H
L_m	magnetizing inductance	H
L_md	magnetizing inductance in d-direction	H
L_mdq	mutual inductance between q and d axes	H
L_mq	magnetizing inductance in q-direction	H

L_{mt}	tangential magnetizing inductance	H
L_{qr}	rotor inductance in q-direction	H
L_{qs}	stator inductance in q-direction	H
L_r	rotor inductance	H
L_r'	rotor transient inductance	H
$L_{r\lambda}$	rotor leakage inductance	H
$L_{r\lambda 1}$	leakage inductance of rotor cage one	H
$L_{r\lambda 2}$	leakage inductance of rotor cage two	H
L_s	stator inductance	H
L_s'	stator transient inductance	H
$L_{s\lambda}$	stator leakage inductance	H
P_e	electrical power	W
p	pole pair number	
Q	reactive power	Ω
s	Laplace operator	
R_{cl}	equivalent resistance representing core losses	Ω
R_k	locked rotor resistance	Ω
R_l	line resistance	Ω
R_m	iron loss equivalent resistance	Ω
R_r	rotor resistance	Ω
R_{r1}	resistance of rotor cage one	Ω
R_{r2}	resistance of rotor cage two	Ω
R_s	stator resistance	Ω
T	rotor temperature	$^\circ$C
T_{dcm}	electrodynamical torque of the dc machine	Nm
T_e	electrodynamical torque	Nm
T_l	load torque	Nm
T_s	shaft torque	Nm
T_w	torque acting on the wind turbine rotor	Nm
U	voltage	V
U_{grid}	local grid voltage	V
U_N	rated voltage	V
u_{ds}	stator voltage in d-direction	V
u_{qs}	stator voltage in q-direction	V
$\underline{u}_s$	stator voltage vector	V
Z	rotor winding impedance	Ω

A	system matrix	
B	input matrix	
I	current column vector	A
L	inductance matrix	H
R	resistance matrix	Ω
U	voltage column vector	V
Ψ	flux vector	
α	torsional stiffness	Nm/rad
δ	load angle	rad
ε	error function	
ξ	damping ratio	
ξ_{NSR}	damping ratio obtained using the NSR-model	
ξ_{ss}	damping ratio obtained using small-signal analysis	
Θ	angle between rotor and load	rad
Ψ_{dr}	rotor flux linkage in d-direction	Wb
Ψ_{ds}	stator flux linkage in d-direction	Wb
Ψ_{m}	main flux linkage	Wb
Ψ_{qs}	stator flux linkage in q-direction	Wb
Ψ_{qr}	rotor flux linkage in q-direction	Wb
Ψ_{xr}	rotor flux linkage in x-direction	Wb
Ψ_{yr}	rotor flux linkage in y-direction	Wb
$\underline{\Psi}_{r}$	rotor flux linkage vector	Wb
$\underline{\Psi}_{r1}$	flux linkage vector of rotor cage 1	Wb
$\underline{\Psi}_{r2}$	flux linkage vector of rotor cage 2	Wb
$\underline{\Psi}_{s}$	stator flux linkage vector	Wb
Ω_{l}	angular speed of load	rad/s
Ω_{m}	angular speed of the rotor	rad/s
ω_{k}	angular velocity of coordinate system	rad/s
ω_{s}	angular supply frequency	rad/s
ω_{s0}	steady-state value of the angular supply frequency	rad/s
ω_{0}	undamped angular eigenfrequency	rad/s

Abbreviation	Meaning
LA-model	load angle model
LD-model	linear damper model
NST-model	neglecting stator transients model
NSR-model	neglecting stator resistance model
ND-model	non-linear damper model

1 INTRODUCTION

1.1 Background

A good number of dynamic and transient models of induction machines has been reported in literature, ranging from first-order models to very complex ones which combine a numerical solution of the magnetic field and circuit equations with the equation of motion. When smaller deviations around an operating point are studied, it is appropriate to use a dynamic model, while a transient model is needed to handle larger disturbances, such as the start-up or short-circuiting of an induction machine. For transient studies, a commonly accepted induction machine model is the non-linear fifth-order Park model, which considers the electrical transients in the rotor and stator windings as well as mechanical transients. This model, in its standard form, ignores the influence of skin effect and saturation of the leakage and magnetizing inductances. If these effects are to be taken into account, the complexity of the model has to be increased.

For dynamic investigations it is often possible to use models of lower order than the Park model. The analysis of power systems is an example where models of lower order have been used. Ohtsuki et al. (1991) and Sekine et al. (1990) used first-order models, Mayeda et al. (1985) and Ueda and Takata (1981) used third-order models and Mohamedein et al. (1986) suggested the usage of second-order models. The proper modelling of induction machines for power system studies is of utmost importance, since they constitute a significant portion of the load. Another example where reduced-order induction machine models have been used, is the modelling of the induction machine in mechanical systems, for instance as a generator in a wind turbine. To model induction machines as wind turbine generators, first-order models (Wilkie et al. 1990, Sheinman & Rosen 1991) and second-order models (Hinrichsen & Nolan 1982) have been used when the wind turbine in itself is the objective of the study. When the power quality impact of wind turbines is investigated, fifth-order models or third-order models have usually been utilized (Estanqueiro et al. 1993, de Mello & Hannet 1981).

The complexity of a multi-machine system can also be reduced by aggregating groups of induction machines. It is important that the machines to be aggregated to single-machine equivalents are of similar sizes (Rahim & Laldin 1987). Hakim and Berg (1976) aggregate induction machines to a first-order model and Crow (1994) as well as Iliceto and Capasso (1974) aggregate the induction machines to third-order models, while Rahim and Laldin (1987) use fifth-order equivalents.

1.2 Related work

Several authors have investigated third-order models of the induction machine based on the negligence of stator transients. Wasynczuk et al. (1985) showed that such a model can predict the same rotor speed response as the Park model for a specific machine up to a 20 Hz perturbation frequency in the voltage magnitude.

Nacke (1962) suggested that the induction machine could be represented by a spring, a mass and a damper if the dynamic response to perturbations in the shaft torque is to be determined. Second-order models based on the load angle have, for instance, been presented by Mohamedein (1978) and Al-Bahrani et al. (1988). Richards and Tan (1981) proposed a second-order model in which the rotor flux linkage magnitude and rotor speed were the state variables, while Derbel et al. (1995) proposed a model where the rotor speed and rotor flux angle were the state variables, in principle, a load angle model.

A possibility to increase the computational speed is to change models during a simulation as suggested by Ertem and Baghzouz (1989). Another possibility is to keep some of the variables constant during a number of time steps. Ertem and Baghzouz (1988) kept the rotor speed constant. If the grid is lost, specially adapted reduced-order models are needed (Richards 1989, Krause et al. 1987).

The inclusion of main flux saturation in the modelling of the induction machine has, for instance, been presented by Deleroi (1970) and Hallenius (1982) and the inclusion of leakage flux saturation has been described by e.g. Healey et al. (1995). Lorenzen (1967) pointed out that also the low-frequency dynamics of the machine can be influenced by the skin effect. A method to model the skin effect has, for instance, been suggested by Adkins and Harley (1975).

The effect of saturation can be taken into account without increasing the order of the induction machine model while the inclusion of skin effect requires that at least two additional differential equations are added to the system of equations, unless only the steady-state performance is of interest. The induction machine models which take the skin effect into account are well suited for model reduction, and reduced-order models of induction machine taking the skin effect into account can be found in literature (Khalil et al. 1982, Richards & Tan 1986).

Several experiments based on step responses have been performed. Experiments to verify induction machine performance based on frequency-analysis methods are harder to find, especially an all-embracing experimental verification of the commonly used induction machine models.

Freise et al. (1964) and Peterson (1991) performed frequency-analysis based experiments in order to determine the damping ratio and eigenfrequency of the induction machine by supplying the stator with dc-current and in this way transforming the synchronous speed to zero.

Leonhard (1966) measured the electrodynamical torque response to shaft torque perturbations and obtained a good agreement between measured and calculated values. Melkebeek (1980, 1983) measured the rotor speed response to perturbations in the magnitude of the voltage. The measurements were performed at no load using different rotors and at various flux levels. The results were compared with calculations performed using a fifth-order non-linear model, in which the effects of saturation were considered. The agreement between measured and calculated results was excellent.

Efforts to generalize the performance of induction machines of arbitrary sizes have been made by Ahmed-Zaid and Taleb (1991). The conclusion drawn in the paper was that a first-order rotor speed model predicts the responses of small machines well while a first-order rotor speed model predicted the responses of larger machines less well. The parameters of the investigated induction machines of various sizes were given by Cathey et al. (1973). Important to note is that the small machines presented by Cathey et al. (1973) had very high slip values, about 5 %.

1.3 Aim and layout of the thesis

The aim of this thesis is to model the induction machine in the simplest appropriate manner, in order to determine the dynamic responses to low-frequency perturbations.

The possibility to use low-order induction machine models to predict the responses to torque, supply frequency and voltage magnitude perturbations is examined. The responses are: rotor speed, electrodynamical torque, stator current as well as active and reactive powers. Furthermore, the calculated induction machine responses are verified by measurements for all the 15 combinations of responses and perturbations.

Models presented in literature, ranging in order from one to seven, are studied and improved wherever possible. Frequency analysis is used as an investigation tool instead of step responses, since the results then become more generally applicable. The possibility of using simplified models is examined for different types of induction machines, and recommendations for the field of application of the simplified models are given. Moreover, the importance of different factors that influence the dynamics of the 15 kW machine investigated is studied. The factors are: skin effect, temperature of the machine, parameters of the machine, iron losses, line impedance, saturation and operating points.

Two main fields of application for the simplified models are identified: 1) modelling of the induction machine by linear first- or second-order models in a mechanical system, where the usage of linear models can facilitate the analysis substantially; 2) modelling of the induction machine for the analysis of power systems containing large numbers of induction machines, where the computational effort is a problem.

In Chapter 2 the investigated induction machine models are presented. After describing the measurement equipment in Chapter 3, the models are compared with measurements in Chapter 4. In Chapter 5 the dynamic influence of various factors on the dynamic behaviour of the machine is examined. Finally, in Chapter 6 the validity of reduced-order models is investigated for induction machines of different sizes.

2 MODELS

A commonly accepted model of the induction machine for dynamic and transient studies is the fifth-order Park model, also referred to as the two-axis model. The equations for this model have been described by e.g. Kovacs (1984). Starting with the Park model as a reference model, simpler and more advanced models are derived in this chapter.

2.1 Park Model

The standard Park model requires some simplifying assumptions:

– the machine is considered to have a smooth air-gap,
– the windings are considered to be sinusoidally distributed on the air-gap surface,
– the effects of saturation and skin effect are ignored.

With these assumptions the equations of the Park model of a cage induction machine are

$$\underline{u}_s = \underline{i}_s R_s + \frac{d\underline{\Psi}_s}{dt} + j\omega_k \underline{\Psi}_s \tag{2.1}$$

$$0 = \underline{i}_r R_r + \frac{d\underline{\Psi}_r}{dt} + j(\omega_k - p\Omega_m)\underline{\Psi}_r \tag{2.2}$$

$$J_m \frac{d\Omega_m}{dt} = T_e - T_s \tag{2.3}$$

$$T_e = p\mathrm{Im}(\underline{\Psi}_s^* \underline{i}_s) \tag{2.4}$$

where $\underline{i}_s$ and $\underline{i}_r$ are the stator and rotor current vectors, respectively, Ω_m is the mechanical rotor speed and ω_k is the angular velocity of the coordinate system, which in this thesis is set equal to the angular supply frequency ω_s. T_s is the applied shaft torque, T_e the electrodynamical torque and $\underline{u}_s$ the supply voltage vector. R_s and R_r are the stator and rotor resistances, respectively, J_m is the moment of inertia of the machine and p the number of pole pairs. Motor references have been used and all rotor quantities are referred to the stator side. The stator and rotor flux linkage vectors are obtained by the expressions

$$\underline{\Psi}_s = L_s \underline{i}_s + L_m \underline{i}_r = (L_{s\lambda} + L_m)\underline{i}_s + L_m \underline{i}_r \tag{2.5}$$

$$\underline{\Psi}_r = L_m \underline{i}_s + L_r \underline{i}_r = L_m \underline{i}_s + (L_{r\lambda} + L_m)\underline{i}_r \tag{2.6}$$

L_s, L_r and L_m are the stator, rotor and magnetizing inductances, respectively. $L_{s\lambda}$ and $L_{r\lambda}$ are the stator and rotor leakage inductances. The system is non-linear as can be noted if (2.5) or (2.6) is inserted into (2.4) or (2.2), respectively.

The induction machine equations can be expressed in matrix form:

$$\mathbf{U} = \mathbf{R}\,\mathbf{I} + \mathbf{L}\,\frac{\mathrm{d}\mathbf{I}}{\mathrm{d}t} \tag{2.7}$$

where $\mathbf{U}$ is the voltage vector, $\mathbf{I}$ is the current vector, $\mathbf{R}$ is the resistance matrix and $\mathbf{L}$ is the inductance matrix. The elements in the vectors and matrices are given by

$$\mathbf{I} = \begin{bmatrix} i_{qs} \\ i_{ds} \\ i_{qr} \\ i_{dr} \\ \Omega_m \end{bmatrix}, \quad \mathbf{U} = \begin{bmatrix} u_{qs} \\ u_{ds} \\ 0 \\ 0 \\ T_s \end{bmatrix}, \quad \mathbf{L} = \begin{bmatrix} L_s & 0 & L_m & 0 & 0 \\ 0 & L_s & 0 & L_m & 0 \\ L_m & 0 & L_r & 0 & 0 \\ 0 & L_m & 0 & L_r & 0 \\ 0 & 0 & 0 & 0 & -J_m \end{bmatrix}$$

and

$$\mathbf{R} = \begin{bmatrix} R_s & L_s\omega_s & 0 & L_m\omega_s & 0 \\ -L_s\omega_s & R_s & -L_m\omega_s & 0 & 0 \\ 0 & L_m(\omega_s - p\Omega_m) & R_r & L_r(\omega_s - p\Omega_m) & 0 \\ L_m(p\Omega_m - \omega_s) & 0 & L_r(p\Omega_m - \omega_s) & R_r & 0 \\ pL_m i_{dr} & 0 & -pL_m i_{ds} & 0 & 0 \end{bmatrix}$$

where u_{ds} and u_{qs} are the direct- and quadrature-axis components of the stator voltages, i_{ds} and i_{qs} are the direct- and quadrature-axis components of the stator currents, i_{dr} and i_{qr} are the direct- and quadrature-axis components of the rotor currents, respectively.

Instead of using the currents as state variables, the flux linkages can be used and then (2.1) and (2.2) are replaced by

$$\underline{u}_s = [\frac{R_s}{L_s} + \mathrm{j}\omega_s]\,\underline{\Psi}_s + \frac{\mathrm{d}\underline{\Psi}_s}{\mathrm{d}t} - k_r\frac{R_s}{L_s}\,\underline{\Psi}_r \tag{2.8}$$

$$0 = -k_s\frac{R_r}{L_r}\,\underline{\Psi}_s + [\frac{R_r}{L_r} + \mathrm{j}(\omega_s - p\Omega_m)]\,\underline{\Psi}_r + \frac{\mathrm{d}\underline{\Psi}_r}{\mathrm{d}t} \tag{2.9}$$

where

16

$$k_s = \frac{L_m}{L_s} \tag{2.10}$$

$$k_r = \frac{L_m}{L_r} \tag{2.11}$$

are the stator and rotor coupling factors, respectively, and

$$L_s' = L_s - \frac{L_m^2}{L_r} \tag{2.12}$$

$$L_r' = L_r - \frac{L_m^2}{L_s} \tag{2.13}$$

are the stator and rotor transient inductances, respectively. The electrodynamic torque can be expressed as

$$T_e = p\,\frac{k_r}{L_s'}\,\mathrm{Im}(\underline{\Psi}_s\underline{\Psi}_r{}^*) \tag{2.14}$$

The state-space equations of the machine with the flux linkages and rotor speed as state variables are

$$\frac{d\Psi}{dt} = \mathbf{A}\Psi + \mathbf{B}\,\mathbf{U} \tag{2.15}$$

where

$$\mathbf{B} = \begin{bmatrix} 1 & 0 & 0 & 0 & 0 \\ 0 & 1 & 0 & 0 & 0 \\ 0 & 0 & 1 & 0 & 0 \\ 0 & 0 & 0 & 1 & 0 \\ 0 & 0 & 0 & 0 & \frac{-1}{J_m} \end{bmatrix}, \Psi = \begin{bmatrix} \Psi_{qs} \\ \Psi_{ds} \\ \Psi_{qr} \\ \Psi_{dr} \\ \Omega_m \end{bmatrix}, \mathbf{U} = \begin{bmatrix} u_{qs} \\ u_{ds} \\ 0 \\ 0 \\ T_s \end{bmatrix}$$

and

$$\mathbf{A} = \begin{bmatrix} \dfrac{-R_s}{L_s'} & -\omega_s & \dfrac{k_r R_s}{L_s'} & 0 & 0 \\[2mm] \omega_s & \dfrac{-R_s}{L_s'} & 0 & \dfrac{k_r R_s}{L_s'} & 0 \\[2mm] \dfrac{k_s R_r}{L_r'} & 0 & \dfrac{-R_r}{L_r'} & p\Omega_m - \omega_s & 0 \\[2mm] 0 & \dfrac{k_s R_r}{L_r'} & \omega_s - p\Omega_m & \dfrac{-R_r}{L_r'} & 0 \\[2mm] \dfrac{p}{J_m}\dfrac{k_r\Psi_{dr}}{L_s'} & -\dfrac{p}{J_m}\dfrac{k_r\Psi_{qr}}{L_s'} & 0 & 0 & 0 \end{bmatrix}$$

Ψ_{ds} and Ψ_{qs} are the direct- and quadrature-axis components of the stator flux linkages, Ψ_{dr} and Ψ_{qr} are the direct- and quadrature-axis components of the rotor flux linkages, respectively.

The currents can be determined from the flux linkages by

$$i_s = \frac{1}{L_s'}\Psi_s - \frac{k_r}{L_s'}\Psi_r \tag{2.16}$$

$$i_r = \frac{1}{L_r'}\Psi_r - \frac{k_s}{L_r'}\Psi_s \tag{2.17}$$

The reason for presenting two models which predict identical results is that simpler and more advanced models presented in this chapter are derived from both models.

The output signals can be the state variables, such as rotor speed and flux linkages or currents as well as the electrodynamical torque. Other output signals that may be of interest are the active power

$$P = u_{qs}i_{qs} + u_{ds}i_{ds} \tag{2.18}$$

and the reactive power

$$Q = u_{qs}i_{ds} - u_{ds}i_{qs} \tag{2.19}$$

2.2 Inclusion of a non-stiff shaft

The performance of an induction machine depends on the mechanical load to which it is attached. A seventh-order model is used to represent the induction machine with a load connected via a non-stiff shaft. The shaft torque of the induction machine is now determined from the shaft stiffness α and damping B as well as the speeds and differences in angles of the machine and the load. The shaft torque is given by

$$T_s = B(\Omega_m - \Omega_l) + \alpha\Theta \tag{2.20}$$

The equations relating the speed of the load, Ω_l, and the mechanical angle between the load and rotor of the machine, Θ, are

$$T_s - T_l = J_l\frac{\Omega_l}{dt} \tag{2.21}$$

$$\Omega_m - \Omega_l = \frac{d\Theta}{dt} \tag{2.22}$$

where J_l is the moment of inertia of the load and T_l is the applied load torque.

2.3 Main flux saturation

If saturation effects are ignored, the inductance matrix is constant and does not need to be recalculated at each time step of a simulation. If only the magnetizing inductance is adjusted, the dynamic effect of the saturation is not accounted for. If the dynamic effect of the saturation is considered, the inductance matrix has to be determined at each time step. According to Hallenius (1982) the main flux saturation is taken into account by modifying the inductance matrix in (2.7) to

$$\mathbf{L} = \begin{bmatrix} L_{qs} & L_{mdq} & L_{mq} & L_{mdq} & 0 \\ L_{mdq} & L_{ds} & L_{mdq} & L_{md} & 0 \\ L_{mq} & L_{mdq} & L_{qr} & L_{mdq} & 0 \\ L_{mdq} & L_{md} & L_{mdq} & L_{dr} & 0 \\ 0 & 0 & 0 & 0 & -J_m \end{bmatrix} \tag{2.23}$$

where

$$L_m = \frac{\Psi_m}{i_m} \tag{2.24}$$

$$i_{dm} = i_{ds} + i_{dr} \tag{2.25}$$

$$i_{qm} = i_{qs} + i_{qr} \tag{2.26}$$

$$i_m = \sqrt{i_{dm}^2 + i_{qm}^2} \tag{2.27}$$

$$L_{mdq} = \frac{i_{dm}i_{qm}}{i_m} \frac{dL_m}{di_m} \tag{2.28}$$

$$L_{md} = L_m + \frac{(i_{dm})^2}{i_m} \frac{dL_m}{di_m} \tag{2.29}$$

$$L_{mq} = L_m + \frac{(i_{qm})^2}{i_m} \frac{dL_m}{di_m} \tag{2.30}$$

$$L_{ds} = L_{s\lambda} + L_{md} \tag{2.31}$$

$$L_{qs} = L_{s\lambda} + L_{mq} \tag{2.32}$$

$$L_{dr} = L_{r\lambda} + L_{md} \tag{2.33}$$

$$L_{qr} = L_{r\lambda} + L_{mq} \tag{2.34}$$

Ψ_m and i_m are the main flux linkage and the magnetizing current, respectively.

At high currents, also the leakage inductances saturate. Since the scope of this thesis is low-frequency perturbations in the steady-state operating region, the leakage inductances have here been considered to be independent of the currents. A method to take the saturation of the leakage inductances into account has been presented by, for example, Healey et al. (1995).

If only small deviations from an operating point are to be investigated, the analysis can be facilitated by rotating the applied voltage vector in such a way that the quadrature-axis component of the magnetizing current is equal to zero (Melkebeek 1980, 1983). An important quantity is now the differential or tangential magnetizing inductance

$$L_{mt} = \frac{d\Psi_m}{di_m} \tag{2.35}$$

In Figure 2.1 Ψ_m is plotted as a function of i_m for the 15 kW machine investigated.
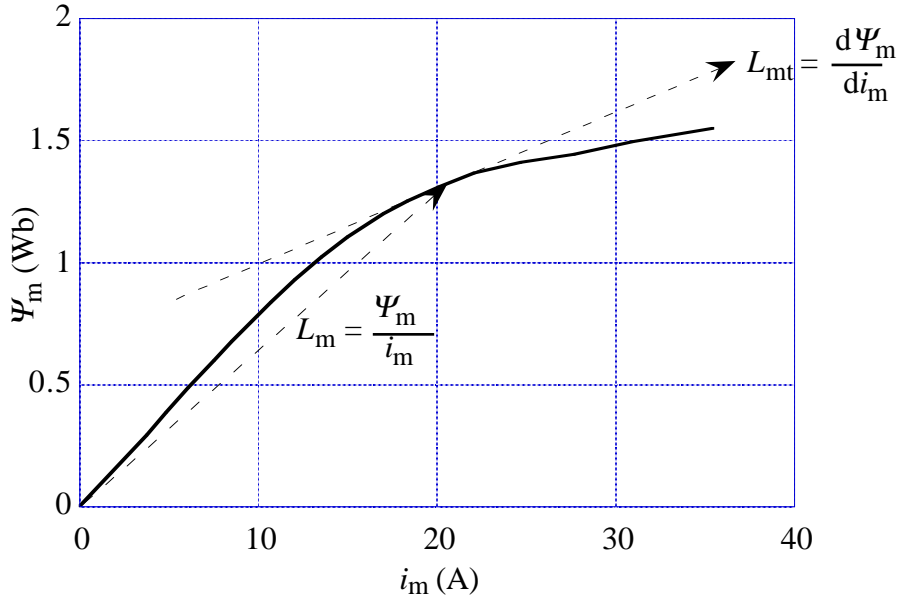
Figure 2.1. Ψ_m as a function of i_m for the 15 kW machine investigated.

The induction matrix (2.23) can now be simplified substantially, since

$$L_{mdq} = 0 \tag{2.36}$$

$$L_{md} = L_{mt} \tag{2.37}$$

$$L_{mq} = L_m \tag{2.38}$$

However, any larger deviations from the operating point investigated require a new determination of the inductance matrix (Ojo et al. 1990).

2.4 Skin effect

The parameters R_r and $L_{r\lambda}$ of the rotor winding depend on the rotor frequency of a cage induction machine. For the investigated 15 kW machine, the rotor resistance has increased by about 60 % at a rotor frequency of 50 Hz and the rotor leakage inductance has decreased by about 8 %. In order to determine the steady-state characteristics, it is possible to simply adjust R_r and $L_{r\lambda}$ in (2.2) and (2.6). However, the dynamic influence of the skin effect is not considered using this method. The most convenient method to take the dynamic influence of the skin effect into account is to use a multiple-cage rotor configuration as suggested by Adkins and Harley (1975).

The rotor winding impedance, rotor resistance and rotor leakage reactance, of the investigated 15 kW machine were determined by means of a locked-rotor test. The test is presented in Appendix A.

The slot shape of the investigated 15 kW machine is shown in Figure 2.2 and the double-rotor bar configuration is presented in Figure. 2.3.
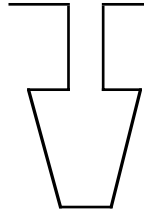
Figure 2.2. The slot shape of the investigated 15 kW machine.
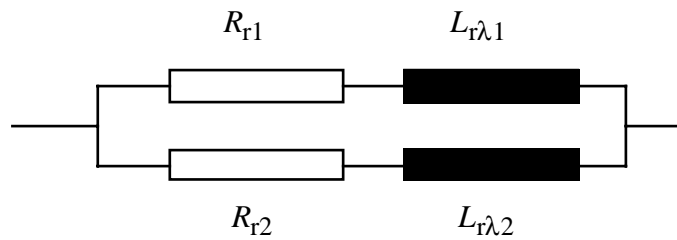
Figure 2.3. Rotor winding impedance of the double-cage rotor.

The rotor winding impedance of the double-cage rotor is

$$Z(s) = \frac{s^2 L_{r\lambda 1} L_{r\lambda 2} + s(L_{r\lambda 1} R_{r2} + L_{r\lambda 2} R_{r1}) + R_{r1} R_{r2}}{R_{r1} + R_{r2} + s(L_{r\lambda 1} + L_{r\lambda 2})} \tag{2.39}$$

The parameters of the double-cage rotor configuration are determined from the measured values using the least square-method. In Figure 2.4 the measured rotor winding impedance is presented together with those calculated using single- and double-cage rotor configurations.
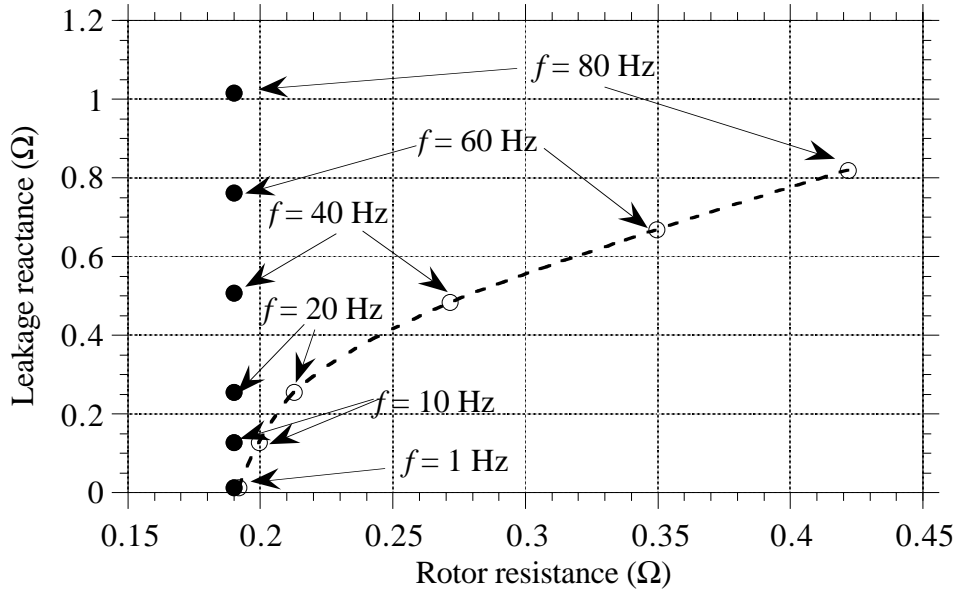
Figure 2.4. Impedance of the double-cage rotor winding. Circles are measured values. Dots are values determined according to a single-cage rotor configuration. Dashed line represents the characteristics of the double-cage rotor configuration.

As can be noted from Figure 2.4, a single-cage rotor configuration is useful in predicting the rotor winding impedance only at very low rotor current frequencies for the investigated 15 kW machine. Furthermore, it can be noted that a very good prediction of the rotor winding impedance is obtained by using the double-cage rotor configuration up to a rotor current frequency of at least 80 Hz for the machine investigated. To represent the double-cage rotor, (2.2), (2.5) and (2.6) are replaced by

$$0 = \underline{i}_{r1}R_{r1} + \frac{d\underline{\Psi}_{r1}}{dt} + j(\omega_s - p\Omega_m)\underline{\Psi}_{r1} \tag{2.40}$$

$$0 = \underline{i}_{r2}R_{r2} + \frac{d\underline{\Psi}_{r2}}{dt} + j(\omega_s - p\Omega_m)\underline{\Psi}_{r2} \tag{2.41}$$

$$\underline{\Psi}_s = L_s\underline{i}_s + L_m\underline{i}_{r1} + L_m\underline{i}_{r2} \tag{2.42}$$

$$\underline{\Psi}_{r1} = (L_m + L_{r\lambda 1})\underline{i}_{r1} + L_m\underline{i}_s + L_m\underline{i}_{r2} \tag{2.43}$$

$$\underline{\Psi}_{r2} = L_m\underline{i}_{r1} + (L_m + L_{r\lambda 2})\underline{i}_{r2} + L_m\underline{i}_s \tag{2.44}$$

If the purpose of the study is to investigate the rotor winding impedance for higher frequency regions, the number of parallel circuits can be increased further. For example, three loops have been used to study an inverter-fed induction machine by Dell'Aquila et al. (1984).

2.5 Inclusion of iron losses

The iron losses are usually neglected when the dynamic and transient performance of the machine is determined. To completely take the iron losses into account is an almost impossible task. However, if only the responses to very low-frequency perturbations in the voltage magnitude are of interest, it is possible to use a simple and straightforward method to take into account the dynamic effect of iron losses. A resistance R_m, representing the iron losses, is added in parallel with the magnetizing inductance in a fashion similar to the steady-state equivalent circuit. As a consequence, the two-axis model consists of seven differential equations. R_m can be obtained from a no load test at variable voltage. The iron loss resistance varies with the supply frequency and has accordingly to be determined for each new supply frequency. If the flux level is at rated or below rated flux level, R_m is rather independent of the flux level in the machine. In order to model the iron losses, (2.2), (2.5) and (2.6) are replaced by

$$0 = \underline{i}_r R_r + \frac{\mathrm{d}\underline{\Psi}_r}{\mathrm{d}t} + \mathrm{j}(\omega_s - p\Omega_m)\underline{\Psi}_r \qquad (2.45)$$

$$0 = \underline{i}_{Rm} R_m + \frac{\mathrm{d}\underline{\Psi}_m}{\mathrm{d}t} + \mathrm{j}\omega_s\underline{\Psi}_m \qquad (2.46)$$

$$\underline{\Psi}_s = L_s\underline{i}_s + L_m\underline{i}_r + L_m\underline{i}_{Rm} \qquad (2.47)$$

$$\underline{\Psi}_r = (L_m + L_{r\lambda 1})\underline{i}_r + L_m\underline{i}_{Rm} + L_m\underline{i}_s \qquad (2.48)$$

$$\underline{\Psi}_m = L_m\underline{i}_s + L_m\underline{i}_r + L_m\underline{i}_{Rm} \qquad (2.49)$$

where R_m is the iron loss equivalent resistance and $\underline{i}_{Rm}$ is the current of the iron loss equivalent resistance.

2.6 Neglecting stator transients model (NST-models)

The induction machine model can be reduced to a third-order system by neglecting the stator flux transients. Several methods have been presented in the literature. Here, two models presented by Rodriguez et al. (1987) have been used.

In the most commonly used variant, NST I, the derivatives of the stator flux linkage of (2.8) are put to zero and the stator flux linkages are then solved as functions of the rotor flux linkages and rotor speed. The stator flux linkages are then inserted into the three rotor equations and a third-order model has been derived. In this model the state variables Ψ_{dr}, Ψ_{qr} and Ω_m are the same as in (2.15). Details about the procedure of deriving the NST I-model can be found in Appendix B.

A more advanced model, NST III, described by Rodriguez et al. (1987) can be obtained by neglecting only the fast components of the stator flux transients. In this model, the three state variables must be transformed in order to obtain Ψ_{dr}, Ψ_{qr} and Ω_m before the stator flux linkages and currents can be determined. The details of the procedure of deriving the NST III-model is presented by Rodriquez et al. (1987).

2.7 Second-order models

2.7.1 Neglecting stator resistance model (NSR-model)

If the stator resistance is neglected and the voltage vector is considered to be constant and oriented in the q-direction, three of the machine flux linkages can be considered to be constants at no load:

$$\Psi_{ds} = \frac{u_{qs}}{\omega_{s0}} \tag{2.50}$$

$$\Psi_{qs} = 0 \tag{2.51}$$

$$\Psi_{dr} = \frac{L_m}{L_s} \Psi_{ds} \tag{2.52}$$

where ω_{s0} is the steady-state value of ω_s. Equation (2.15) can now be reduced to a linear second-order system at no load with the supply frequency and shaft torque as input signals,

$$\begin{bmatrix} \dfrac{\mathrm{d}\Psi_{qr}}{\mathrm{d}t} \\ \dfrac{\mathrm{d}\Omega_m}{\mathrm{d}t} \end{bmatrix} = \begin{bmatrix} \dfrac{-R_r}{L_r'} & p\,\dfrac{L_m}{L_s}\Psi_{ds} \\ -\dfrac{p}{J_m L_s'}\dfrac{k_r}{}\Psi_{ds} & 0 \end{bmatrix} \begin{bmatrix} \Psi_{qr} \\ \Omega_m \end{bmatrix} + \begin{bmatrix} -\dfrac{L_m}{L_s}\Psi_{ds} & 0 \\ 0 & \dfrac{-1}{J_m} \end{bmatrix} \begin{bmatrix} \omega_s \\ T_s \end{bmatrix} \tag{2.53}$$

Very simple transfer functions of the induction machine can be obtained from this model (2.53). For instance, the transfer function from shaft torque to electrodynamical torque can be expressed as

$$\frac{\Delta T_e}{\Delta T_s} = \frac{\left(\dfrac{L_m}{L_s}\right)^2 \dfrac{p^2 \Psi_{ds}^2}{J_m L_r'}}{s^2 + s\,\dfrac{R_r}{L_r'} + \left(\dfrac{L_m}{L_s}\right)^2 \dfrac{p^2 \Psi_{ds}^2}{J_m L_r'}} \tag{2.54}$$

The induction machine can now be represented by the mechanical analogy shown in Figure 2.5, as proposed by Nacke (1962). Since the induction machine rotor speed and electrodynamical torque responses to supply frequency and shaft torque perturbations varies only slightly with the static shaft torque, (2.53) predicts these responses well, not only at no load but also at other operating points. The performance of this model is usually good with one exception: if the stator resistance is relatively large compared to the reactances of the machine. This is the case in smaller machines or if the supply frequency is low. The result is that the damping of the machine will be overestimated. The larger the machine, the lower the supply frequency can be without the NSR-model loosing too much in accuracy.
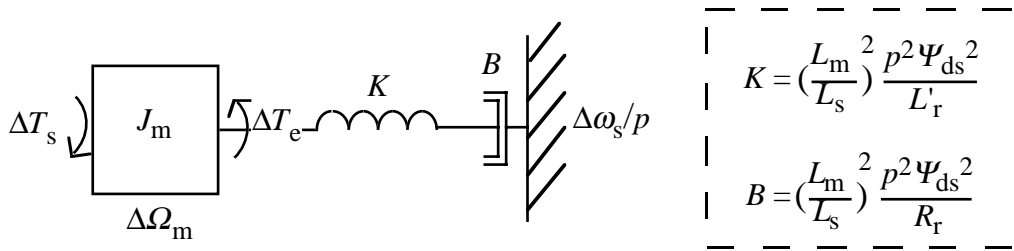
Figure 2.5. Mechanical analogy of the induction machine, NSR-model.

2.7.2 Load angle model (LA-model)

Since the stator resistance is neglected in the NSR-model derived above, there will be a steady-state error as well as a changed dynamic performance. A second-order model that correctly predicts the steady-state responses of the machines, the Load Angle model, will be derived in this section. The rotor speed and load angle are used as state variables. The magnitudes of the stator and rotor flux linkages are considered to vary slowly and not to affect the dynamic response of the model. The magnitudes of the stator and rotor flux linkages, Ψ_s and Ψ_r, are determined from the speed by

$$\begin{bmatrix} \underline{\Psi}_s \\ \underline{\Psi}_r \end{bmatrix} = \begin{bmatrix} \dfrac{-R_s}{L_s'} + j\omega_s & \dfrac{k_r R_s}{L_s'} \\ -\dfrac{k_s R_r}{L_r'} & j(\omega_s - p\Omega_m) \end{bmatrix}^{-1} \begin{bmatrix} \underline{u}_s \\ 0 \end{bmatrix} \tag{2.55}$$

The flux linkages at motor operation as well as the load angle δ are presented in Figure 2.6. A coordinate system oriented in the same direction as the stator flux linkage is also introduced.
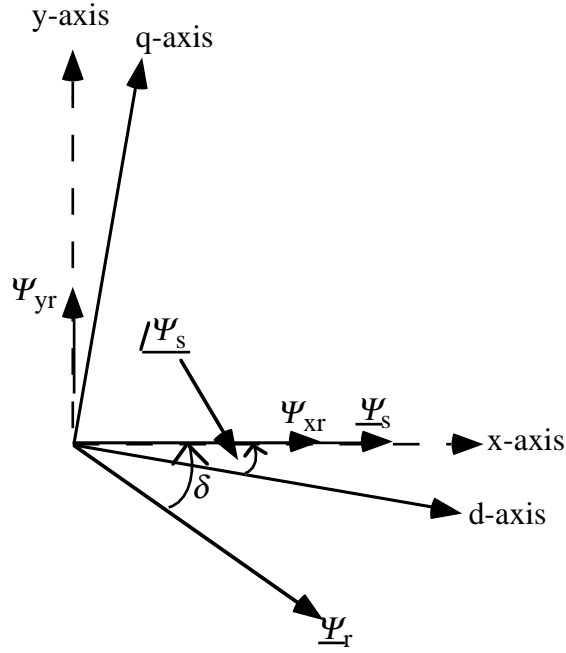
Figure 2.6. Flux linkages and δ at motor operation.

The load angle is related to the x- and y- components of the axes rotor flux linkages by

$$\Psi_{yr} = -\ \Psi_r \sin\delta \qquad\qquad (2.56)$$

$$\Psi_{xr} = \Psi_r \cos\delta \qquad\qquad (2.57)$$

Differentiating (2.56) and (2.57) with the rate of change of the rotor flux linkage magnitude neglected gives

$$\frac{\mathrm{d}\Psi_{yr}}{\mathrm{d}t} = -\frac{\mathrm{d}\delta}{\mathrm{d}t}\Psi_r \cos\delta \qquad\qquad (2.58)$$

$$\frac{\mathrm{d}\Psi_{xr}}{\mathrm{d}t} = -\frac{\mathrm{d}\delta}{\mathrm{d}t}\Psi_r \sin\delta \qquad\qquad (2.59)$$

Equations (2.56)-(2.59) are now inserted into (2.9), resulting in

$$\frac{\mathrm{d}\delta}{\mathrm{d}t} = \frac{-R_r}{L_r{}'}\tan\delta + \omega_s - p\Omega_m \qquad\qquad (2.60)$$

for the imaginary part of the resulting equation and the real part ignored. The electrodynamical torque can be expressed as a function of the flux linkage magnitudes and the load angle by

$$T_e = p \frac{k_r}{L'_s} \Psi_s \Psi_r \sin\delta \tag{2.61}$$

and the differential equation of the rotor speed is obtained as

$$J_m \frac{d\Omega_m}{dt} = p \frac{k_r}{L'_s} \Psi_s \Psi_r \sin\delta - T_s \tag{2.62}$$

Equation (2.60) can be simplified by using the approximation

$$\tan\delta \approx \delta \tag{2.63}$$

and (2.62) can be simplified by letting

$$\sin\delta \approx \delta \tag{2.64}$$

The dynamics is only slightly altered by these two simplifications. A steady-state error, however, is introduced as well. The load angle of an induction machine is usually about 10 degrees at rated load. At 10 degrees the simplifications (2.63) and (2.64) give a steady-state slip error of 1.5 %. At the pull-out torque, the slip error is 30 %.

By using the more detailed approximations,

$$\sin\delta \approx (\delta - \frac{\delta^3}{6}) \tag{2.65}$$

$$\tan\delta \approx (\delta + \frac{\delta^3}{3}) \tag{2.66}$$

the steady-state slip error is reduced to 0.02 % at rated load and 5 % at the pull-out point. The proposed load angle model can now be written as

$$\begin{bmatrix} \frac{d\delta}{dt} \\ \frac{d\Omega_m}{dt} \end{bmatrix} = \begin{bmatrix} \frac{-R_r}{L'_r}(1 + \frac{\delta^2}{3}) & -p \\ p \frac{L_m}{L_s L'_r} \Psi_s \Psi_r(1 - \frac{\delta^2}{6}) & 0 \end{bmatrix} \begin{bmatrix} \delta \\ \Omega_m \end{bmatrix} + \begin{bmatrix} 1 & 0 \\ 0 & \frac{-1}{J_m} \end{bmatrix} \begin{bmatrix} \omega_s \\ T_s \end{bmatrix} \tag{2.67}$$

The rotor flux linkages are determined by

$$\Psi_{qr} = -\Psi_r \sin(\delta - \underline{/\Psi_s}) \tag{2.68}$$

$$\Psi_{dr} = \Psi_r \cos(\delta - \underline{/\Psi_s})$$ (2.69)

Finally, knowing the flux linkages, the currents as well as the active and reactive powers can be determined using (2.16)-(2.19).

The second-order model derived here is similar to the one derived by Derbel et al. (1995). Compared to load angle models presented earlier by Mohamedein (1978) and Al-Bahrani et al. (1988), the second-order model presented here is less complex but combines the best of the previously presented load angle models: an almost correct steady-state response and a good dynamic response. Since the magnitudes of the rotor and stator flux linkages vary slower than the load angle, it is possible to decrease the simulation time by determining these quantities only at every n:th step, if the LA-model is used in a simulation.

2.8 First-order models (ND-model and LD-model)

In the first-order model of the induction machine, the only state variable is the rotor speed. The electrodynamical torque is now a function of the rotor speed and is determined by

$$T_e = p\, \frac{k_r}{L'_s}(\Psi_{qs}\Psi_{dr} - \Psi_{ds}\Psi_{qr})$$ (2.70)

The flux linkages, which are functions of the applied voltage and rotor speed, are determined by (2.55). By combining the expression for the electrodynamical torque with (2.3), a first-order non-linear model of the induction machine is obtained, the ND-model (non-linear damper model). Knowing the flux linkages, the currents as well as the active and reactive powers can be determined using (2.16)-(2.19).

In many cases, it is possible to use a first-order model linearized at no load with the stator resistance and leakage reactances neglected. The linearized model predicts almost the same rotor speed and electrodynamical torque responses to shaft torque and supply frequency perturbations as the non-linear model, also at other operating points. The expression for the electrodynamical torque is now:

$$T_e = p\left(\frac{L_m}{L_s}\right)^2 \frac{(u_{ds}^2 + u_{qs}^2)}{\omega_s^2 R_r}(\omega_s - p\Omega_m)$$ (2.71)

This model is referred to as the LD-model, linear damper model. The induction machine can now be represented by the mechanical analogy presented in Figure 2.7
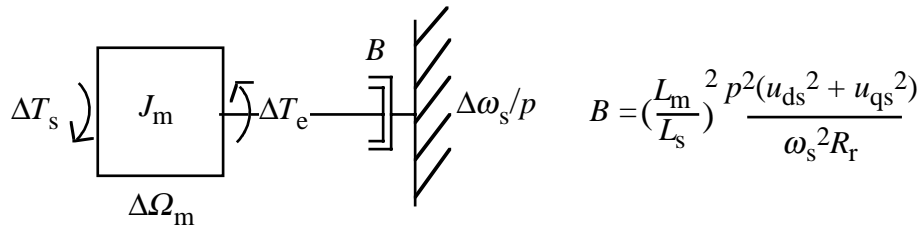
Figure 2.7. Mechanical analogy of the induction machine, LD-model.

$$B = \left(\frac{L_m}{L_s}\right)^2 \frac{p^2(u_{ds}^2 + u_{qs}^2)}{\omega_s^2 R_r}$$

3 EXPERIMENTAL SET-UP

3.1 Main components

The experimental object, a 15 kW six-pole cage induction machine equipped with thermal sensors, was attached to a dc machine via a torque transducer. The dc machine was fed by a four-quadrant thyristor converter and could thus produce any desired shaft torque. The induction machine was connected to an autonomous grid, created by a forced-commutated converter. The forced-commutated converter kept the voltages regardless of the currents of the induction machine, i.e. it compensated for the voltage drops in the converter caused by components and blanking time. Another feature of the forced-commutated converter was that it could generate desired deviations in the frequency and magnitude of the supply voltage. The experimental set-up with the measuring system is illustrated in Figure 3.1 and the main components of the experimental set-up are presented in Table 3.1.
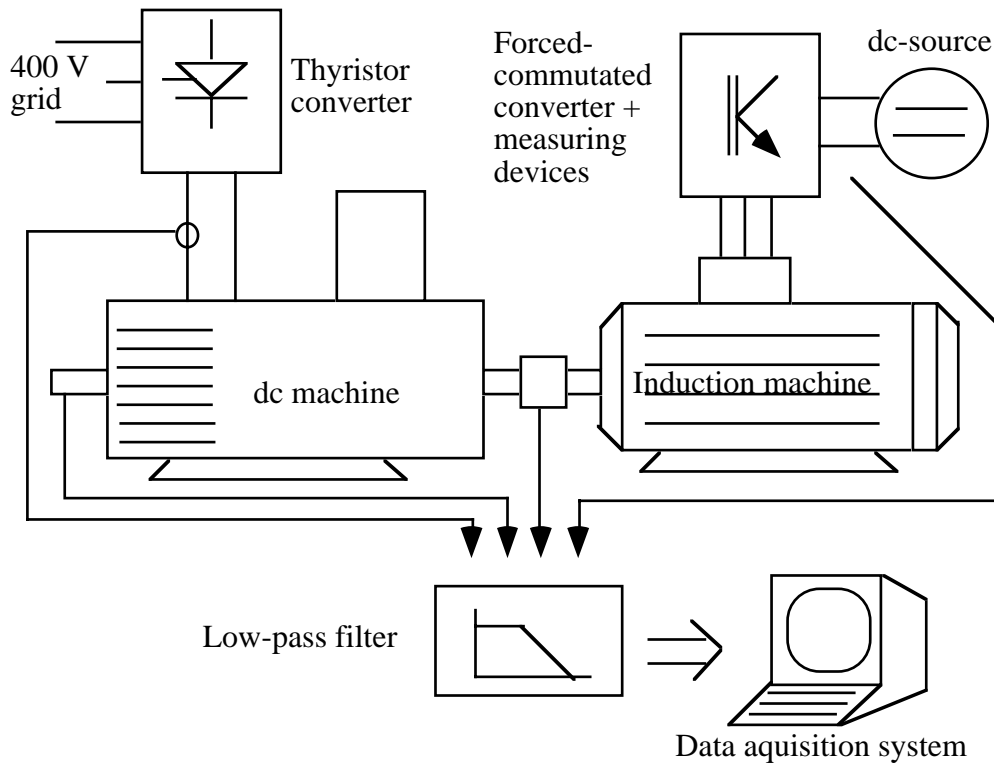
Figure 3.1. Experimental set-up and measuring system.

31

Table 3.1. Main components.

Component	Description
induction machine	ABB MBT-180L 15 kW 970 rpm 380 V 32 A
dc machine	DMP 160-4S 40.1 kW 2470 rpm
thyristor converter	TYRAK S 120 A
forced-commutated converter	Designed at the department 5 kHz switching frequency

The rotor speed is measured by an analogue tachometer attached to the dc machine, and the currents and voltages are measured by transducers with a high bandwidth. The active and reactive powers as well as the stator voltages and currents in field coordinates are determined on-line. The shaft torque is measured by means of the torque transducer, and the dc machine torque is determined by measuring the armature current of the dc machine. All the signals are filtered before being sampled by a data acquisition system.

3.2 Experimental method

Small sinusoidal perturbations in the frequency or magnitude of the voltage were generated by controlling the forced-commutated converter. Torque perturbations were generated by controlling the four-quadrant thyristor converter.

Since the moments of inertia of the two machines and the electrodynamic torque of the dc machine were known, it was possible to determine the variations in the electrodynamical torque of the induction machine from the measured shaft torque. This method to determine the electrodynamical torque of the induction machine is especially suitable when the torque of the dc machine is constant and requires that the perturbation frequency is several times lower than the shaft resonance frequency, 210 Hz.

The electrodynamical torque was also determined from the measured currents and voltages as well as the estimated stator iron losses. To determine the electrodynamic torque response to frequency and voltage perturbations, the two methods provided the same response except for perturbation frequencies below a few Hz, where the second method predicted less accurate results.

The first method was used to determine the electrodynamical torque response to frequency and voltage perturbations while the second method was used to determine the same response to torque perturbations.

3.3 Description and accuracy of measuring equipment

Since the active and reactive powers as well as the currents and voltages in field coordinates are determined using several components with an accuracy of 1-2 %, the accuracy is worst for these signals. However, these signals were calibrated with dc voltages and dc currents, giving a result not deviating more than 1 % from the calibration equipment. The accuracy of this calibrating equipment is 1 %. The active power and current were also checked against a digital power meter using the ac network from the forced-commutated converter. The frequency used was 43.5 Hz, i.e., the same as during most of the measurements. The current predicted by the measuring equipment deviates less than 1 % from the values obtained by the digital power meter. The linear discrepancy in the power prediction between the measuring equipment and the digital power meter is less than 1 %.

The dc machine torque was calibrated against the torque transducer. The linear error is less than 2 %. The analogue tachometer signal is problematic, since the speed deviations are sometimes very small. Another problem is the suspension of the tachometer, which limits the frequency range of the tachometer to about 15 Hz. At a perturbation frequency of 35 Hz, the signal from the analogue tachometer is amplified by about 10 %. The fact that the tachometer is mounted on the dc machine is of less importance since the torsional stiffness of the torque transducer is rather high, giving a torsional eigenfrequency of 210 Hz. The accuracy of the measured signals is considered, after calibration, to be within 2 % except for the rotor speed signal, which is considered to be less accurate. Information about the location and accuracy of the thermal sensors is given by Kylander (1995).

The different measuring devices and their accuracy are presented in Table 3.2.

Table 3.2. Description and accuracy of measuring equipment.

Device	Type	Typical maximum error
torque transducer	HBM T30FN	1 %
power meter	Yokogawa 2533	1 %
phase current transducer	LEM-modules 200-S	2 %
dc machine current transducer	LEM-modules 300-S	4 %
voltage transducer	AD 210 J	2%
power measurement		2 %
digital tachometer	BREMI BRI-5045	0.02%
analogue tachometer	Radio-Energie Type RE0 444R1	1 % below 15 Hz
data acquisition system	National Instruments NB-MIO-16 L card	0.5 %

4. COMPARISON BETWEEN MODELS AND MEASUREMENTS

In this chapter, the responses predicted by the Park model are compared with measured responses to perturbations in the shaft torque, supply frequency and voltage magnitude. The responses are: rotor speed, electrodynamical torque, electric power, reactive power and stator current. Further, the responses of the simpler models are compared with the results obtained using the Park model.

The measurements and calculations in this chapter were performed on the 15 kW machine operating at 43.5 Hz and 288 V, which corresponds to a flux reduction of 13 %. The measurements were performed at no load as well as in motor and generator operation. The shaft torque was 70 Nm both in motor and generator operation, which gave a slip of about two thirds of the rated one.

Since the responses to shaft torque and supply frequency perturbations do not depend on the static shaft torque significantly, only the results from one operating point are presented. The response to voltage magnitude perturbations is presented for both motor and generator operation because the static shaft torque plays an important role in this case.

The responses of the machine were measured at perturbation frequency points ranging from 1 to 35 Hz. When the response to voltage magnitude perturbations was determined, two lower frequency points, 0.25 and 0.5 Hz, were also used. The perturbation magnitude was about 15 % in the shaft torque perturbation case, 1 % in the supply frequency perturbation case and 4 % in the voltage magnitude perturbation case. The perturbation magnitudes were selected to be small enough, not to affect the magnitudes and phase shifts of the investigated transfer functions.

The measured results are presented in Bode diagrams together with the results obtained by using four different models: the Park model, the NST I-model, the LA-model and the ND-model. When results of the other derived models are of interest, these are also presented.

There are two reasons for displaying the results of the NST I-model instead of the ones obtained using the NST III-model although the results predicted by the NST III-model in many cases are excellent. First, the results of the NST III-model are often very similar to the results predicted by the Park model. Secondly, the NST III-model sometimes needs the derivatives of the input signals in order to predict a correct response at very low-frequency perturbations, for example when predicting the electrodynamic torque response to voltage magnitude

perturbations. If the system order is increased, the error at very low-frequency perturbations can be eliminated.

The second-order models, the LA-model and the NSR-model, predict similar rotor speed and electrodynamical torque responses. However, the NSR-model should not be used to predict the stator current, electric power and reactive power responses, since three of the fluxes are considered to be constant. Therefore, only the results of one second-order model, the LA-model, are compared to the results of the Park model in the Bode diagrams. The same reasoning can be used for the non-linear and linear first-order model and, accordingly, only the results of the non-linear model are compared to the results of the Park model in the Bode diagrams.

In addition to presenting the results of some of the models together with the measurements in the Bode diagrams, the results of all the models are compared in tables. An error ε, indicating the discrepancy between a simplified model and the Park model, is introduced. The error is defined as

$$\varepsilon = \frac{1}{n} \sum_{i=1}^{n} \frac{\left| H_p(j2\pi f_i) - H(j2\pi f_i) \right|}{\left| H_p(j2\pi f_i) \right|} \tag{4.1}$$

where $H_p(j2\pi f)$ and $H(j2\pi f)$ are the transfer functions derived using the Park model and the model that is to be compared to the Park model, respectively. The components f_i of the frequency vector are logarithmically distributed between 0.1 Hz and 15 Hz.

4.1 Torque perturbation

The responses to torque perturbations were determined with the electrodynamical torque of the dc-machine as input. The electrodynamical torque of the dc machines was determined from the armature current of the dc-machine. The field current of the dc machine was constant. Consequently, the inertia of the dc machine is added to the inertia of the induction machine. Thus, we have a 15 kW induction machine with an inertia of 0.45 kgm^2.

In Figures 4.1.a-e the measured responses to torque perturbations (ΔT_{dcm}) are presented and compared with the results predicted by the different induction machine models. The machine is operating as motor loaded by an average shaft torque of 70 Nm.
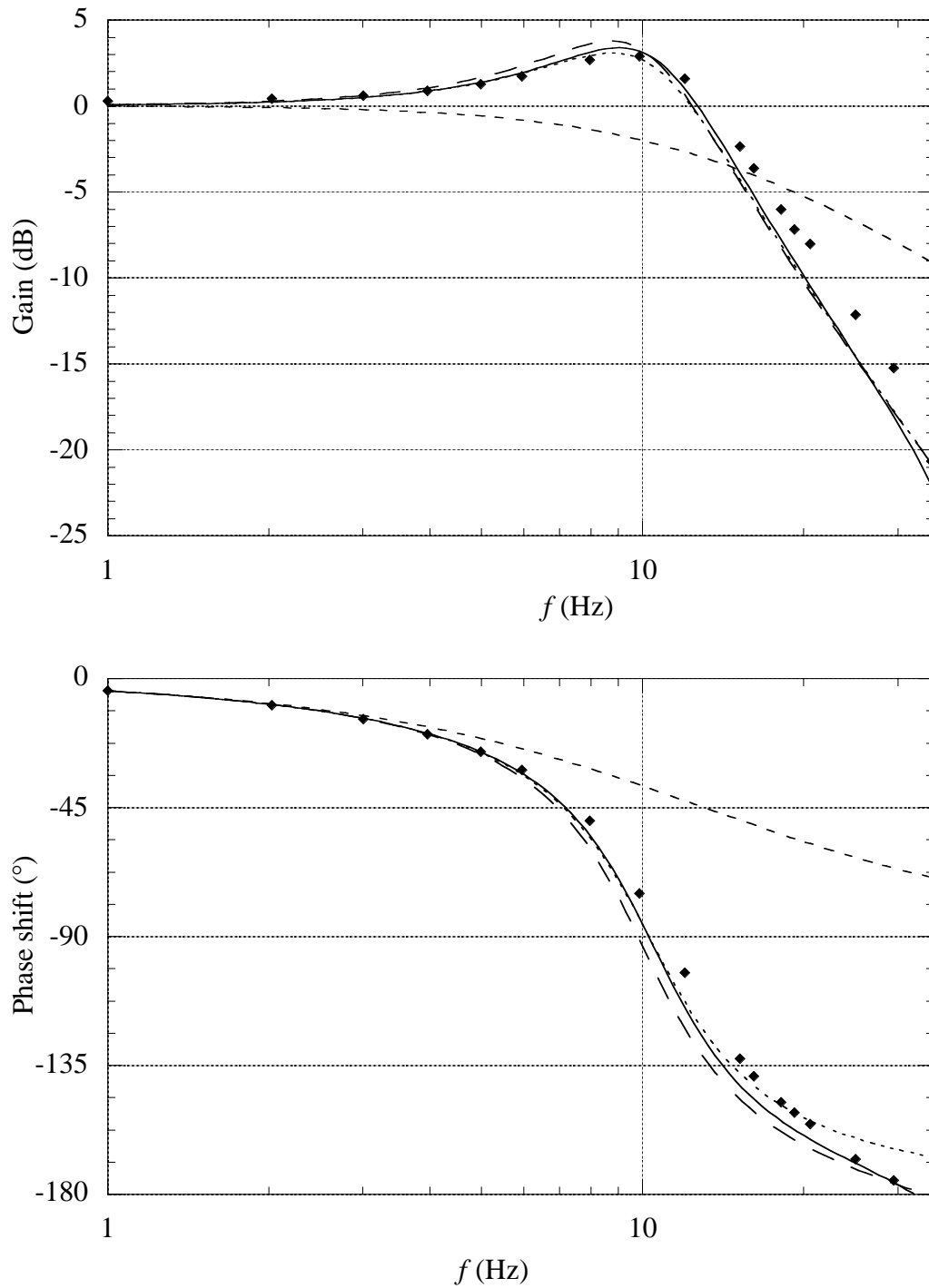
Figure 4.1.a.   Measured and calculated gains and phase shifts of $\Delta T_e/\Delta T_{dcm}$. Dots are measured values and lines are values determined according to the different models. Park model (——), NST I (··········), LA (— — —) and ND (- - - - -).
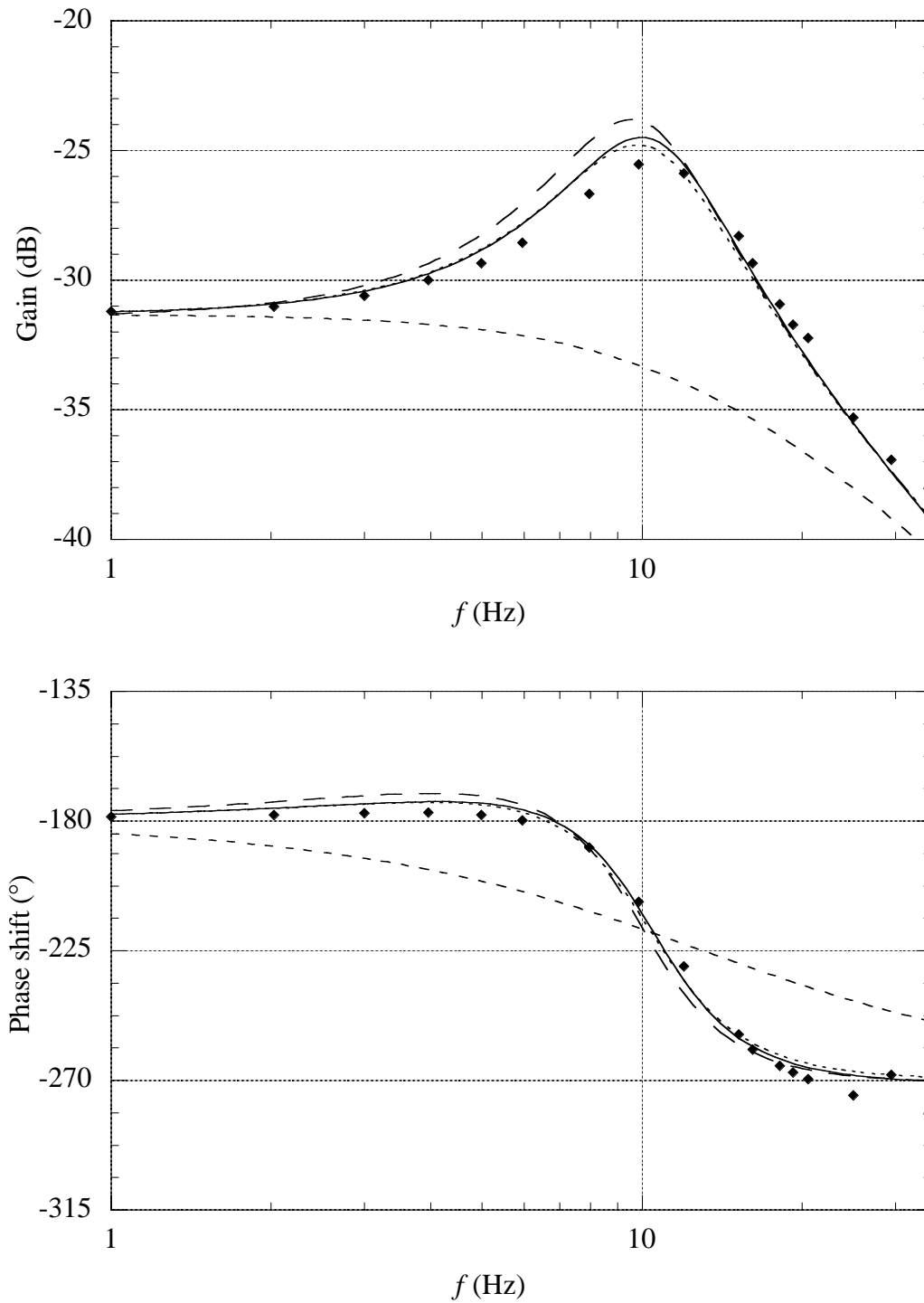
Figure 4.1.b. Measured and calculated gains and phase shifts of $\Delta\Omega_m/\Delta T_{dcm}$. Dots are measured values and lines are values determined according to the different models. Park model (——), NST I (··········), LA (— — —) and ND (- - - - -).
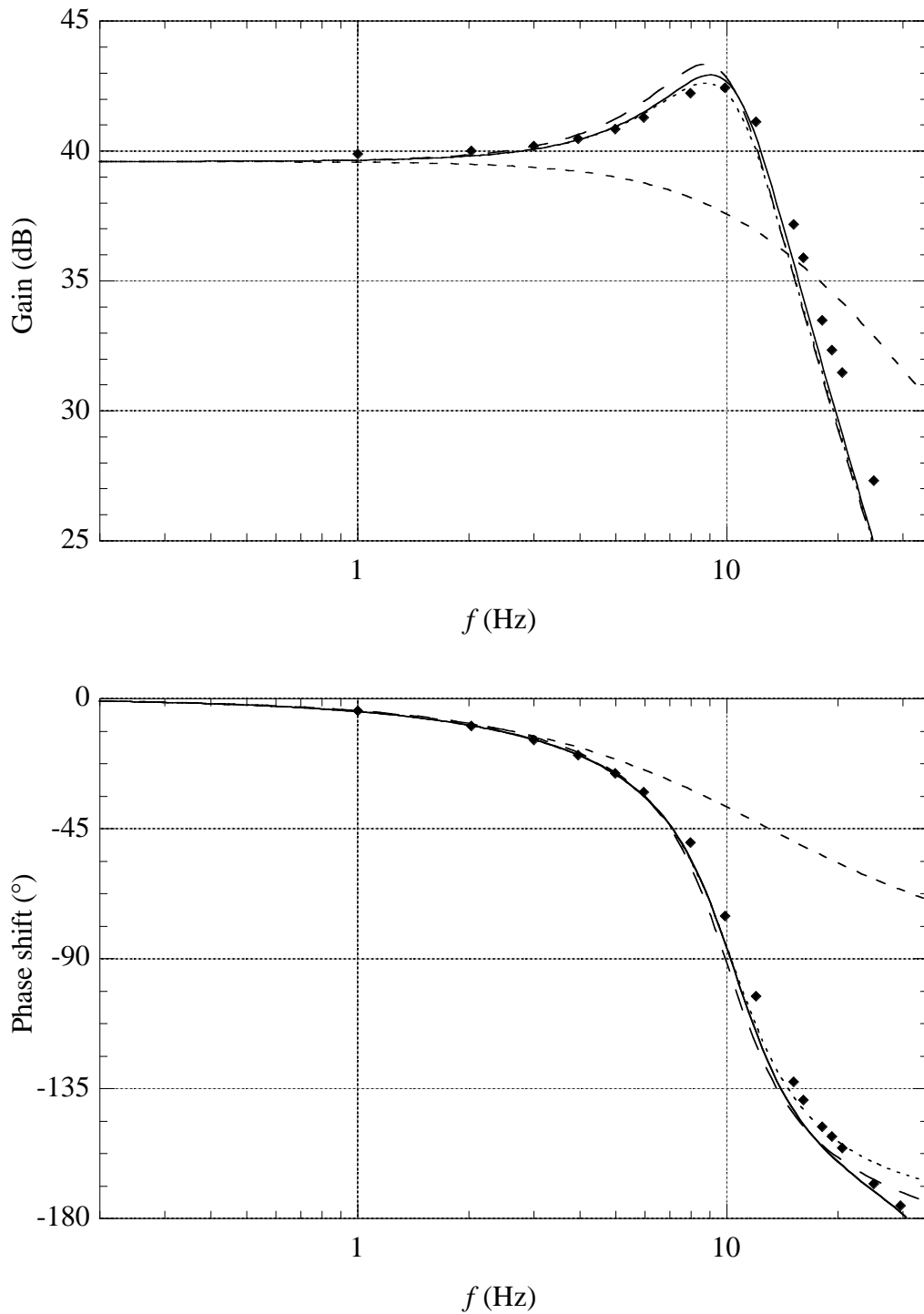
Figure 4.1.c. Measured and calculated gains and phase shifts of $\Delta P_e/\Delta T_{dcm}$. Dots are measured values and lines are values determined according to the different models. Park model (——), NST I (·········), LA (— — —) and ND (- - - - -).
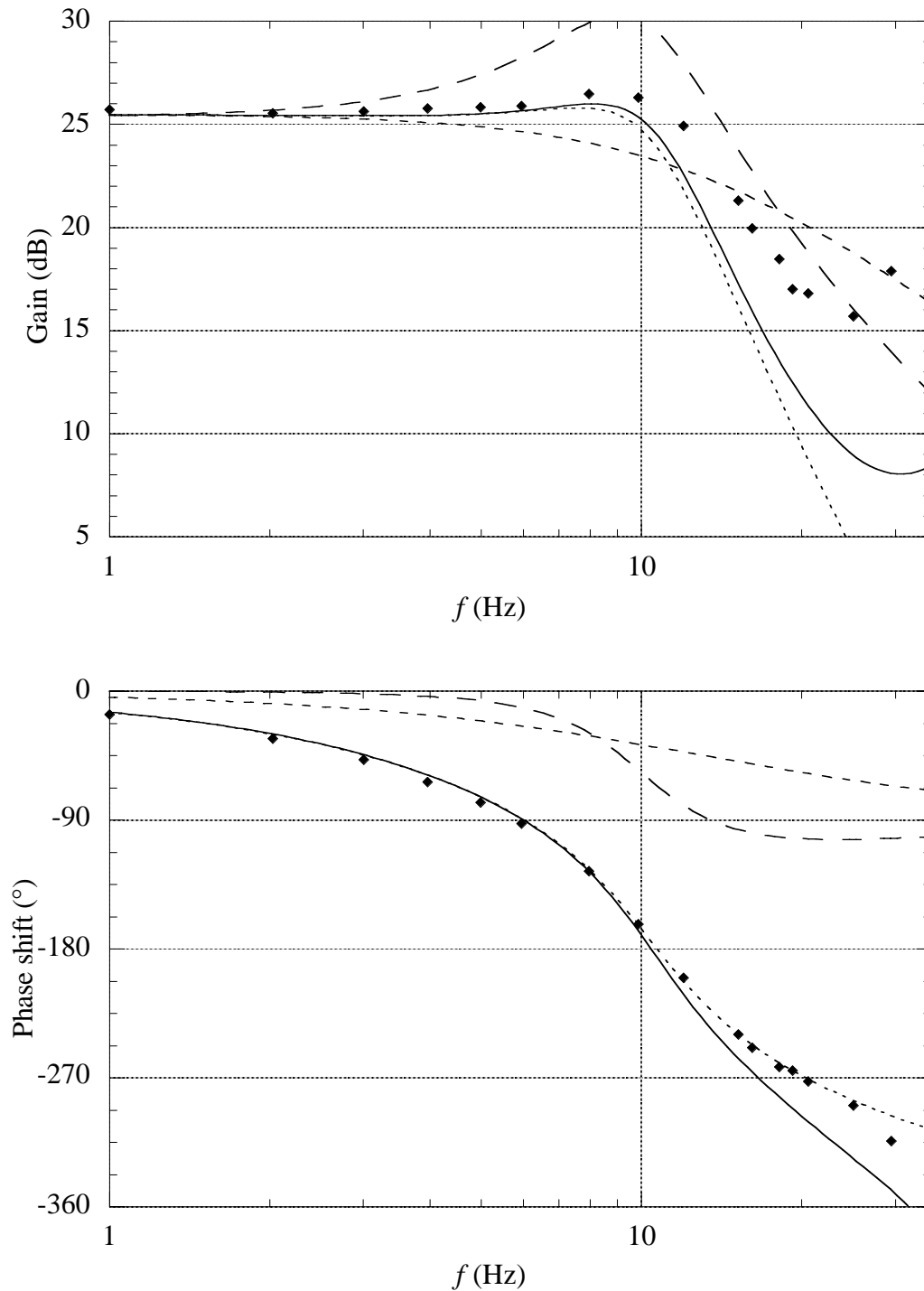
Figure 4.1.d. Measured and calculated gains and phase shifts of ΔQ/ΔT$_{dcm}$. Dots are measured values and lines are values determined according to the different models. Park model (——), NST I (·········), LA (— — —) and ND (- - - - -).
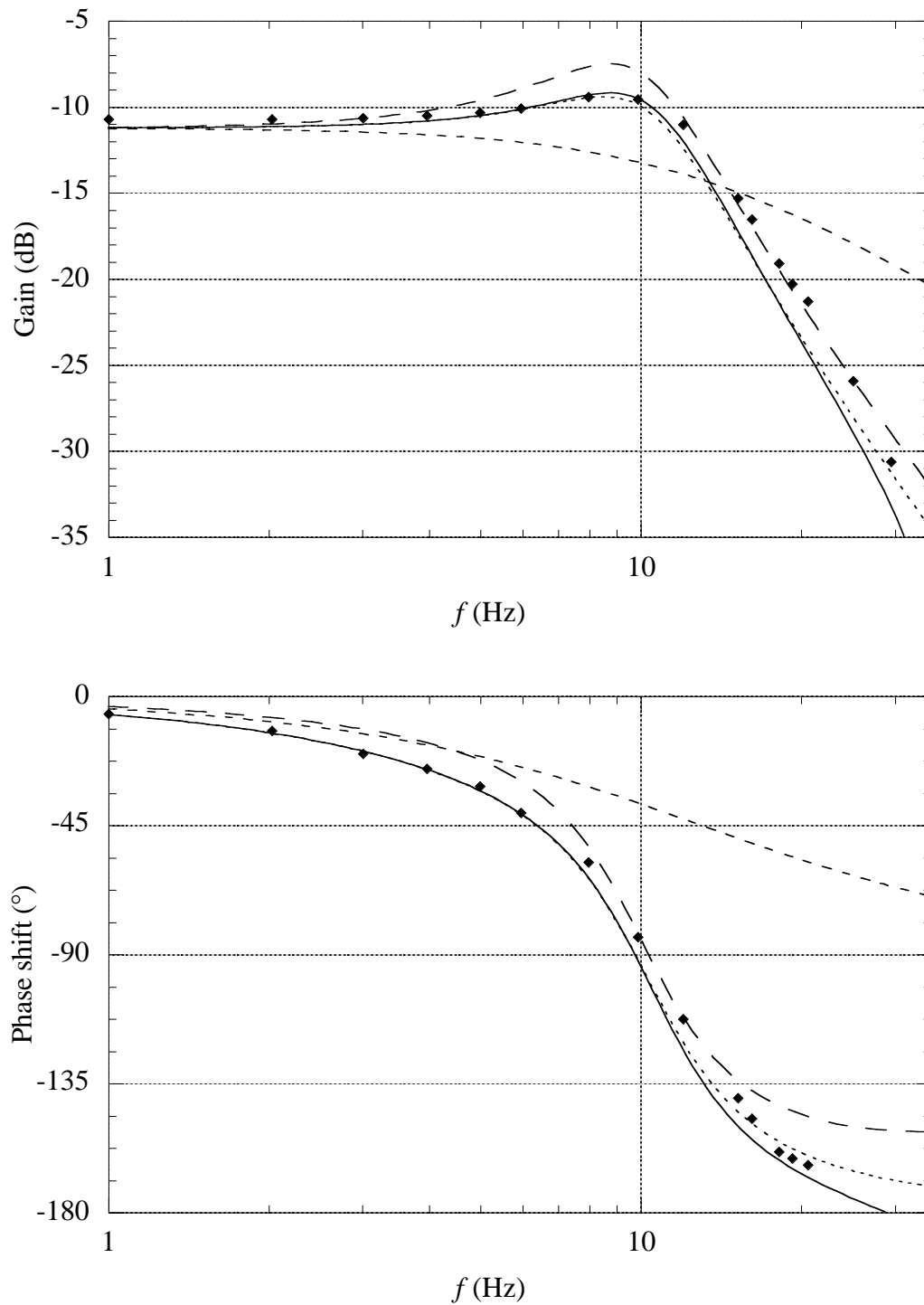
Figure 4.1.e. Measured and calculated gains and phase shifts of $\Delta I_s/\Delta T_{dcm}$. Dots are measured values and lines are values determined according to the different models. Park model (——), NST I (··········), LA (— — —) and ND (- - - - -).

The measured electrodynamical torque, electric power and stator current responses agree well with the values predicted by the Park model, while the reactive power response agrees only up to a perturbation frequency of 10 Hz. The rotor speed response has a 10 % discrepancy above a perturbation frequency of 5 Hz. Similar observations were made when the machine was operating as generator. The dominating eigenfrequency of the 15 kW machine operating at 288 V and 43.5 Hz with a moment of inertia of 0.45 kgm^2, 10 Hz, is visible in Figures 4.1.a-e.

A first-order model is possible to use up to a perturbation frequency of about 3 Hz if an error of 10 % is the maximum allowed. This frequency is a third of the dominating eigenfrequency of the 15 kW machine. The rotor speed, electrodynamical torque and electric power responses predicted by the LA-model have a maximum error of about 10 % compared to the Park model. Finally, the NST I-model is almost as good as the Park model.

In Table 4.1 the error ε defined by (4.1) is presented for the different models and different outputs. It can be noted that the NST III-model predicts excellent characteristics of the induction machine when the responses to shaft torque disturbances is to be determined. It can further be observed that the NSR-model has a larger rotor speed response error than the LA-model. In Figure 4.2 the calculated gains of $\Delta\Omega_m/\Delta T_s$ predicted by the NSR-model and LA-model are compared to the one obtained using the Park model.

Table 4.1. Error values of the simplified models.

	$\Delta T_e/\Delta T_{dcm}$	$\Delta\Omega_m/\Delta T_{dcm}$	$\Delta P_e/\Delta T_{dcm}$	$\Delta Q/\Delta T_{dcm}$	$\Delta I_s/\Delta T_{dcm}$
NST III-model	0.0013	0.0010	0.0014	0.0010	0.0022
NST I-model	0.0089	0.0083	0.0089	0.0196	0.0094
NSR-model	0.019	0.067			
LA-model	0.0233	0.034	0.021	0.42	0.078
ND-model	0.17	0.25	0.17	0.35	0.19
LD-model	0.17	0.28	0.21	0.37	0.24
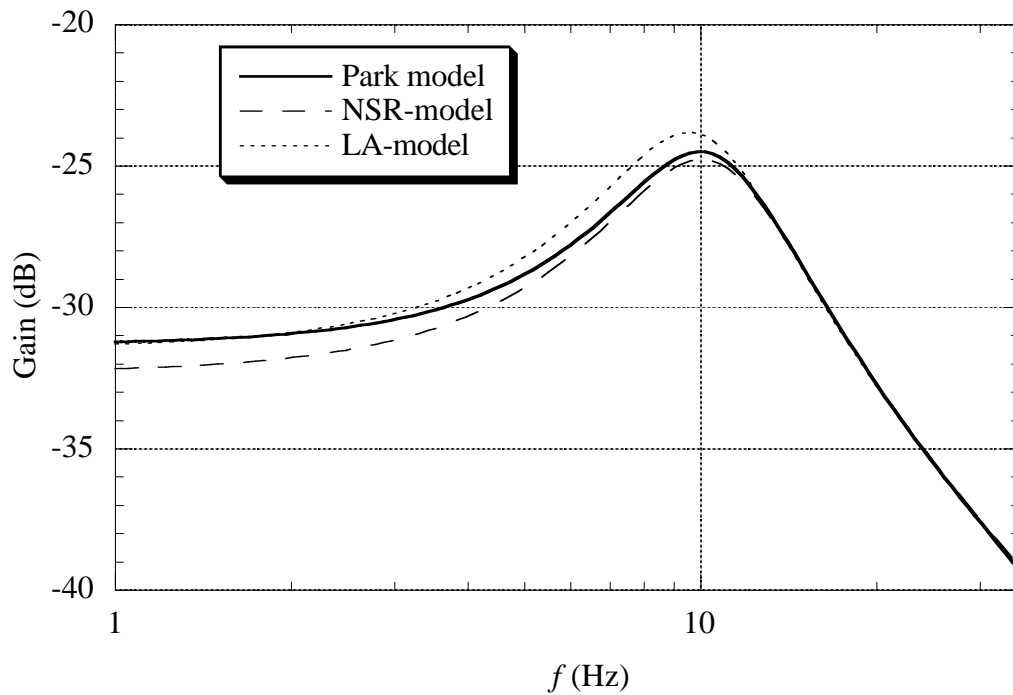
Figure 4.2. Calculated gain of $\Delta\Omega_m/\Delta T_s$ for the Park model and the two second-order models.

In Figure 4.2 it can be observed that the NSR-model predicts a rather good rotor speed response around the eigenfrequency of the machine. The reason for the high error value in Table 4.1 can be found in the lower frequency region, where the NSR-model does not predict a correct steady-state response. However, keeping in mind that this model is very simple, it provides good characteristics of the induction machine, suitable for many applications.

In Figure 4.3 the calculated gains of $\Delta\Omega_m/\Delta T_s$ predicted by the linear and non-linear first-order models are compared to the one obtained using the Park model. Again it can be observed from the figure that the dynamics of the models are quite similar but the linear model fails to predict a correct steady-state response.
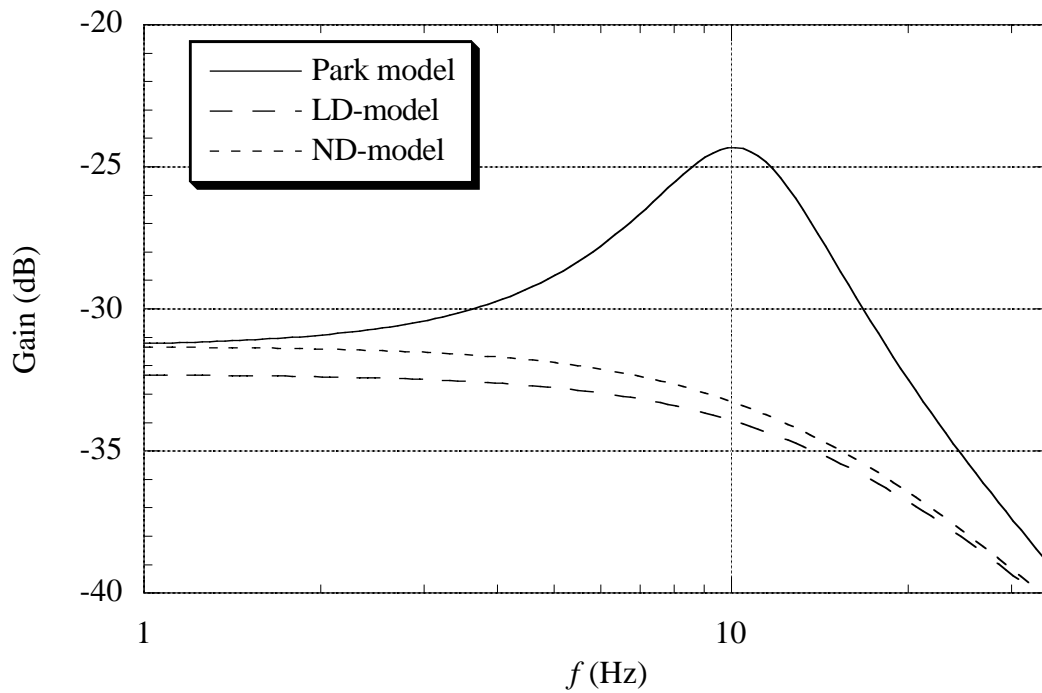
Figure 4.3. Calculated gain of ΔΩ$_m$/ΔT$_s$ for the Park model and the first-order models.

4.2 Supply frequency perturbation

The measured and calculated responses to perturbations in the supply frequency are shown in Figs. 4.4.a-e. Measured and calculated results are presented only for motor operation since the induction machine response to perturbations in the supply frequency does not depend much on the static shaft torque.
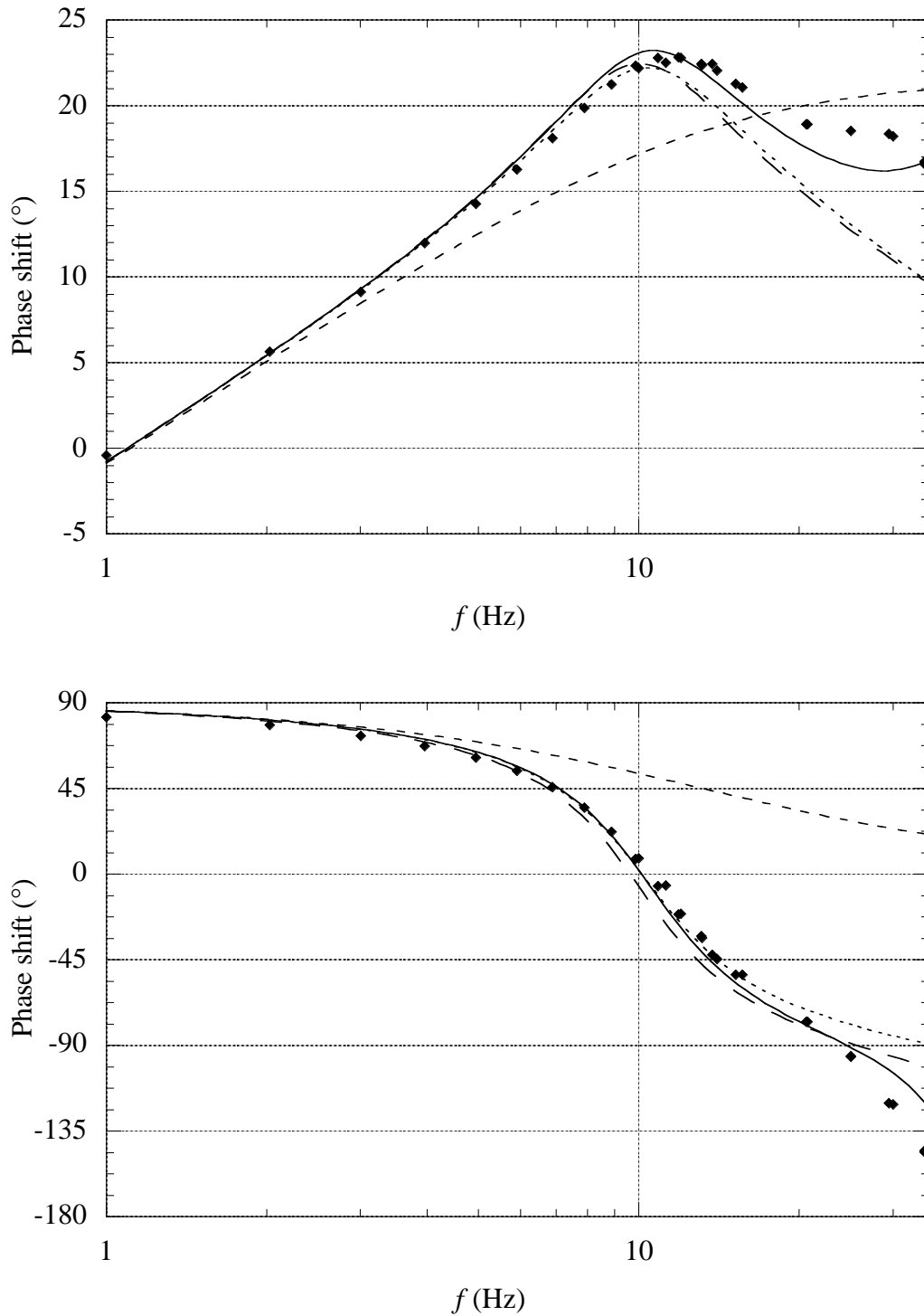
Figure 4.4.a.   Measured and calculated gains and phase shifts of $\Delta T_e/\Delta \omega_s$. Dots are measured values and lines are values determined according to the different models. Park model (——), NST I (·········), LA (— — —) and ND (- - - - -).
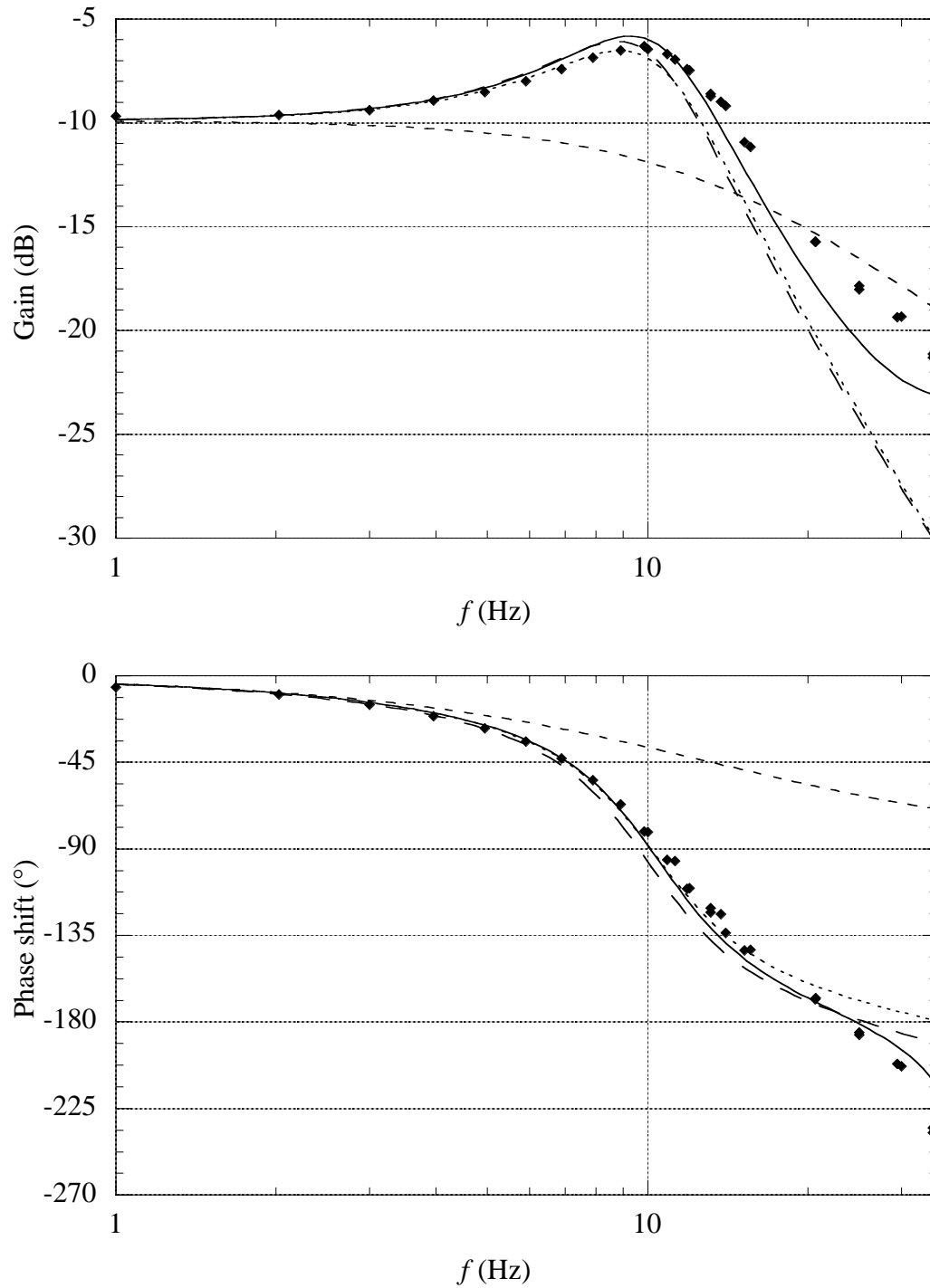
Figure 4.4.b. Measured and calculated gains and phase shifts of $\Delta\Omega_m/\Delta\omega_s$. Dots are measured values and lines are values determined according to the different models. Park model (——), NST I (·········), LA (— — —) and ND (- - - - -).
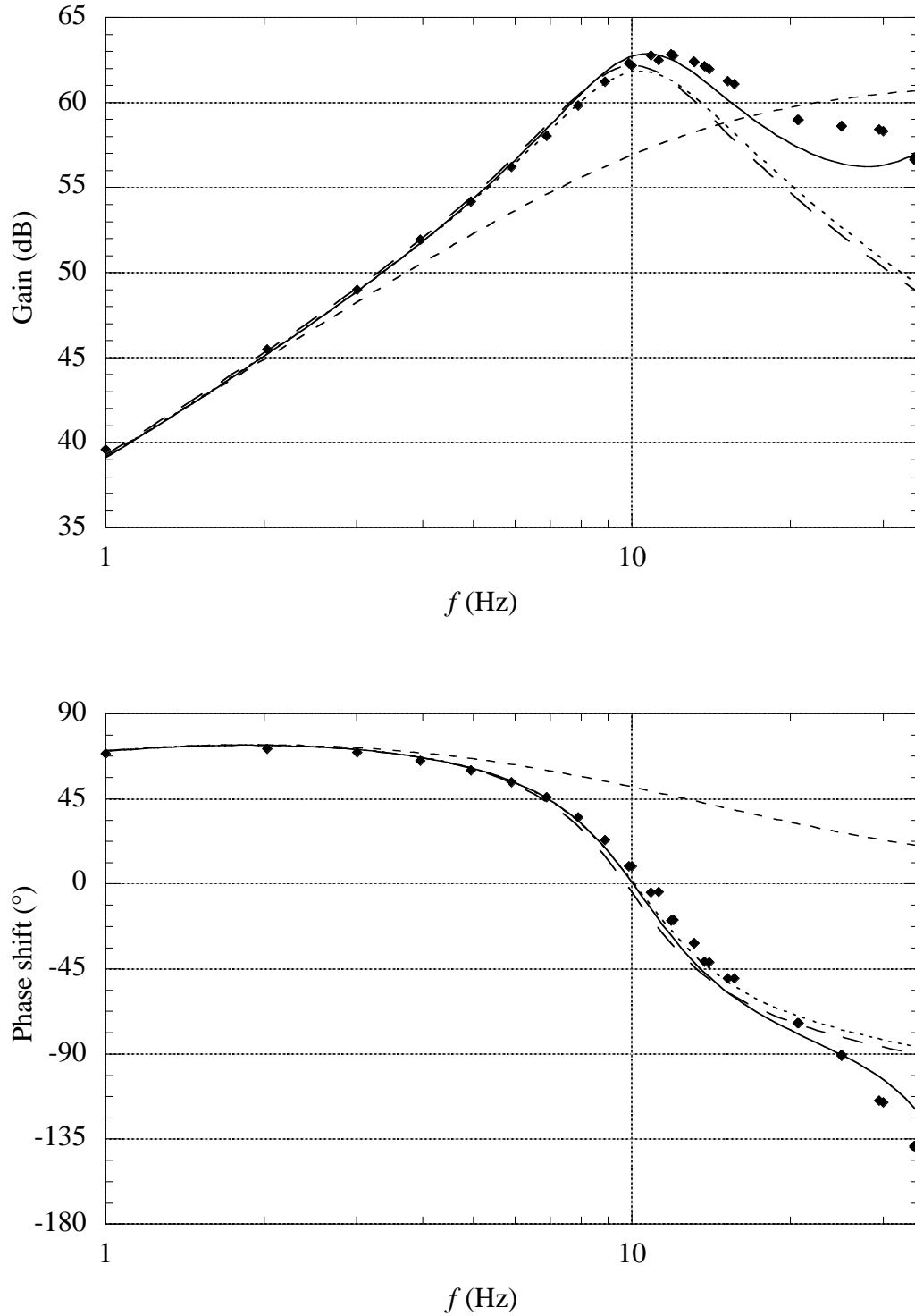
Figure 4.4.c. Measured and calculated gains and phase shifts of $\Delta P_e/\Delta\omega_s$. Dots are measured values and lines are values determined according to the different models. Park model (——), NST I (·········), LA (— — —) and ND (- - - - -).
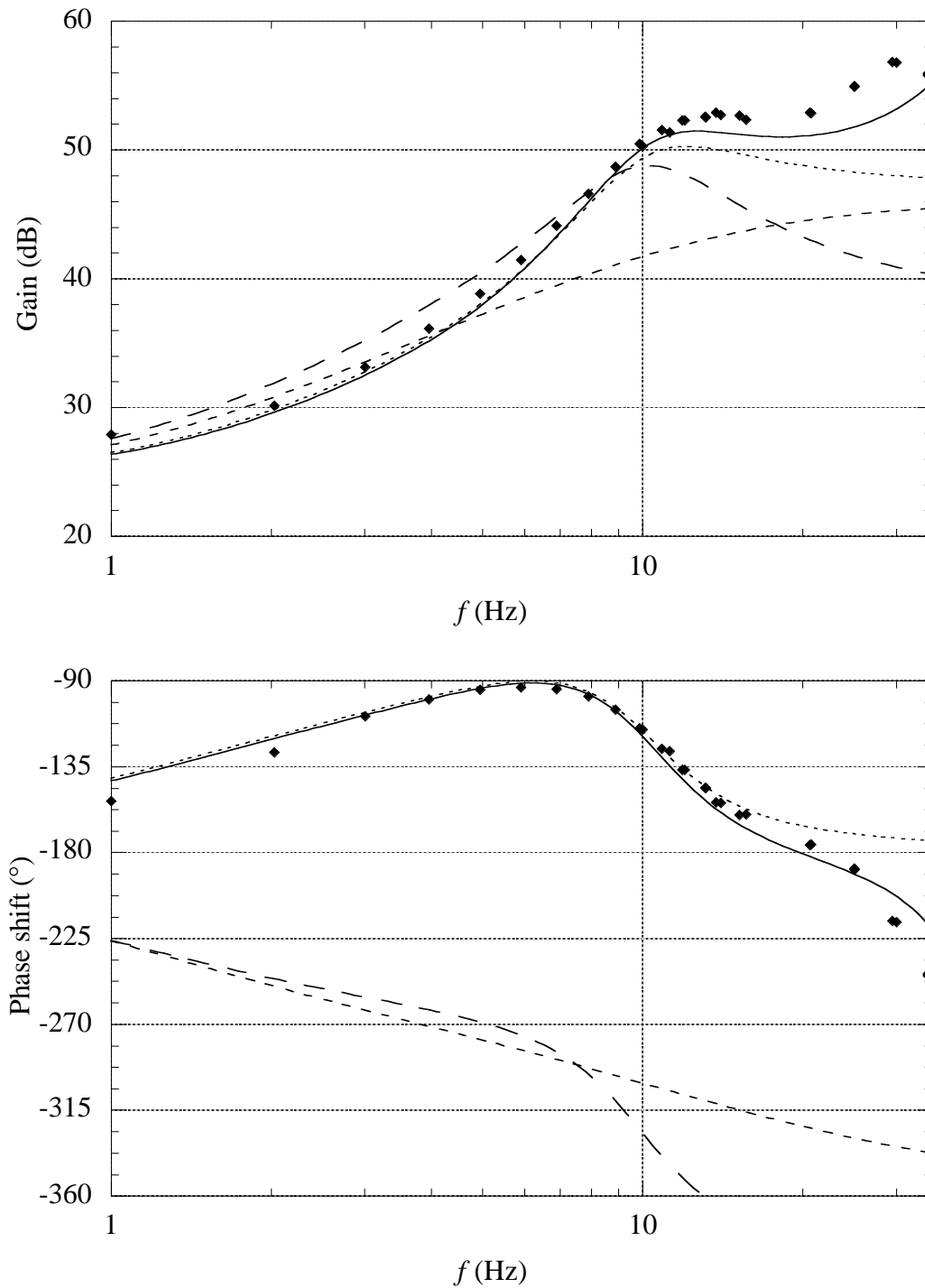
Figure 4.4.d.   Measured and calculated gains and phase shifts of ΔQ/Δω$_s$. Dots are measured values and lines are values determined according to the different models. Park model (——), NST I (··········), LA (— — —) and ND (- - - - -).
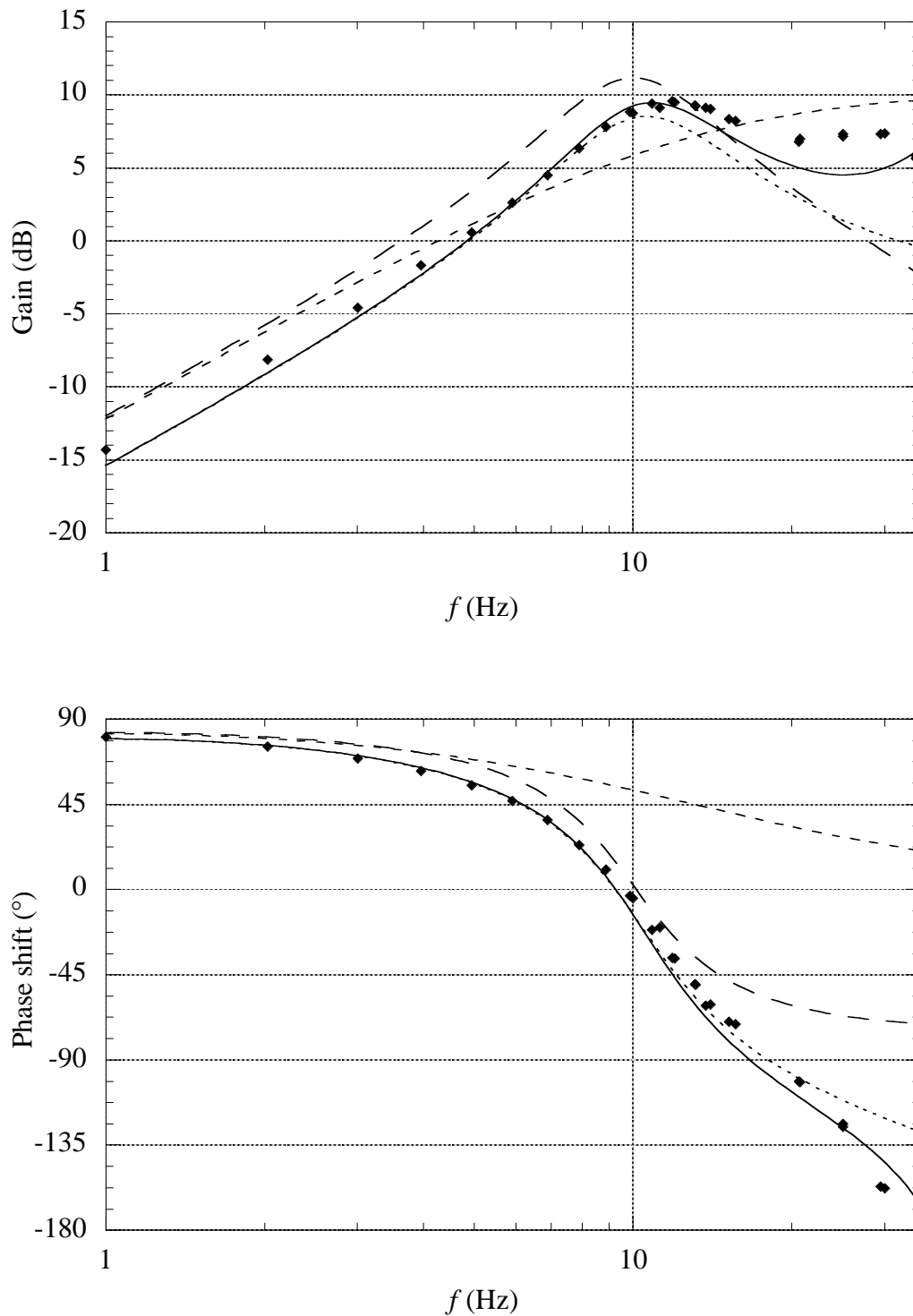
Figure 4.4.e.   Measured and calculated gains and phase shifts of $\Delta I_s/\Delta\omega_s$. Dots are measured values and lines are values determined according to the different models. Park model (——), NST I (··········), LA (— — —) and ND (- - - - -).

The measured responses to supply frequency perturbations agree well with those predicted by the Park model up to a perturbation frequency of 15 Hz. The predicted rotor speed response is somewhat higher than the measured one, for perturbations frequencies between 5 and 10 Hz, but the discrepancy is smaller than in the case where the response to torque perturbations was investigated.

At low frequencies, the different models predict similar induction machine responses, but at a frequency above a few Hz, the discrepancy between the first-order model and the Park model becomes significant. The approximation of an upper perturbation frequency of 3 Hz for the first-order model is useful also as an upper limit in determining the responses to supply frequency perturbations.

The NST I-model predicts the responses to supply frequency perturbations rather well. The discrepancy compared to the Park model grows as the perturbation frequency increases and reaches 10 % at the dominating eigenfrequency. However, the discrepancy is larger in the prediction of the reactive power and stator current responses.

The LA-model predicts similar rotor speed, electrodynamical torque and electric power responses as the NST I-model, while the stator current and reactive power responses are much less accurate.

The error values determined according to (4.1) are presented in Table 4.2. It can be observed that the linear NSR-model predicts similar rotor speed and electrodynamical torque responses to supply frequency perturbations as the LA-model, in fact, the error values are even lower for the NSR-model. Moreover, it can be seen that the NST III-model predicts the transfer function $\Delta\Omega_m/\Delta\omega_s$ excellently while the prediction of the other responses to the supply frequency perturbations using the NST III-model is less good. In Figure 4.5 the magnitudes of $\Delta T_e/\Delta\omega_s$ is presented for the Park model and the two NST-models.

Table 4.2. Error values of the simplified models.

	$\Delta T_e/\Delta\omega_s$	$\Delta\Omega_m/\Delta\omega_s$	$\Delta P_e/\Delta\omega_s$	$\Delta Q/\Delta\omega_s$	$\Delta I_s/\Delta\omega_s$
NST III-model	0.053	0.0027	0.051	0.056	0.047
NST I-model	0.019	0.019	0.021	0.033	0.020
NSR-model	0.027	0.027			
LA-model	0.036	0.036	0.040	0.92	0.36
ND-model	0.18	0.18	0.18	0.87	0.43
LD-model	0.18	0.18	0.22	0.82	0.34
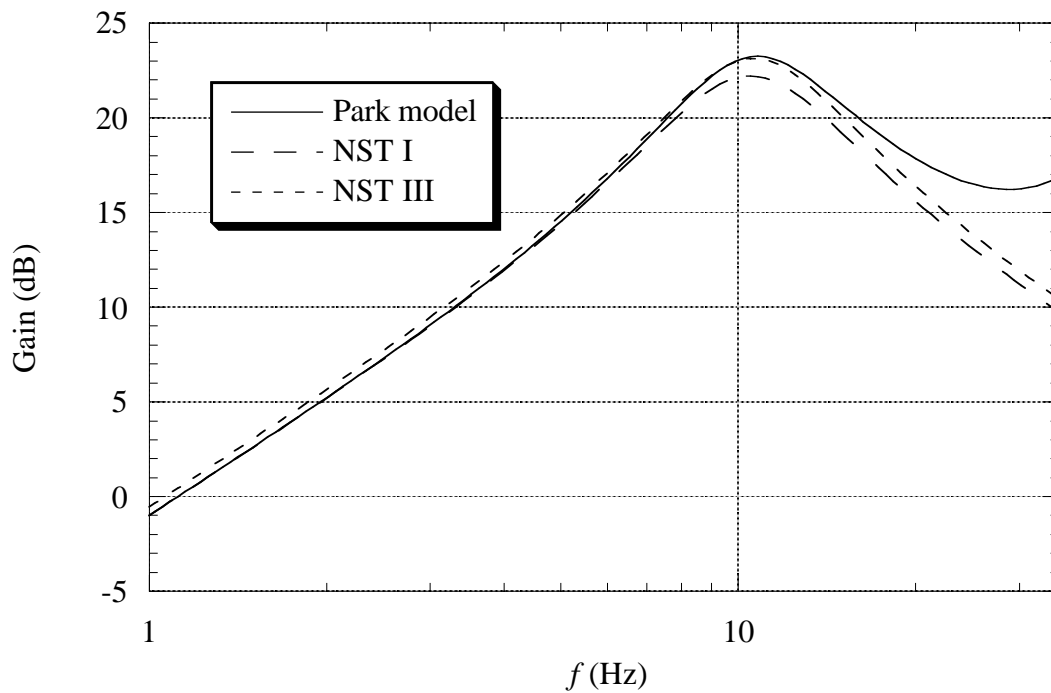
Figure 4.5. Calculated gain of $\Delta T_e/\Delta\omega_s$ for the Park model and the NST-models.

The NST III-model predicts an excellent electrodynamical torque response around the eigenfrequency but it predicts 6 % too high an electrodynamic torque response to perturbation frequencies below 7 Hz, which causes the large error value in Table 4.2.

4.3 Perturbations in the supply voltage magnitude

The responses to voltage magnitude perturbations depend on the steady-state shaft torque of the machine. In Figures 4.6.a-e and Figures 4.7.a-e the responses to voltage magnitude perturbations are presented at generator and motor operation, respectively. In the cases where the effect of saturation and iron losses are of importance, results calculated taking these effects into account are also presented.
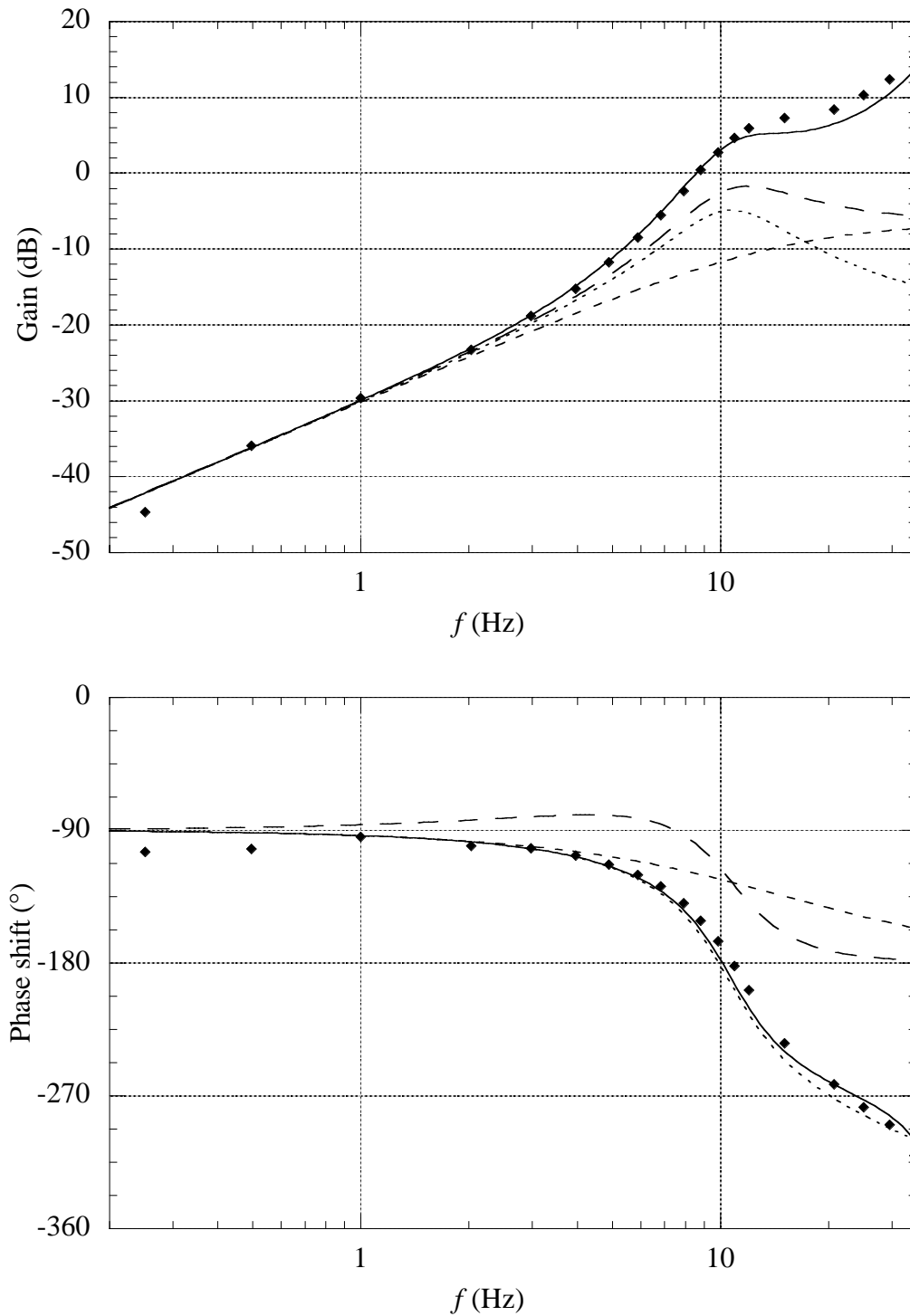
Figure 4.6.a. *Measured and calculated gains and phase shifts of $\Delta T_e/\Delta U$. Dots are measured values and lines are values determined according to the different models. Park model (———), NST I (·········), LA (— — —) and ND (- - - - -).*
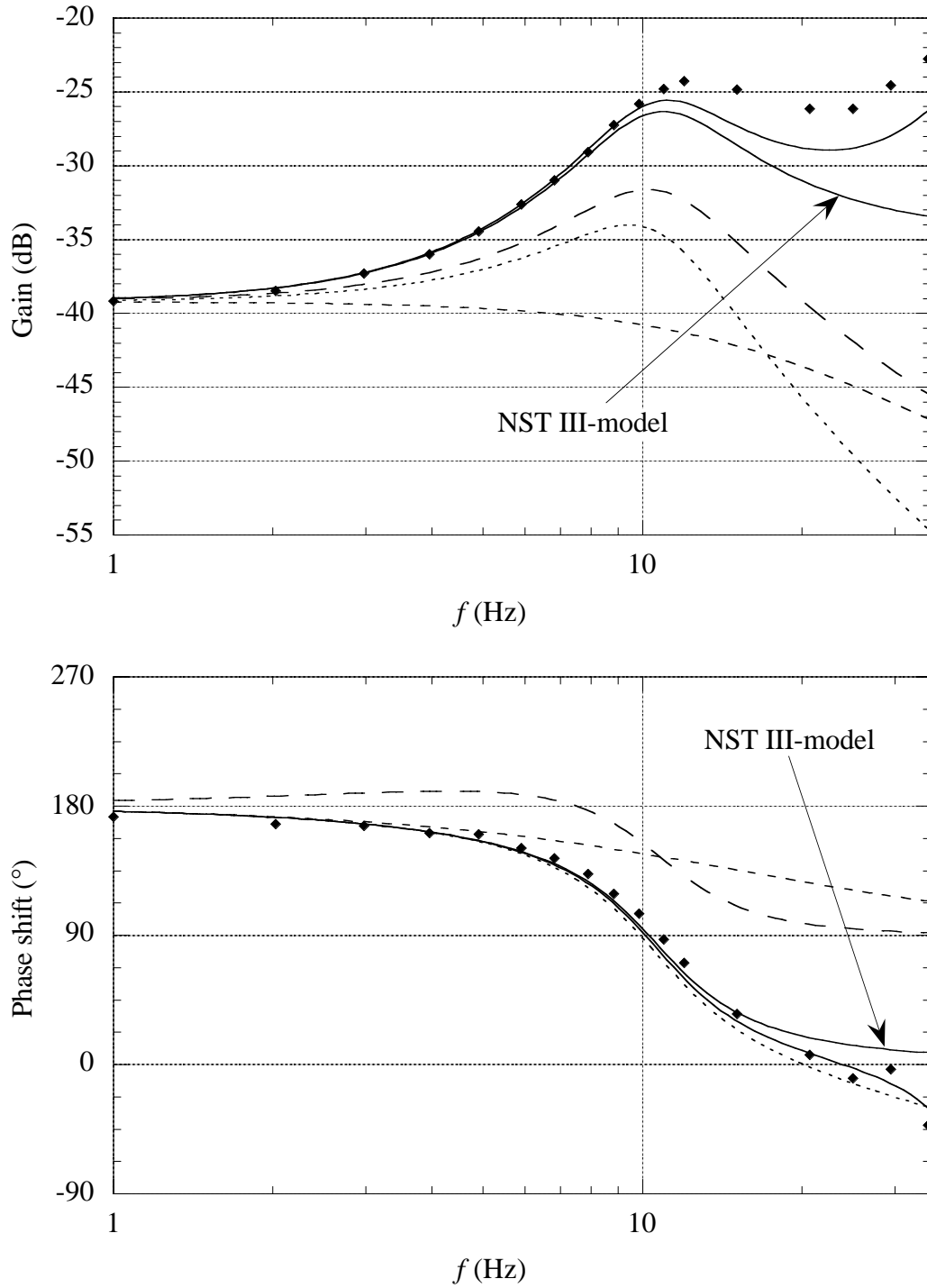
Figure 4.6.b. Measured and calculated gains and phase shifts of ΔΩ$_m$/ΔU. Dots are measured values and lines are values determined according to the different models. Park model (——), NST III (——), NST I (··········), LA (— — —) and ND (- - - - -).

Figure 4.6.c. Measured and calculated gains and phase shifts of ΔP$_e$/ΔU. Dots are measured values and lines are values determined according to the different models. Park model (⎯⎯), Two-axis model with saturation and iron losses considered (⎯⎯), NST I (·········), LA (— — —) and ND (- - - - -).
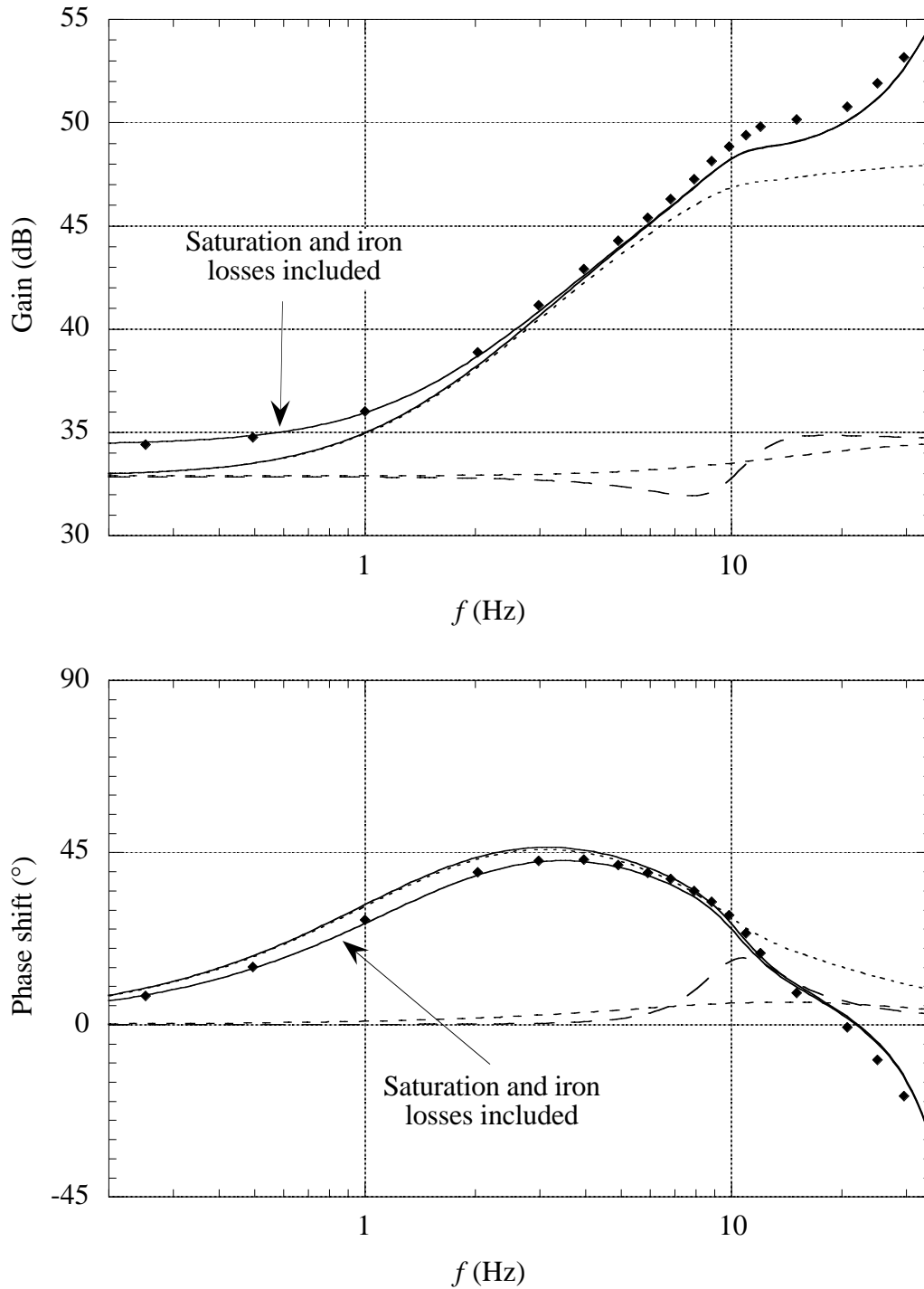
Figure 4.6.d. Measured and calculated gains and phase shifts of ΔQ/ΔU. Dots are measured values and lines are values determined according to the different models. Park model (——), Two-axis model with saturation and iron losses considered (——), NST I (··········), LA (— — —) and ND (- - - - -).
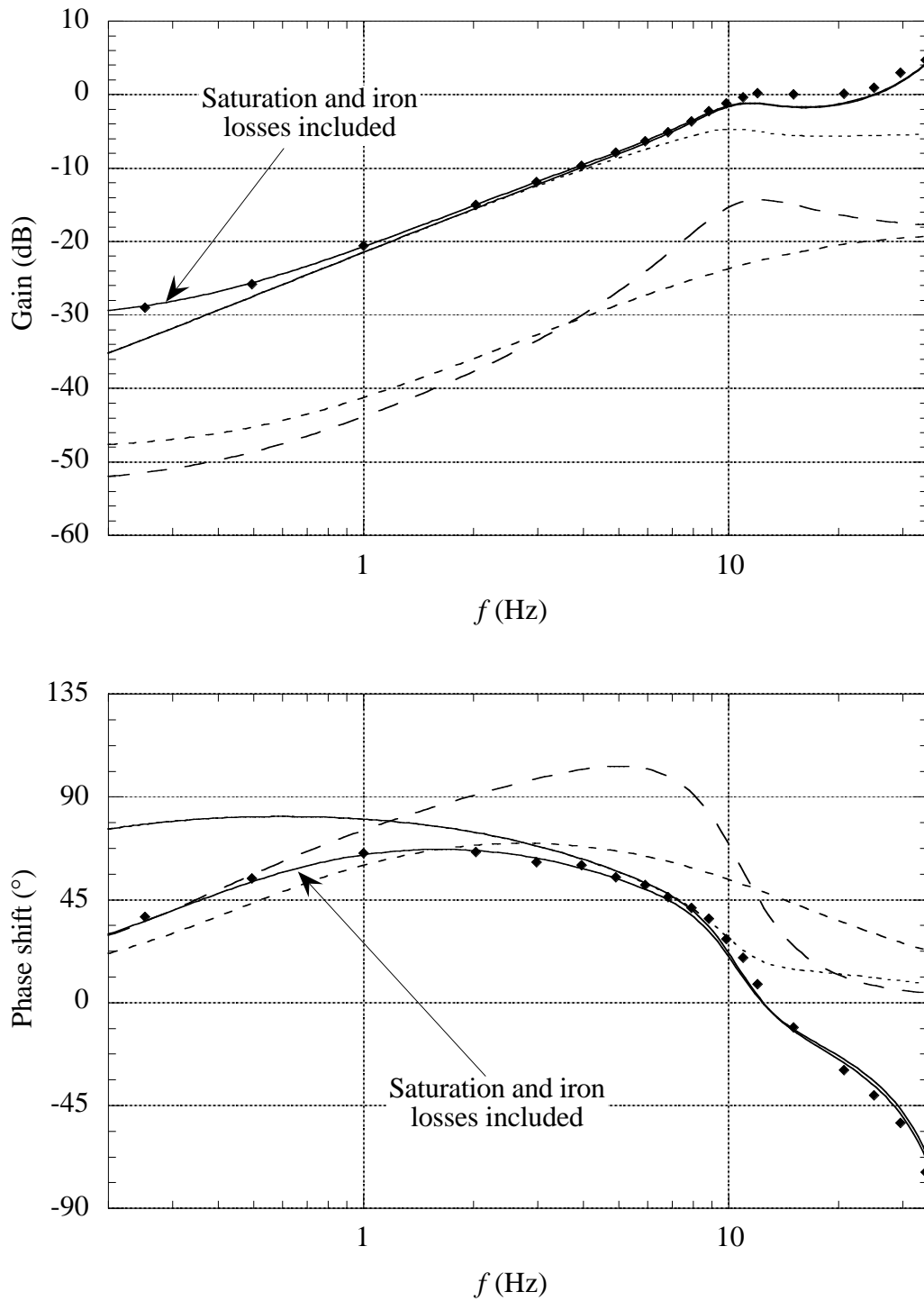
Figure 4.6.e. Measured and calculated gains and phase shifts of $\Delta I_S/\Delta U$. Dots are measured values and lines are values determined according to the different models. Park model (——), Two-axis model with saturation and iron losses considered (——), NST I (·········), LA (— — —) and ND (- - - - -).
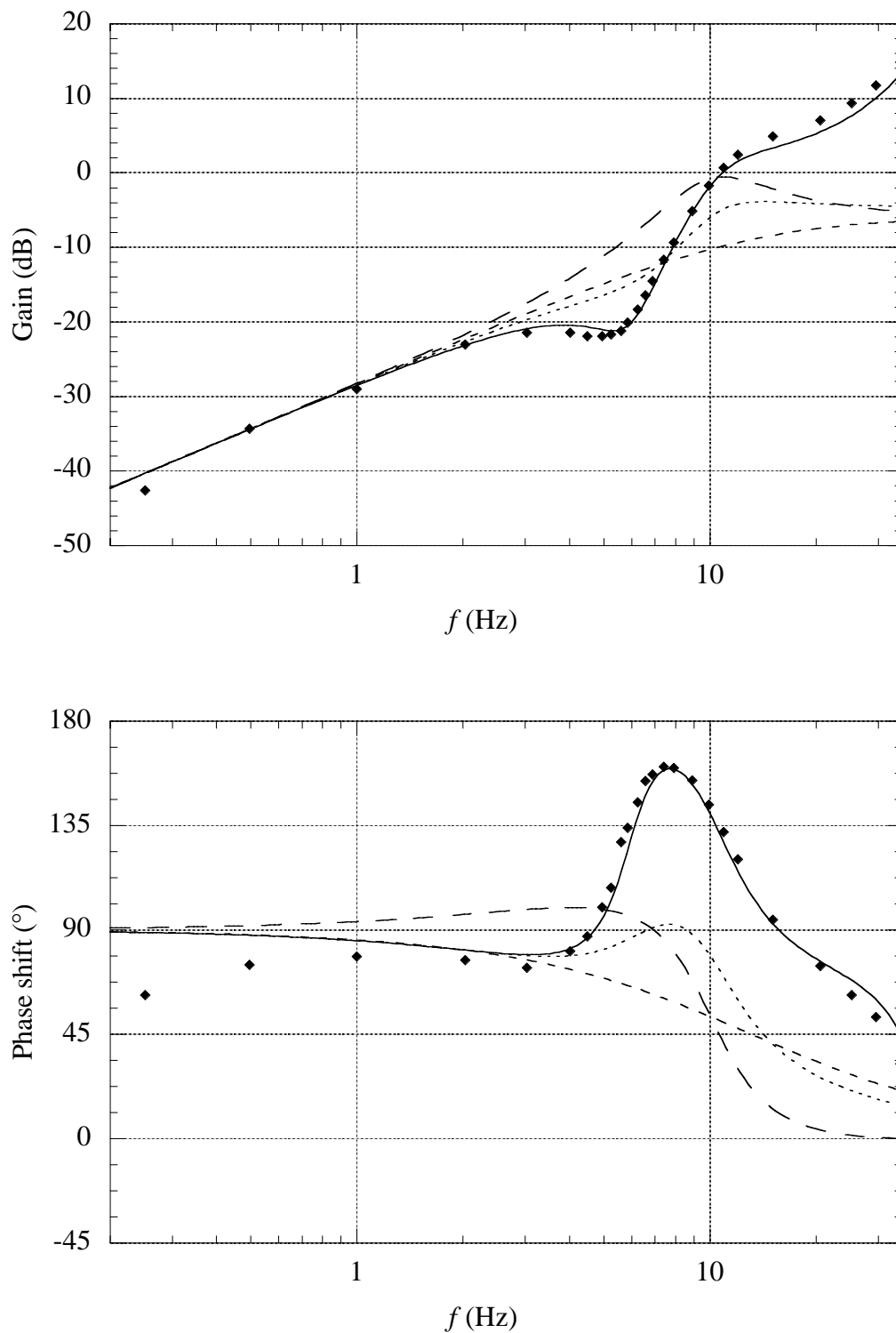
Figure 4.7.a. *Measured and calculated gains and phase shifts of $\Delta T_e/\Delta U$. Dots are measured values and lines are values determined according to the different models. Park model (——), NST I (··········), LA (— — —) and ND (- - - - -).*
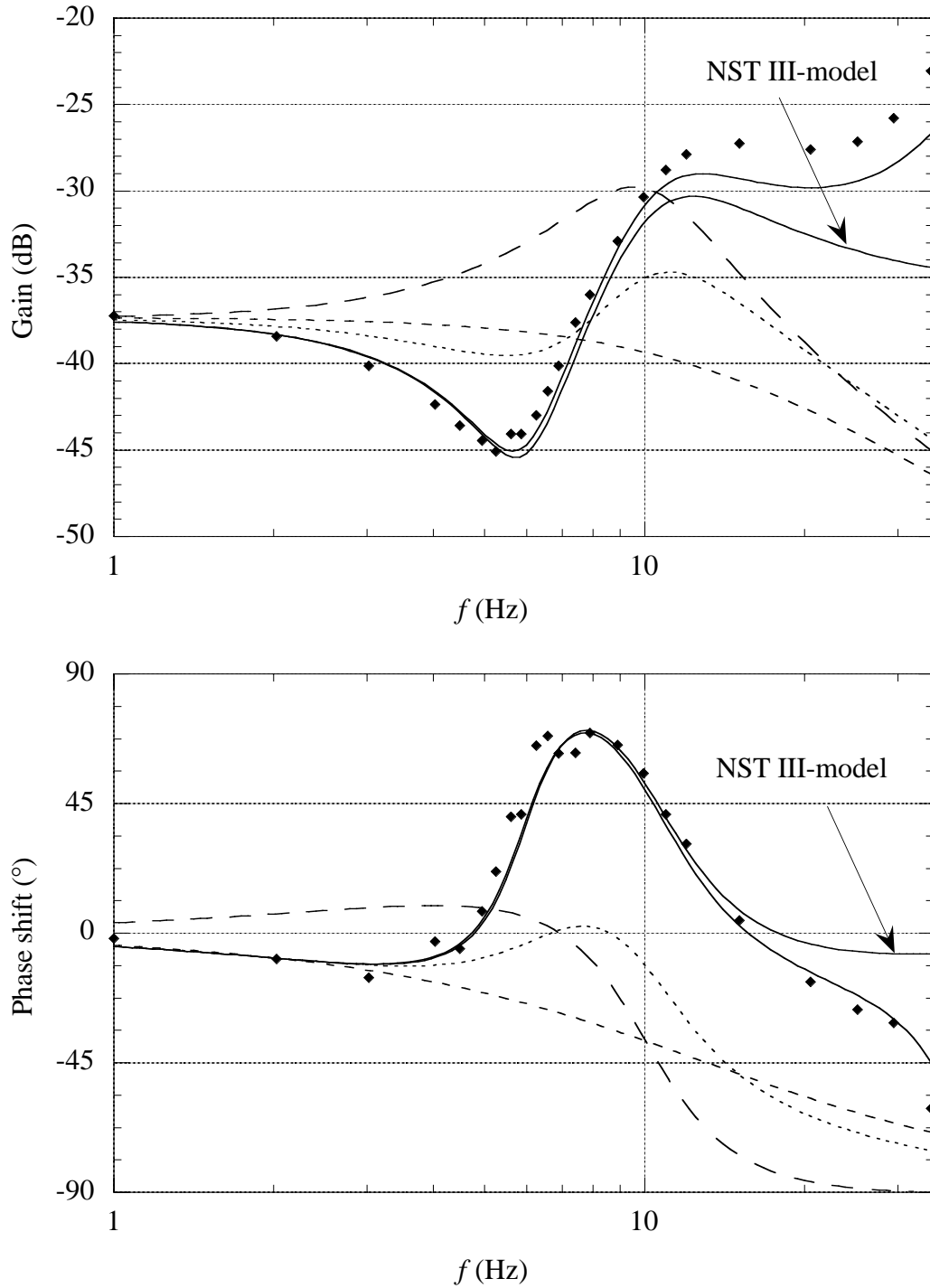
Figure 4.7.b. Measured and calculated gains and phase shifts of $\Delta\Omega_m/\Delta U$. Dots are measured values and lines are values determined according to the different models. Park model (——), NST III (——), NST I (·········), LA (— — —) and ND (- - - - -).
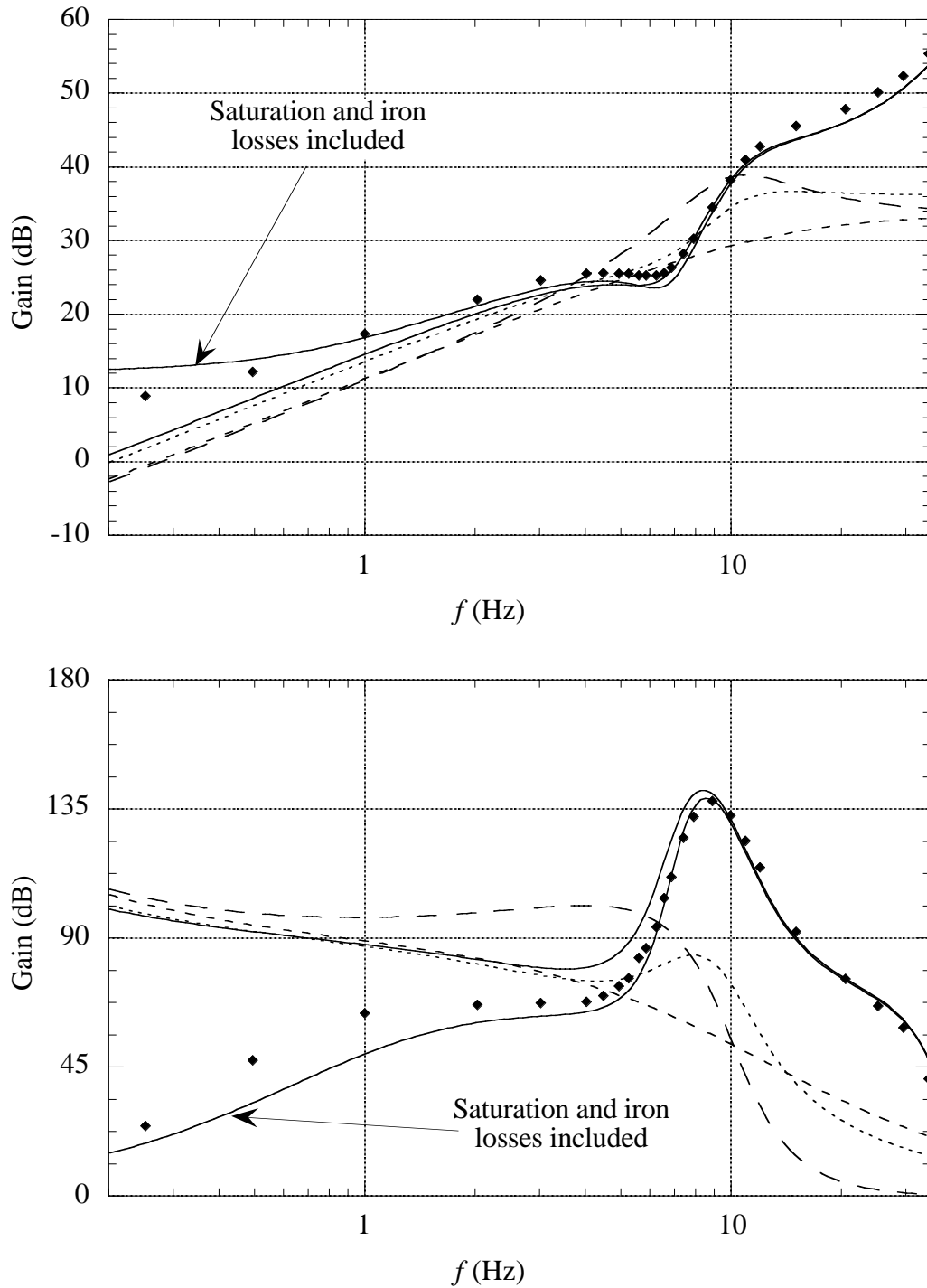
Figure 4.7.c. Measured and calculated gains and phase shifts of ΔP$_e$/ΔU. Dots are measured values and lines are values determined according to the different models. Park model (——), Two-axis model with saturation and iron losses considered (——), NST I (·········), LA (— — —) and ND (- - - - -).
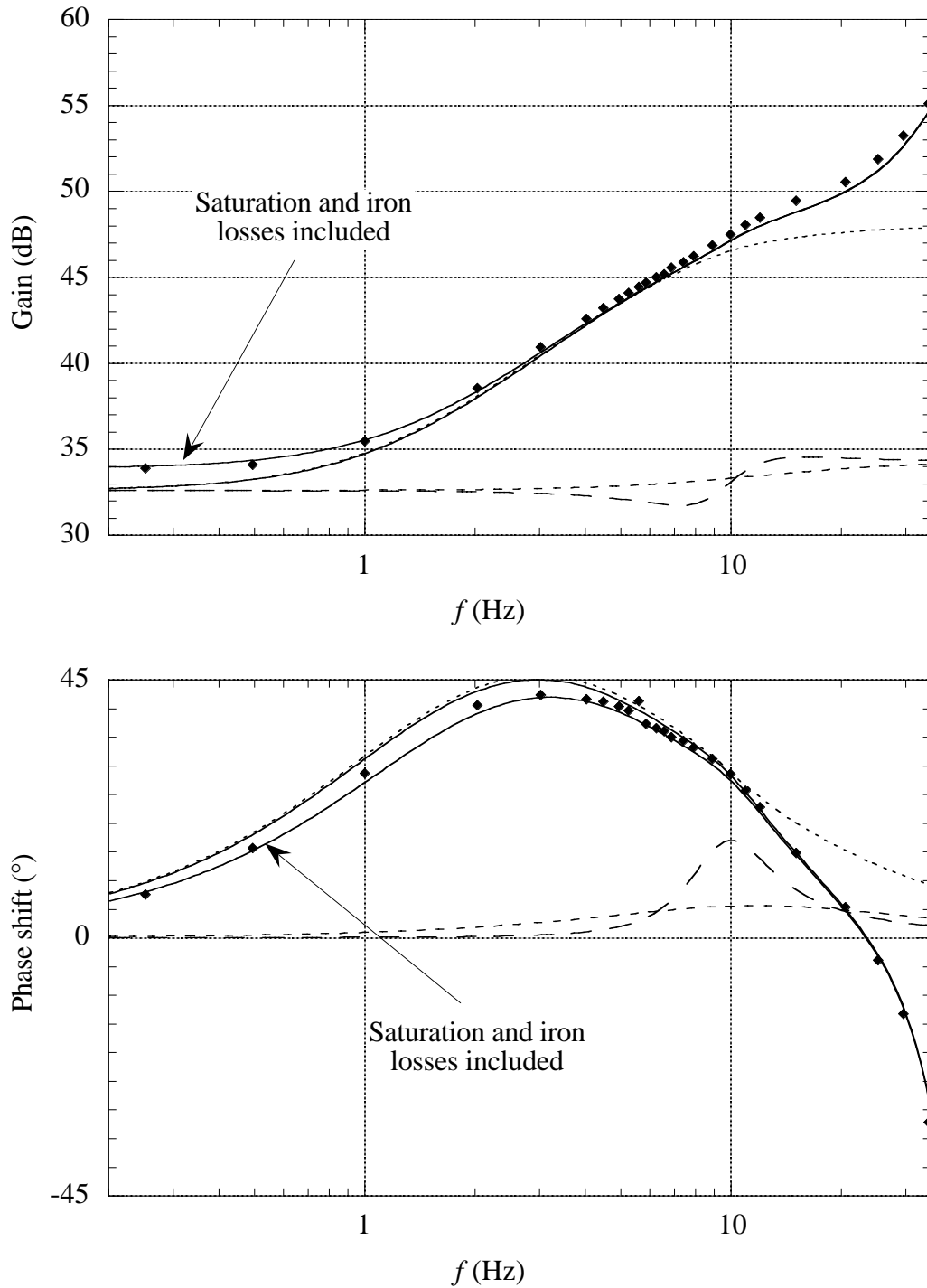
Figure 4.7.d. Measured and calculated gains and phase shifts of ΔQ/ΔU. Dots are measured values and lines are values determined according to the different models. Park model (——), Two-axis model with saturation and iron losses considered (——), NST I (·········), LA (— — —) and ND (- - - - -).
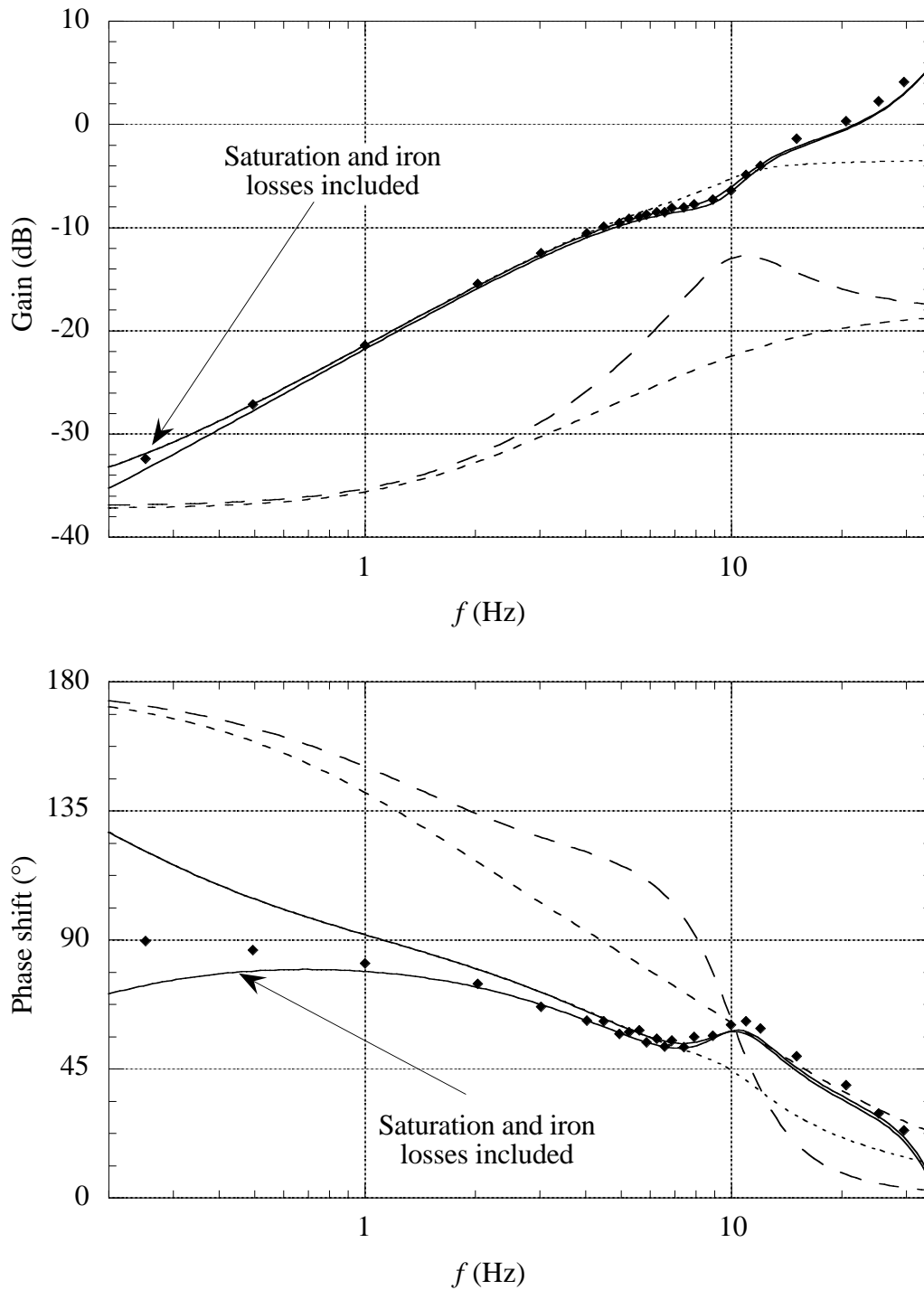
Figure 4.7.e.   Measured and calculated gains and phase shifts of $\Delta I_S/\Delta U$. Dots are measured values and lines are values determined according to the different models. Park model (———), Two-axis model with saturation and iron losses considered (———), NST I (··········), LA (— — —) and ND (- - - - -).

61

The standard Park model predicts the rotor speed and electrodynamical torque responses rather well but it is necessary to consider the iron losses when the electric power and stator current responses are determined.

The error values determined according to (4.1) are presented in Table 4.3. Since the performance of the models varies with the operating point, when the machine is subjected to voltage magnitude perturbations, the average values of the error at motor and generator operation are presented.

Table 4.3. Error values of the simplified models.

	$\Delta T_e/\Delta U$	$\Delta \Omega_m/\Delta U$	$\Delta P_e/\Delta U$	$\Delta Q/\Delta U$	$\Delta I_s/\Delta U$
NST III-model	1.3	0.020	2.2	0.038	0.15
NST I-model	0.21	0.21	0.36	0.027	0.053
LA-model	0.46	0.46	0.97	0.52	0.86
ND-model	0.30	0.30	0.81	0.51	0.86

The ND-model predicts the rotor speed and electrodynamical torque responses rather well up to a perturbation frequency of about 2 Hz. The upper frequency limit below which the first-order model can predict accurate responses thus is somewhat lower in the voltage magnitude perturbation case than in the torque or supply frequency perturbation case. The LA-model is approximately as useful as a first-order model in predicting the responses to voltage magnitude perturbations.

The NST I-model is not much better than the LA-model in determining the rotor speed, electrodynamical torque and electric power responses to voltage magnitude perturbations. However, the stator current and reactive power responses predicted by the NST I-model are much better compared to the ones obtained using the LA-model. The NST III-model predicts an excellent rotor speed response while it do not predict the electrodynamical torque, electric power and stator current responses as well as the NST I-model. This fact demonstrates that it is dangerous to validate a model based on only one transfer function as Wasynczuk et al. (1985) did. In Figure 4.8 the magnitudes of $\Delta T_e/\Delta U$ is presented in motor operation for the Park model and the two NST models.

Again, the observation can be made that the values obtained using the NST III-model differ from those obtained using the Park model for very low perturbation frequencies, which causes the large error in Table 4.3. The reason for this error is the fact that the derivatives of the input signals are needed to predict a correct answer.
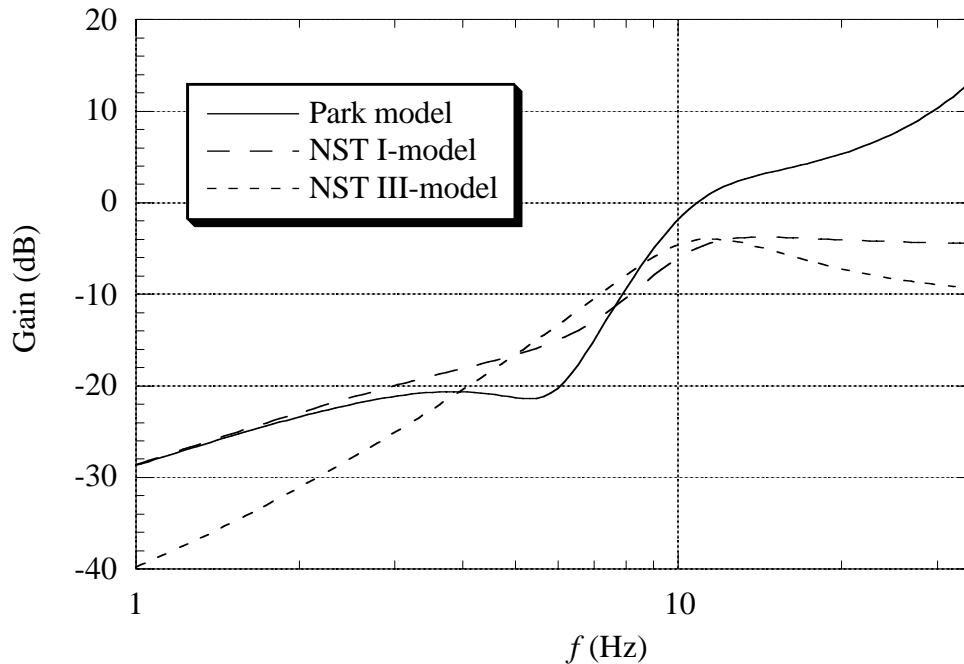
Figure 4.8. Calculated gain of $\Delta T_e/\Delta U$ for the Park model and the NST-models.

4.4 Response of a two-machine group

There are two methods of reducing the order of a multi-machine system: reduction of induction machine groups to single-unit equivalents, i.e. aggregate models, and simplified representation of each machine. If the interior signals are of no interest, the model order of a multi-machine system can be reduced by replacing the machines with one equivalent machine, i.e. an aggregate model. However, if the interior signals are of interest, the approach of simplified representation of each machine must be used.

When the response of a two-machine group was investigated, an additional converter-fed dc machine-induction machine set-up was used, identical to the one described in Chapter 3. The two induction machines were connected to the forced-commutated converter via a resistance, $R_1 = 0.72$ Ω, and an inductance, $L_1 = 2$ mH. Figure 4.9 shows the set-up consisting of the line impedances and the induction machines.
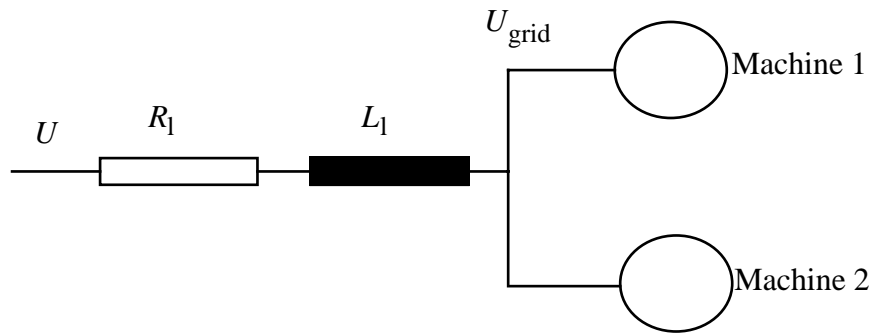
Figure 4.9. The investigated two-machine system.

The two-machine system was modelled in the following way: The two machines, represented by Park models/NST-models/LA-models/ND-models were connected to a local grid, which was connected to an infinite bus via a line inductance and resistance. The dynamic influence of the line inductance was taken into account. In power system analysis programs, the dynamic influence of the line inductances is usually neglected, i.e. the line impedance current derivatives are neglected.

If the derivatives of the line impedance currents were neglected, the maximum magnitudes of the transfer functions were typically reduced by 10 % for the two-machine systems based on the Park models and NST I-models. For the LA-model and ND-model, the neglection of the derivatives had a very small influence. Figure 4.10 presents the calculated magnitudes of the transfer function $\Delta T_{e1}/\Delta T_{dcm1}$ using the Park model-based two-machine system with and without the dynamics of the line impedance incorporated.

The line resistance used here is 0.72 Ω, i.e. 0.16 p.u. if 288 V and 64 A are used as the base voltage and base current, respectively. If the machines operate at rated current, the losses in the line resistance will be 3 kW, i.e., 10 % of the rated power of the two machines. The line inductance was 2 mH (j0.55Ω). This gives a short-circuit capacity of 90 kVA at the machines, i.e., only three times the rating of the two machines. This was done in order to obtain a strong interaction between the induction machines.
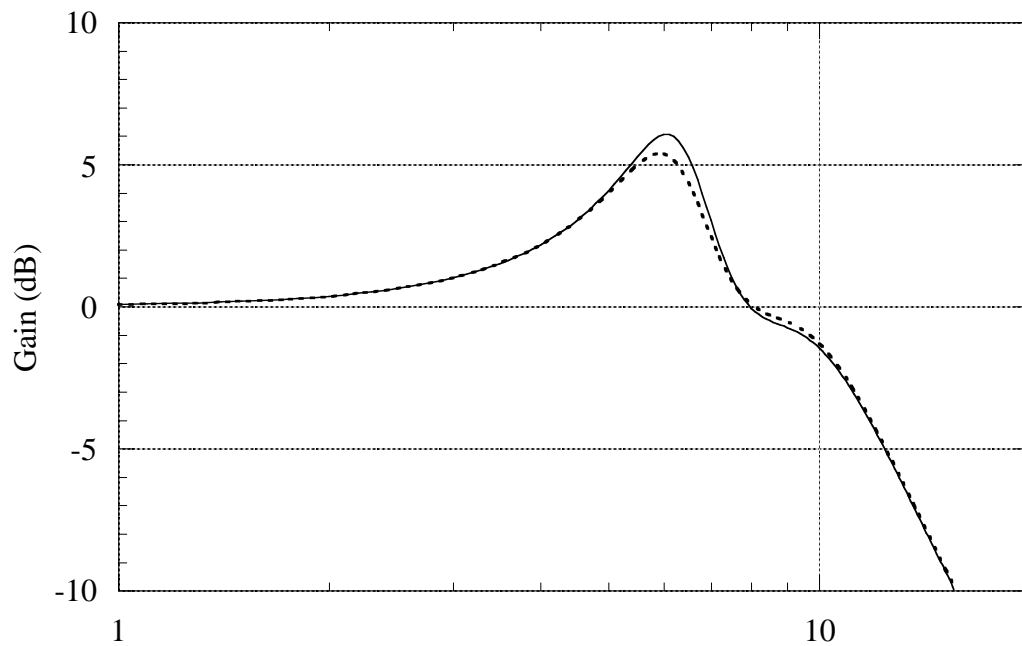
Figure 4.10. Calculated gains of $\Delta T_{e1}/\Delta T_{dcm1}$. Solid line represents the calculations performed taking the dynamic influence of the line impedance into account and the dashed curve represents the calculations where the dynamic influence of the line impedance has been ignored.

The high value of the line impedance led to an unexpected problem: the simulation of the two-machine system using the NST-models to represent the machines did not work unless the line impedance was reduced by 30 %. However, a model producing very similar results was used instead: A new sixth-order model was derived starting from the equations of the whole two-machine system which is a tenth-order system. The procedure suggested by Wasynczuk et al. (1985) was then applied to this system. All four stator flux linkage transients were neglected resulting in a sixth-order model. This model and a two-machine model with single-machine NST-models produced very similar responses when a system with only one third of the used line impedance was investigated.

In Figures 4.11-4.13, the responses predicted by the different models are presented together with the measured ones for some selected responses to torque, supply frequency and voltage magnitude perturbations.

Machine 1 is operating as motor and Machine 2 is operating as generator, loaded and driven by a shaft torque of 35 Nm. A shaft torque of 35 Nm at the used voltage level and supply frequency corresponds to a slip of approximately one third of the rated value.

65

4.4.1 Torque perturbation

Figures 4.11.a-c present the rotor speed response $(\Delta\Omega_{m1})$, the electrodynamical torque response (ΔT_{e1}) and the reactive power response (ΔQ_1) of Machine 1 to perturbations in the torque (ΔT_{dcm2}) of the dc machine connected to Machine 2.
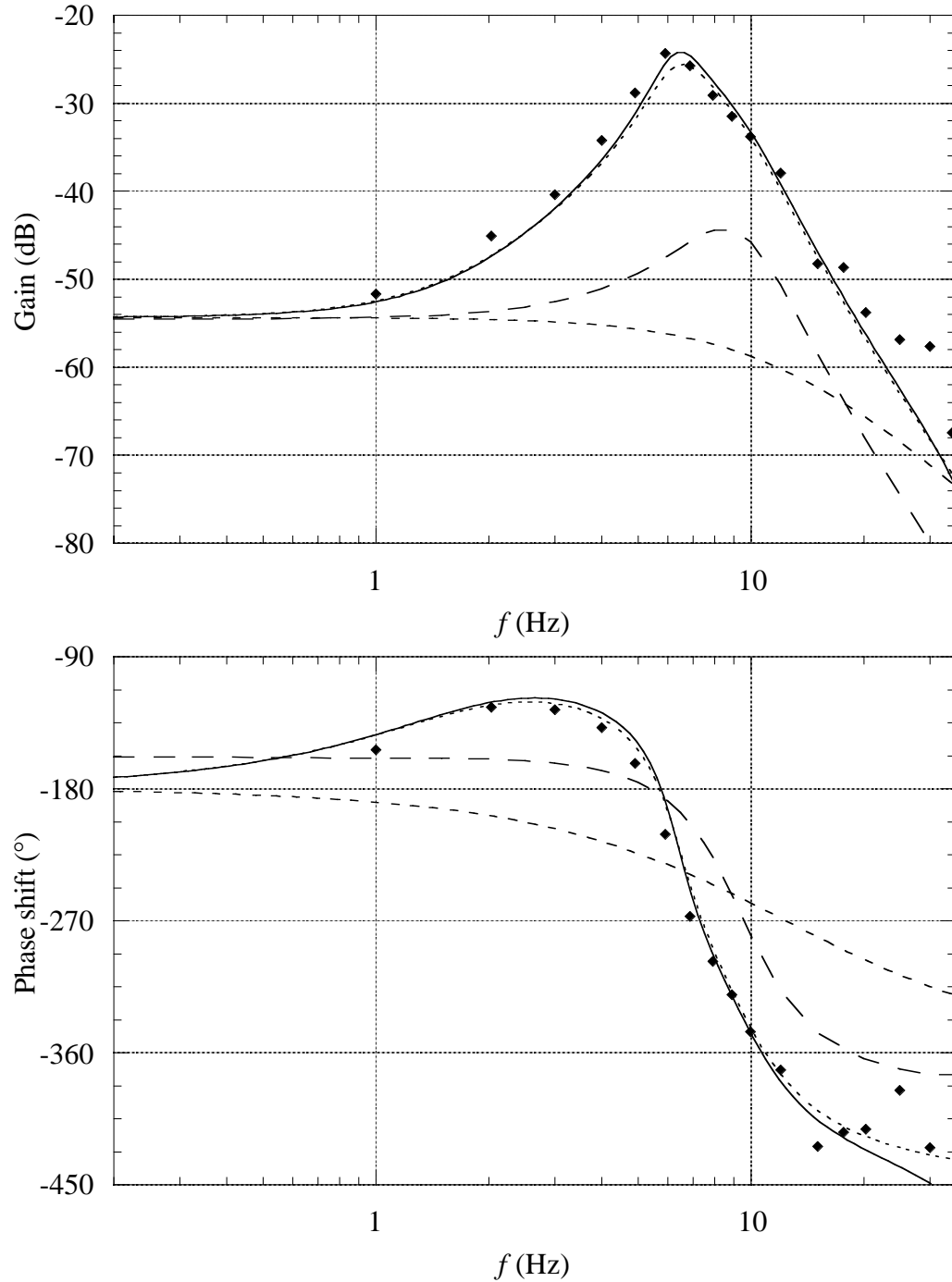
Figure 4.11.a. Measured and calculated gains and phase shifts of $\Delta\Omega_{m1}/\Delta T_{dcm2}$. Dots are measured values and lines are values determined according to the different models. Park model (——), NST I (··········), LA (— — —) and ND (- - - - -).
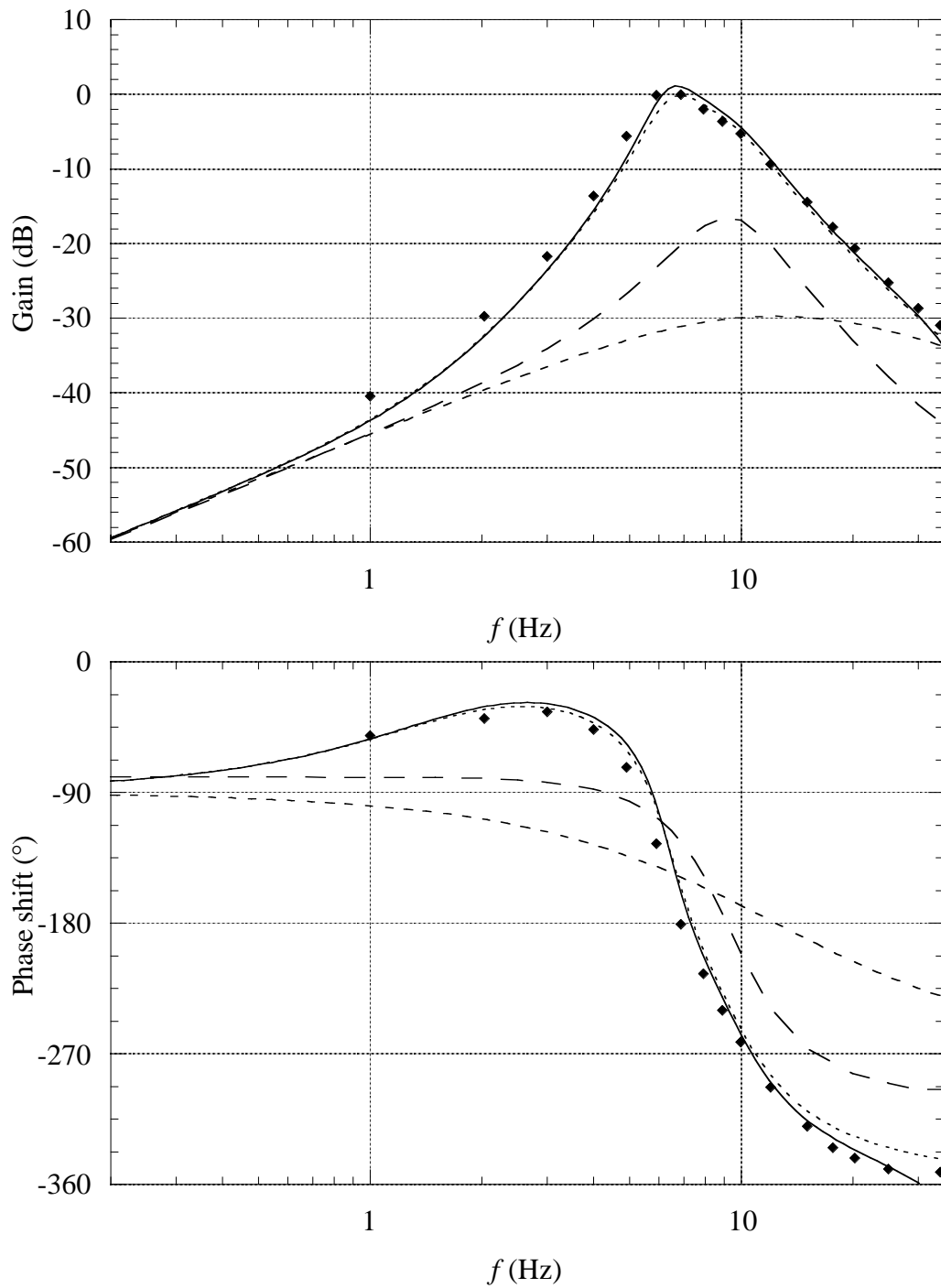
Figure 4.11.b. Measured and calculated gains and phase shifts of $\Delta T_{e1}/\Delta T_{dcm2}$. Dots are measured values and lines are values determined according to the different models. Park model (——), NST I (·········), LA (— — —) and ND (- - - - -).
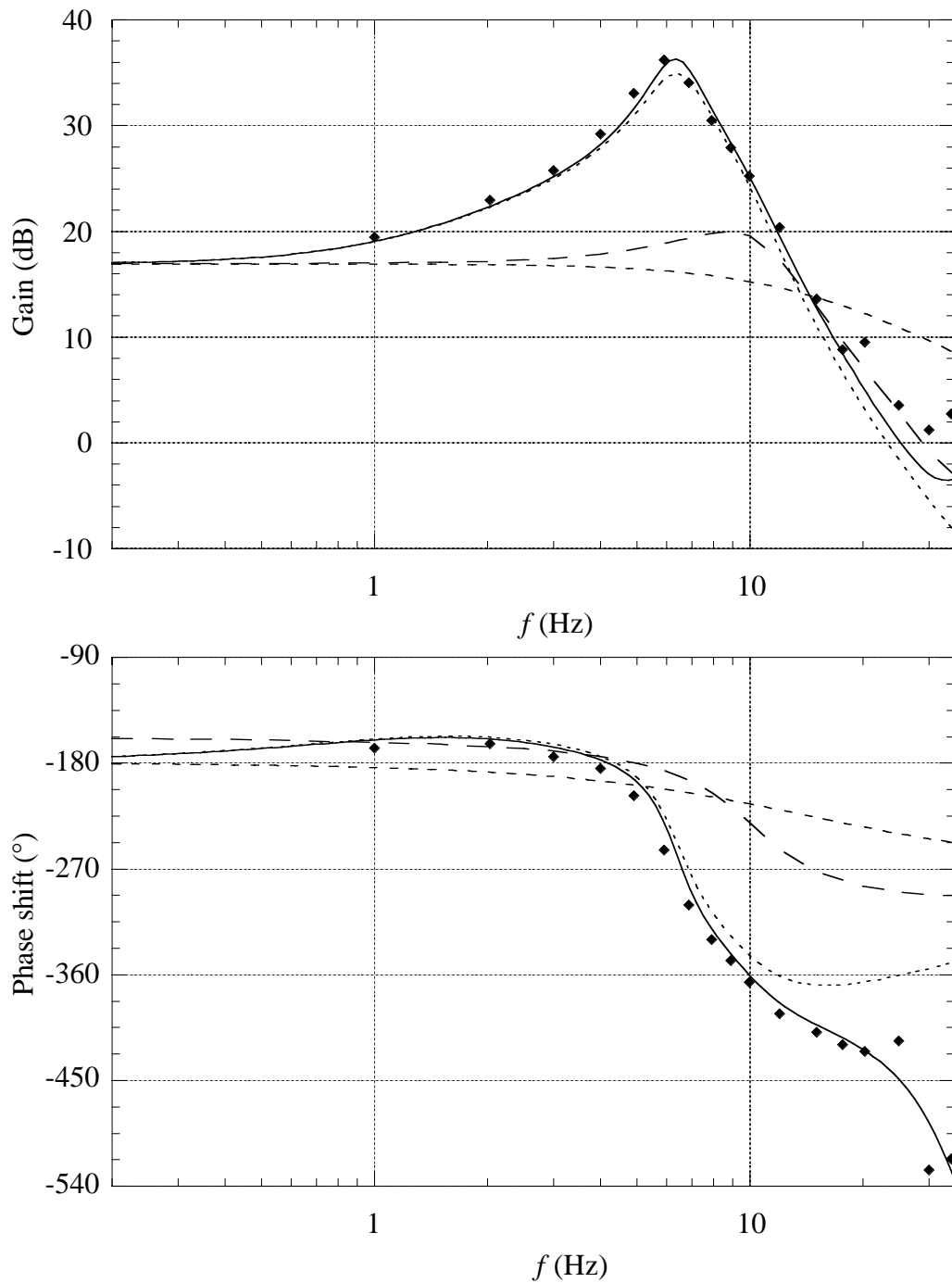
Figure 4.11.c. Measured and calculated gains and phase shifts of $\Delta Q_1/\Delta T_{dcm2}$. Dots are measured values and lines are values determined according to the different models. Park model (——), NST I (··········), LA (— — —) and ND (- - - - -).

The values determined using the Park model coincide well with the measured ones. The NST-model predicts similar results as the Park model. The LA-model and the ND-model can be used to predict the induction machine responses to shaft torque perturbations for perturbation frequencies below 1-2 Hz.

4.4.2 Supply frequency perturbation

Figures 4.12.a-c present the rotor speed response of Machine 1 ($\Delta\Omega_{m1}$), the electrodynamical torque response of Machine 2 (ΔT_{e2}) and the active power response of machine two (ΔP_2) to perturbations in the supply frequency ($\Delta\omega_s$).
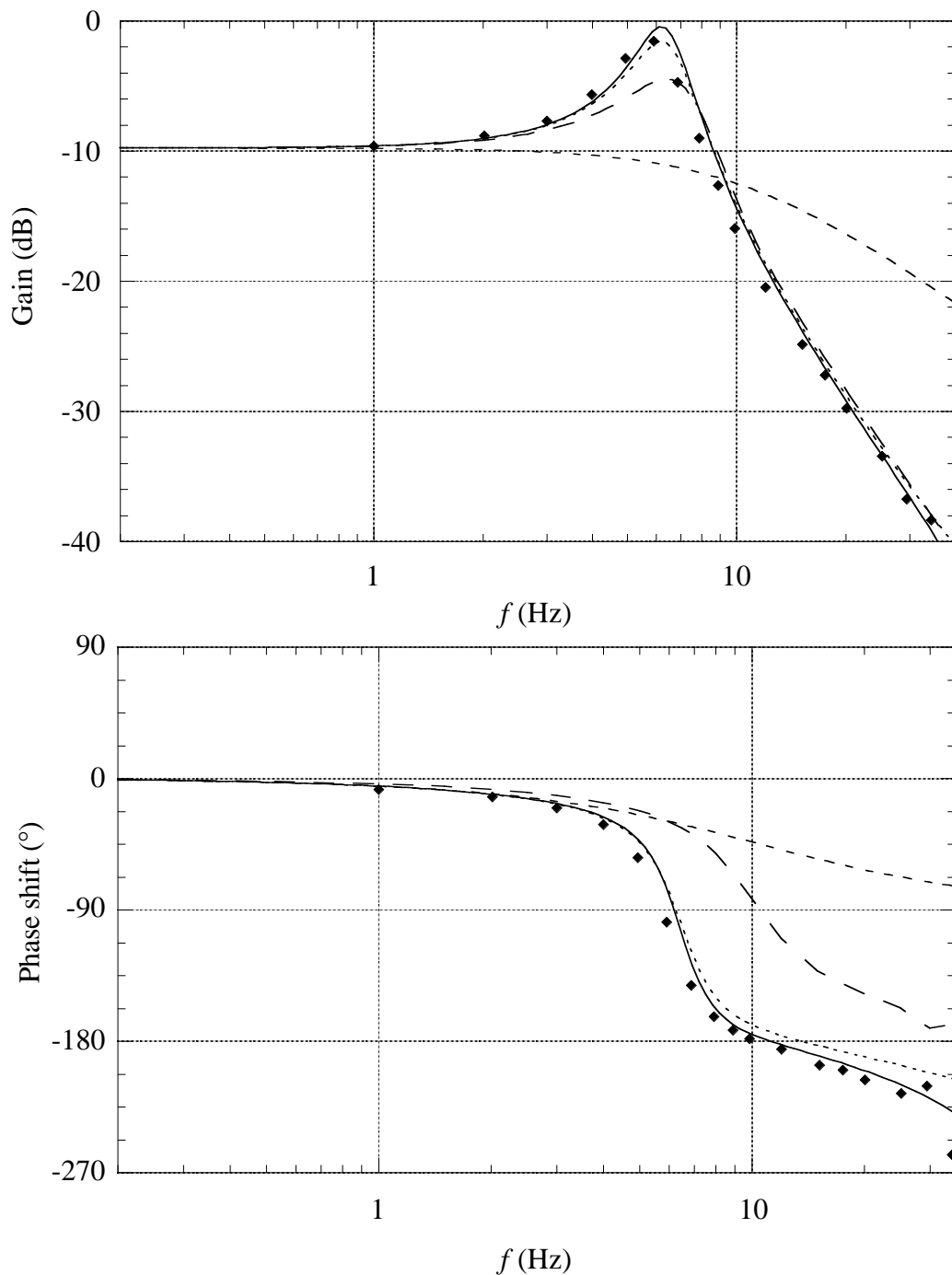
Figure 4.12.a. Measured and calculated gains and phase shifts of $\Delta\Omega_{m1}/\Delta\omega_s$. Dots are measured values and lines are values determined according to the different models. Park model (——), NST I (·········), LA (— — —) and ND (- - - - -).
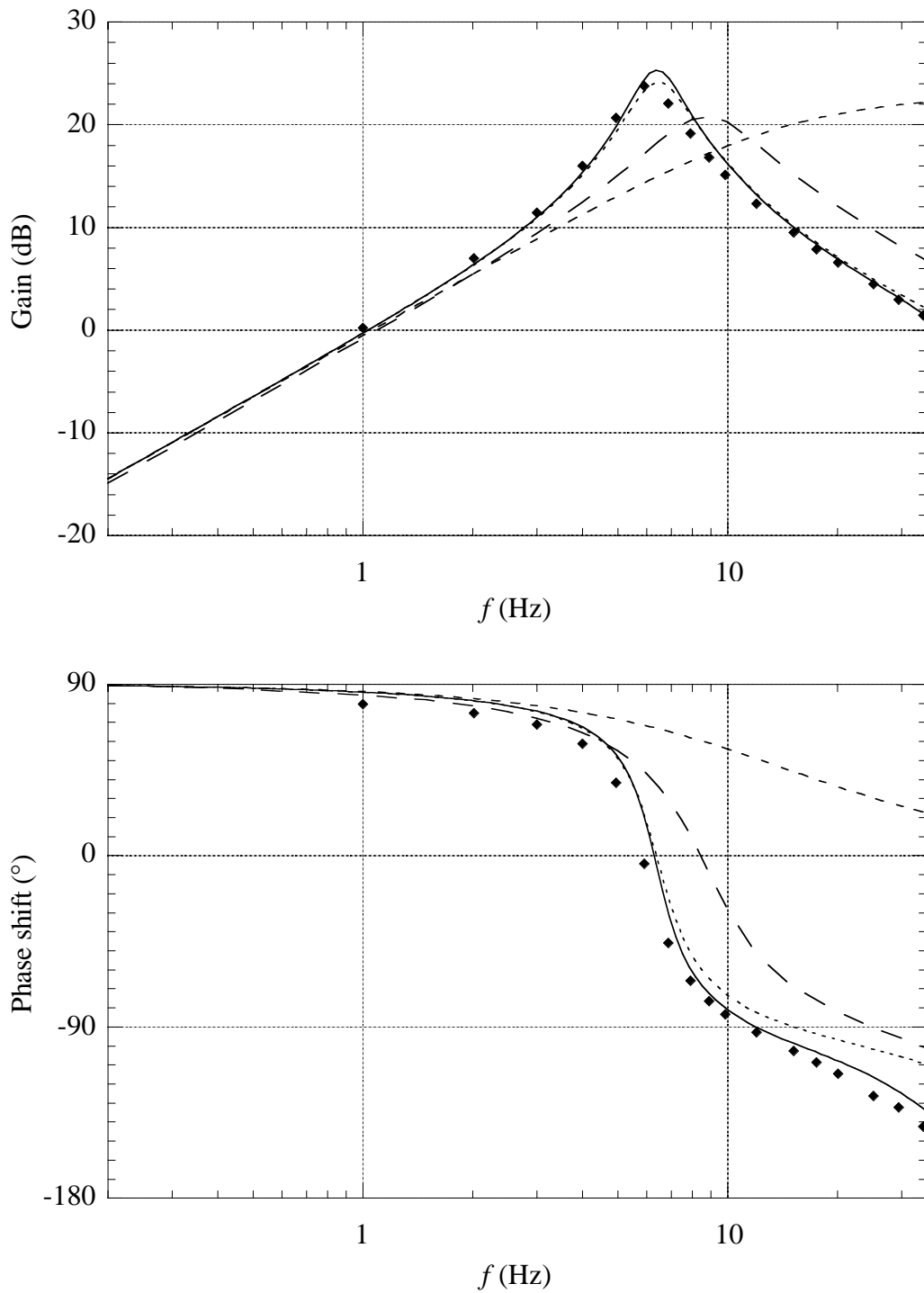
Figure 4.12.b. Measured and calculated gains and phase shifts of $\Delta T_{e2}/\Delta \omega_s$. Dots are measured values and lines are values determined according to the different models. Park model (——), NST I (··········), LA (— — —) and ND (- - - - -).
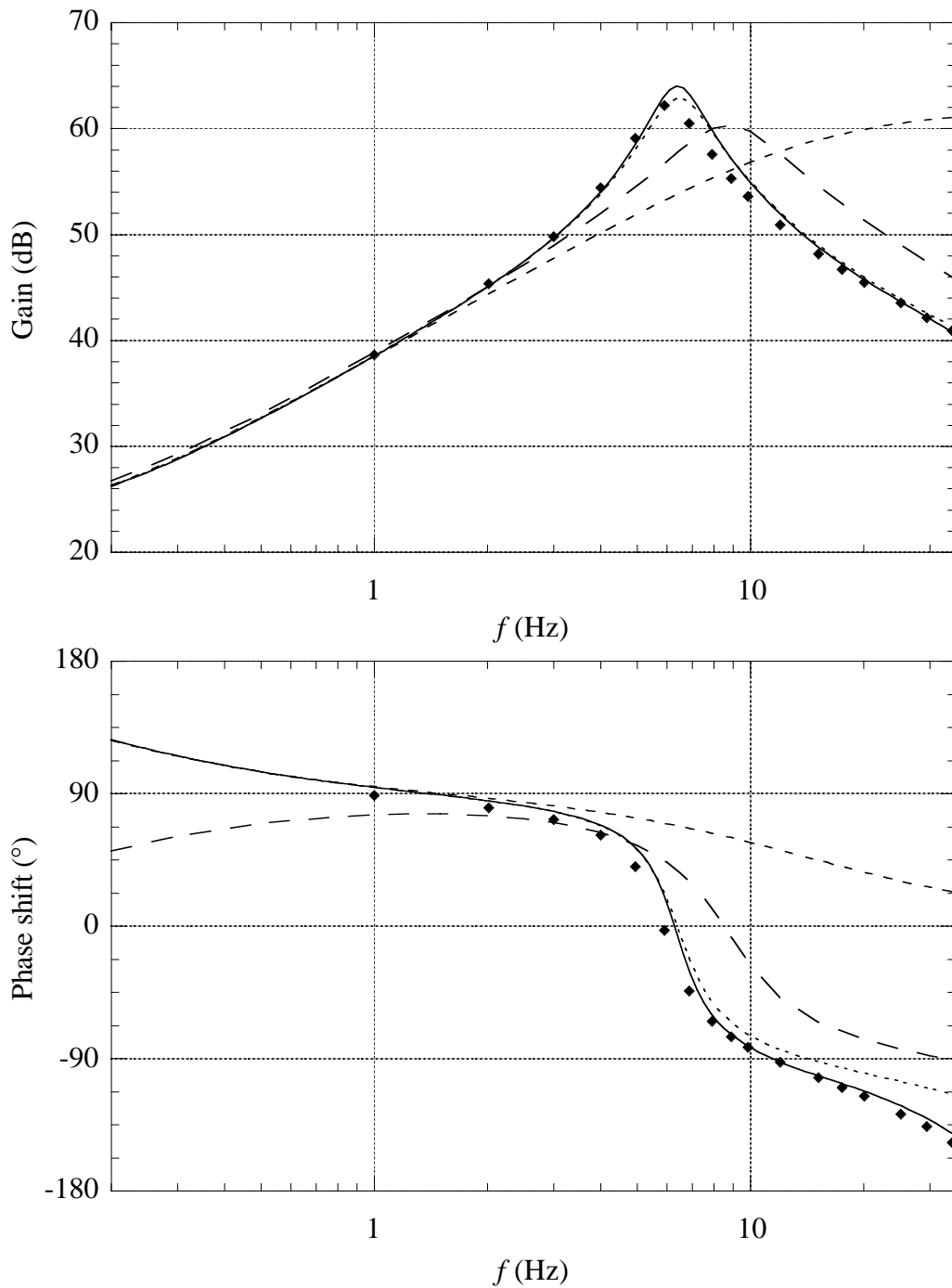
Figure 4.12.c. Measured and calculated gains and phase shifts of $\Delta P_2/\Delta \omega_s$. Dots are measured values and lines are values determined according to the different models. Park model (——), NST I (·········), LA (— — —) and ND (- - - - -).

The Park model calculations agree well with the measured values. The NST-model predicts almost the same result as the Park model. Again, the LA-model and the ND-model is useful up to a perturbation frequency of about 1-2 Hz.

4.4.3 Voltage magnitude perturbation

Figures 4.13.a-c present the rotor speed responses of machines one and two, as well as the local grid voltage response (ΔU_{grid}) to perturbations in the voltage magnitude (ΔU).
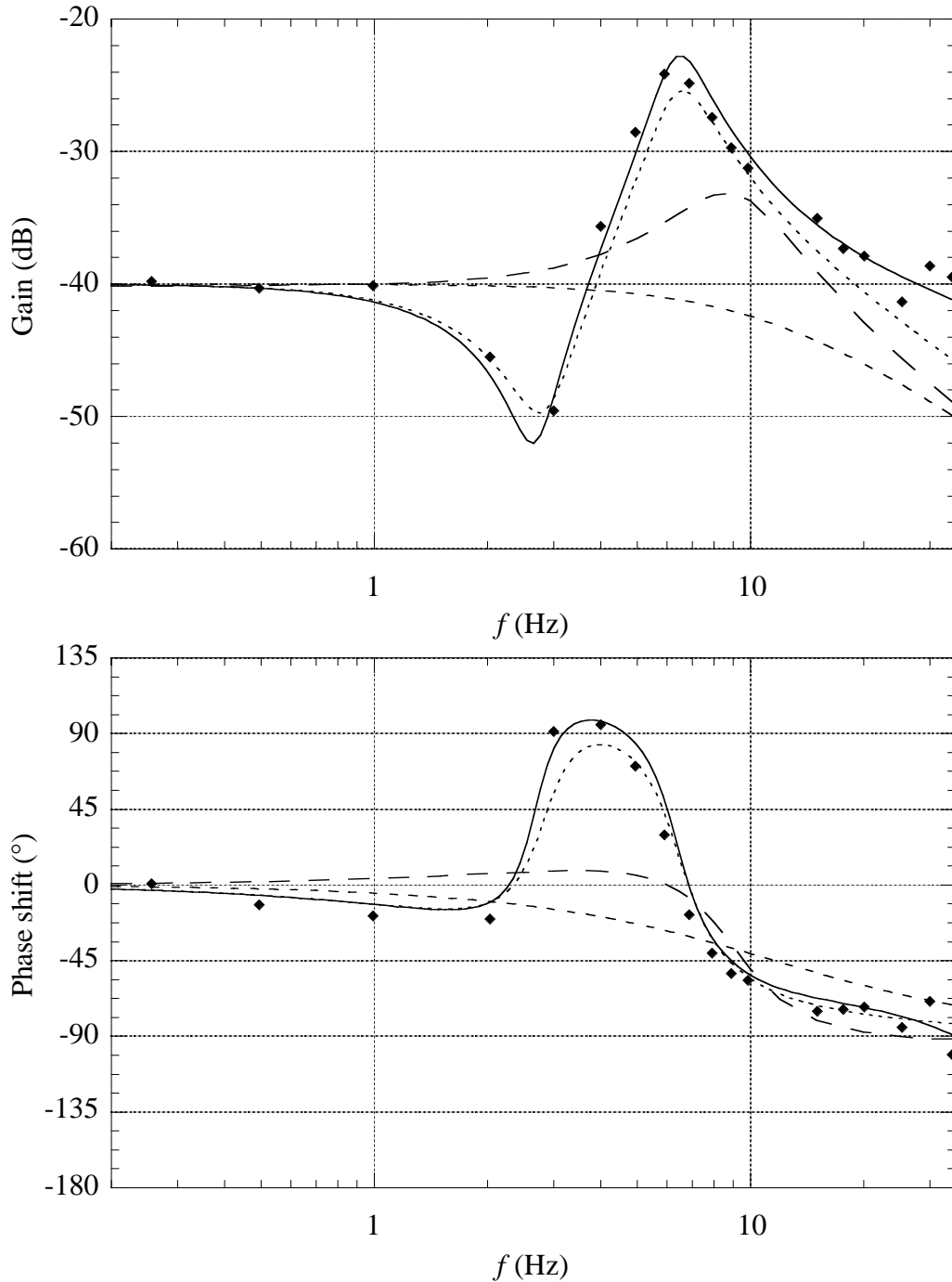
Figure 4.13.a. Measured and calculated gains and phase shifts of $\Omega_{m1}/\Delta U$. Dots are measured values and lines are values determined according to the different models. Park model (——), NST I (··········), LA (— — —) and ND (- - - - -).

72
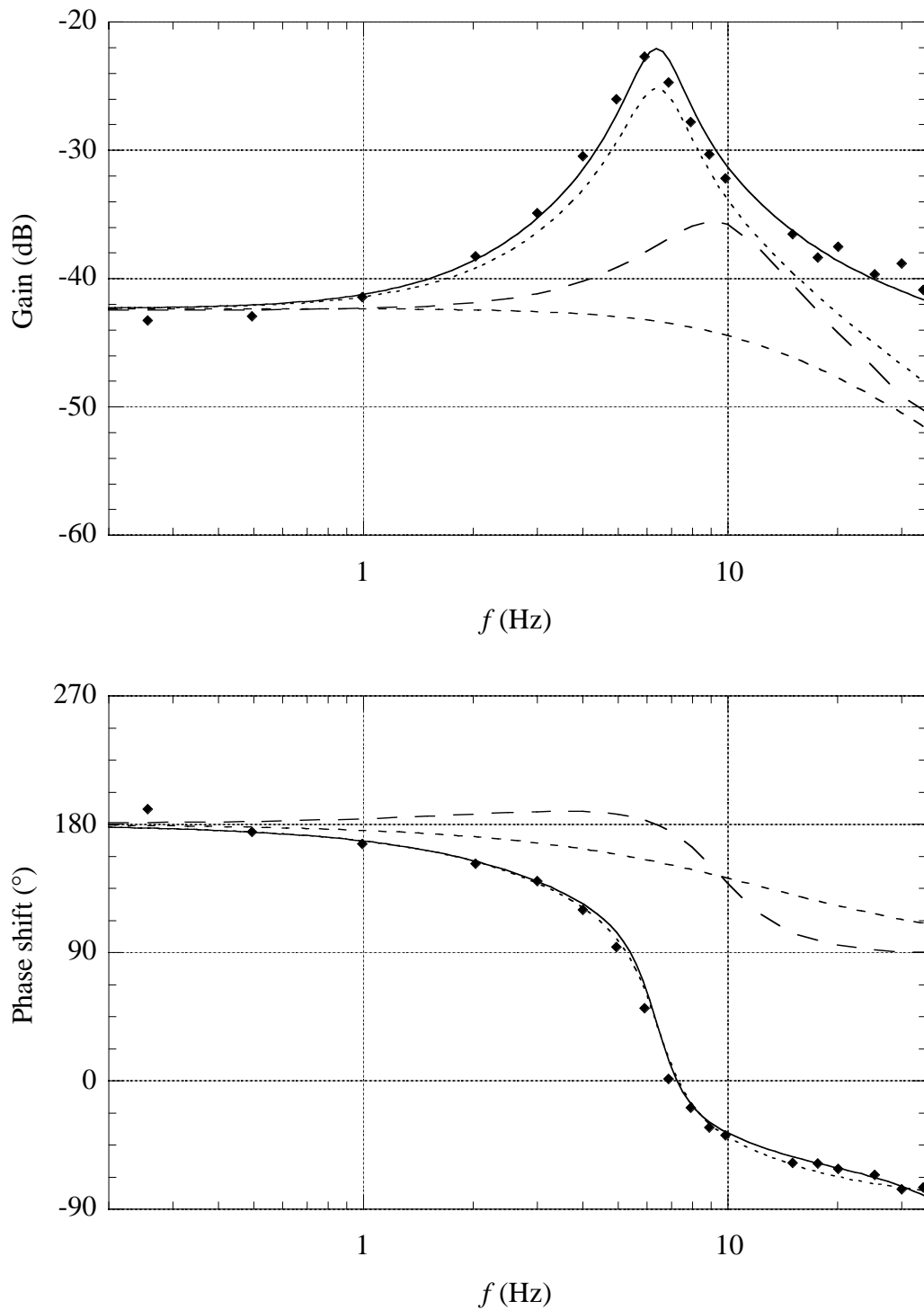
Figure 4.13.b. Measured and calculated gains and phase shifts of ΔΩ_{m2}/ΔU. Dots are measured values and lines are values determined according to the different models. Park model (——), NST I (·········), LA (— — —) and ND (- - - - -).
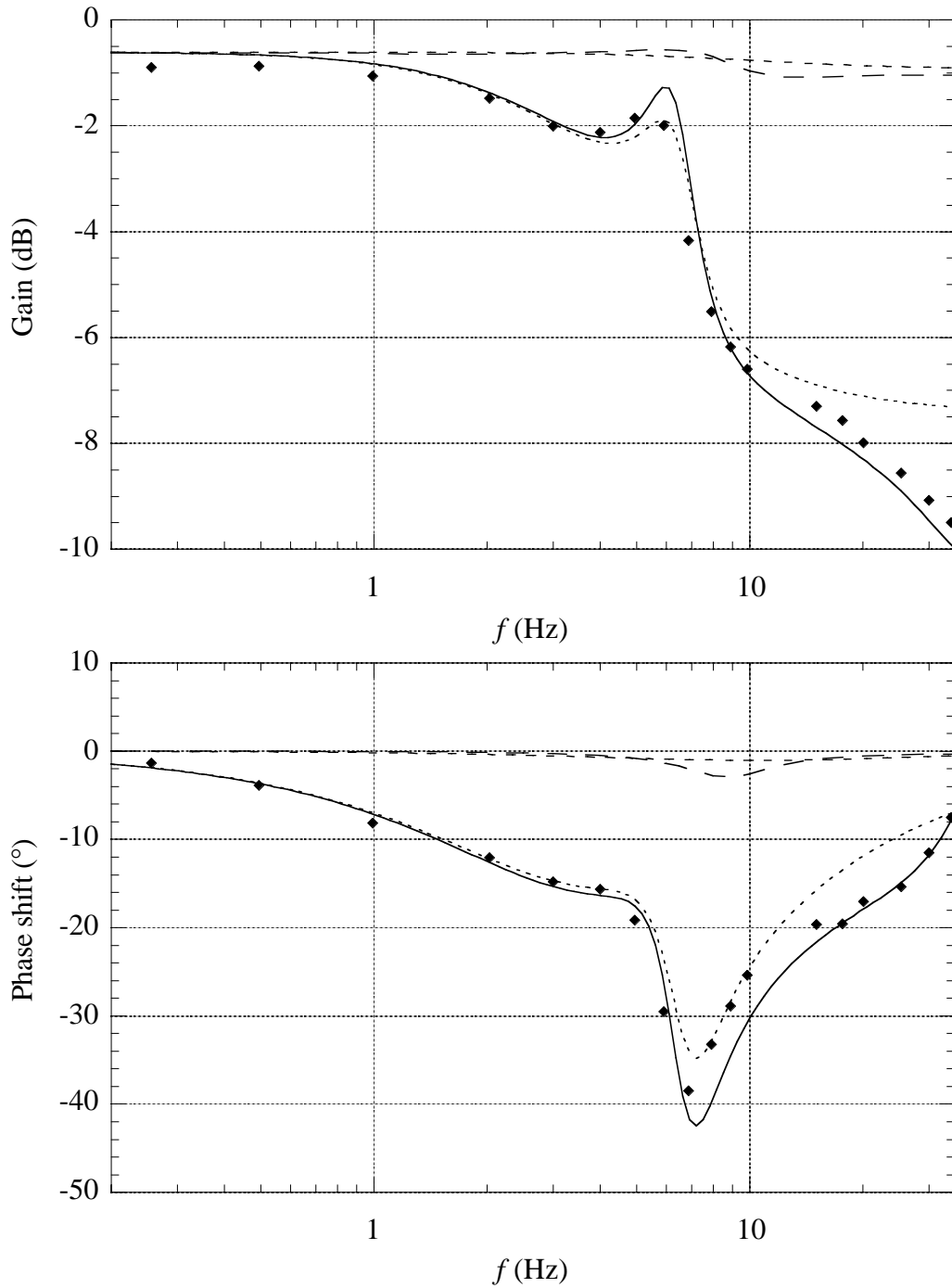
Figure 4.13.c. Measured and calculated gains and phase shifts of ΔU$_{grid}$/ΔU. Dots are measured values and lines are values determined according to the different models. Park model (——), NST I (·········), LA (— — —) and ND (- - - - -).

The values determined using the Park model and the NST-model coincide well with the measured ones. The only exception is that the iron losses should be taken into account to obtain a correct active power response to very low-frequency voltage magnitude perturbations, below approximately 3 Hz for the investigated system. The LA-model is as useful as the ND-model, i.e. valid up to a perturbation frequency of about 1 Hz.

5 SOME ASPECTS ON INDUCTION MACHINE DYNAMICS

The purpose of this chapter is to discuss different aspects that influence the induction machine dynamics, such as different operating points, disturbance magnitude, skin effect, iron losses, main flux saturation, line impedance and variable frequency.

The magnitude of $\Delta T_e/\Delta T_s$ is typically shown in this chapter in order to reduce the number of cases presented. However, other transfer functions are also shown when they are of interest.

5.1 Steady-state shaft torque

In a linear system, the gain is always independent of the operating point. Since the induction machine is a non-linear system this is not the case. However, the steady-state shaft torque is not of such great importance in the steady-state operating region of the inductance machine, as will be shown in this section. The calculations in this section are performed on the 15 kW machine at a voltage level of 400 V and at a supply frequency of 50 Hz using the Park model.

Within the normal operating region of the machine, the electrodynamical torque response to shaft torque perturbations is only slightly influenced by the static shaft torque (Kovacs 1984). Figure 5.1 presents the calculated magnitudes $\Delta T_e/\Delta T_s$ at no load operation and at rated motor operation. The reason for selecting these operating points is that the lowest damping and the highest damping occur close to no load operation and in rated motor operation, respectively.
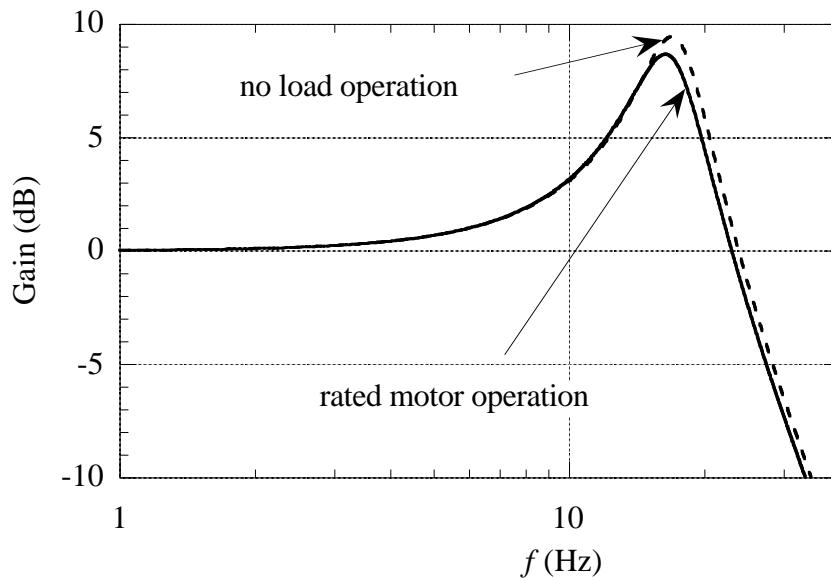
Figure 5.1. Calculated magnitudes of $\Delta T_e/\Delta T_s$. The machine is operating as motor loaded by rated torque and at no load. Temperature variations are not taken into account.

As can be noted from the figure, the discrepancy between the ratios $\Delta T_e/\Delta T_s$ for the two different cases is only notable for perturbation frequencies around and above the eigenfrequency, where it is about 10 %. In the normal steady-state operating region it is more important that the damping is improved as the temperature in the machine increases. As the temperature raises, the stator resistance increases, which leads to reduced damping, and the rotor resistance also grows leading to improved damping. The total effect is that the damping increases as the temperature raises.

In Figure 5.2 the calculated ratios of $\Delta T_e/\Delta T_s$ are presented for some operating points taking temperature variations into account. As can be noted the maximum magnitude of $\Delta T_e/\Delta T_s$ is 50 % lower at rated load than in the case where the machine is cold and operating at no load.
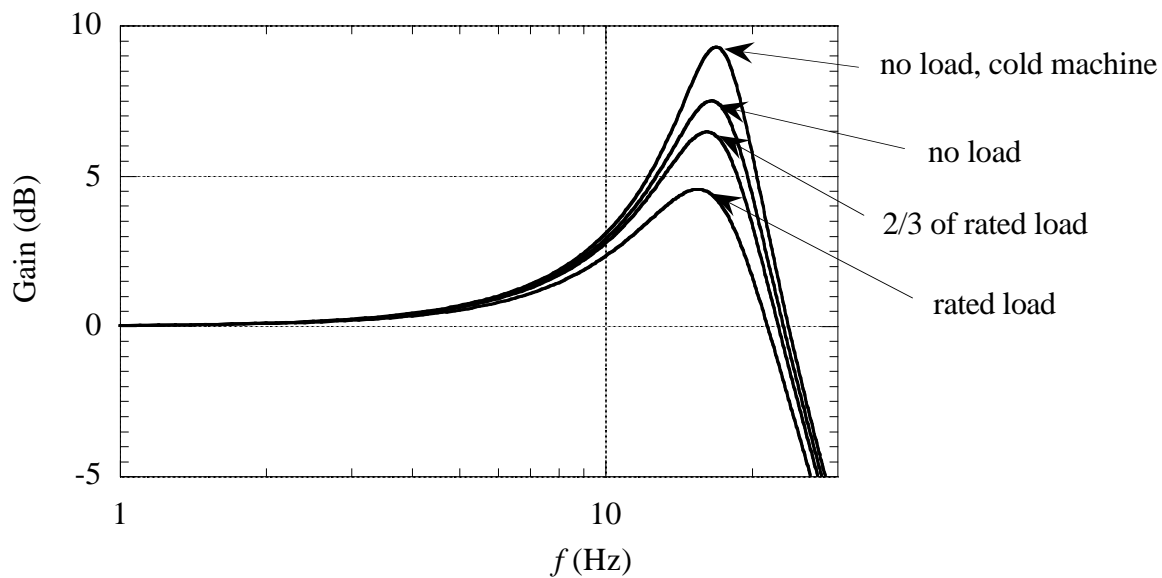
Figure 5.2. Calculated magnitudes of $\Delta T_e/\Delta T_S$ at some operating points with temperature variations taken into account.

The induction machine response to frequency perturbations also varies only slightly in the normal steady-state operating region, if temperature changes are not taken into account. The stator current and especially the reactive power responses to shaft torque and supply frequency perturbations, however, depend strongly on the operating point, even if temperature changes are not accounted for.

The response to perturbations in the magnitude of the supply voltage depends strongly on the static shaft torque even if temperature changes are not taken into account. Figure 5.3 presents the calculated rotor speed response to perturbations in the magnitude of the supply voltage when the machine is operating in generator and in motor operation, driven and loaded by rated torque.
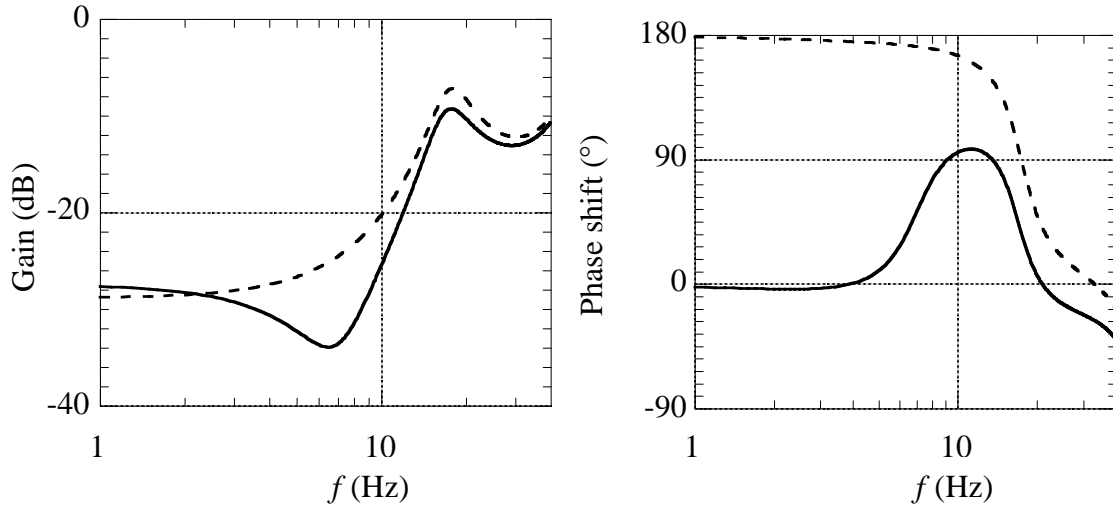
Figure 5.3. Magnitudes and arguments of $\Delta\Omega_m/\Delta U$ in motor (solid curve) and in generator operation (dashed curve).

In motor operation there exists an anti-resonance at 7 Hz which does not occur in generator operation. If small-signal analysis is applied on the machine operating as motor, a complex-conjugated double-zero can be observed which corresponds to the anti-resonance. In generator operation no complex-conjugated double-zero exists, but instead a zero can be found in the right half of the *s*-plane making the induction machine in this case to a mixed-phase system (Proakis & Manolakis 1988). This means that if the voltage is increased in generator operation, the immediate rotor speed response will be opposite to the final change.

5.2 Disturbance magnitude

In a linear system the gain is always independent of the perturbation magnitude. However, in a non-linear system this is not the case. For instance, if the induction machine is subjected to a large shaft torque disturbance, this will cause the machine to pass the pull-out point. An important question is thus: how large input perturbation magnitudes can be tolerated before the results of a small-signal analysis become inaccurate?

By applying small signal analysis on (2.4), we get

$$T_{e0} + \Delta T_e = p \, \mathrm{Im}(\underline{\Psi}_{s0}{}^* \underline{i}_{s0} + \underline{\Psi}_{s0}{}^* \Delta \underline{i}_s + \Delta \underline{\Psi}_s{}^* \underline{i}_{s0} + \Delta \underline{\Psi}_s{}^* \Delta \underline{i}_s) \qquad (5.1)$$

and with the steady-state solution subtracted

$$\Delta T_e = p \, \mathrm{Im}(\underline{\Psi}_{s0}{}^* \Delta \underline{i}_s + \Delta \underline{\Psi}_s{}^* \underline{i}_{s0} + \Delta \underline{\Psi}_s{}^* \Delta \underline{i}_s) \qquad (5.2)$$

The last term in (5.2), a product of small disturbances, is neglected in small signal analysis, which finally gives

$$\Delta T_e = p \ \text{Im}(\underline{\Psi}_{s0}{}^* \Delta \underline{i}_s + \Delta \underline{\Psi}_s{}^* \underline{i}_{s0}) \tag{5.3}$$

As a large pulsation in the supply voltage magnitude, 20% of the nominal grid voltage was selected and 3 % was selected as a small perturbation magnitude. The reason for selecting 3 % is that this is the highest voltage magnitude perturbation allowed by IEC 555-3 for extremely low-frequency voltage perturbations. In fact, for perturbation frequencies between 1 and 30 Hz, the limit is less than 1 %. In Figure 5.4 the magnitudes of $\Delta \Omega_m / \Delta U$ for the two perturbation magnitudes are presented. The machine is operating at 400 V and 50 Hz as motor loaded by rated torque. Again, small-signal analysis was applied but the results did not differ from those obtained using the small perturbation magnitude and accordingly the small-signal results are not presented.
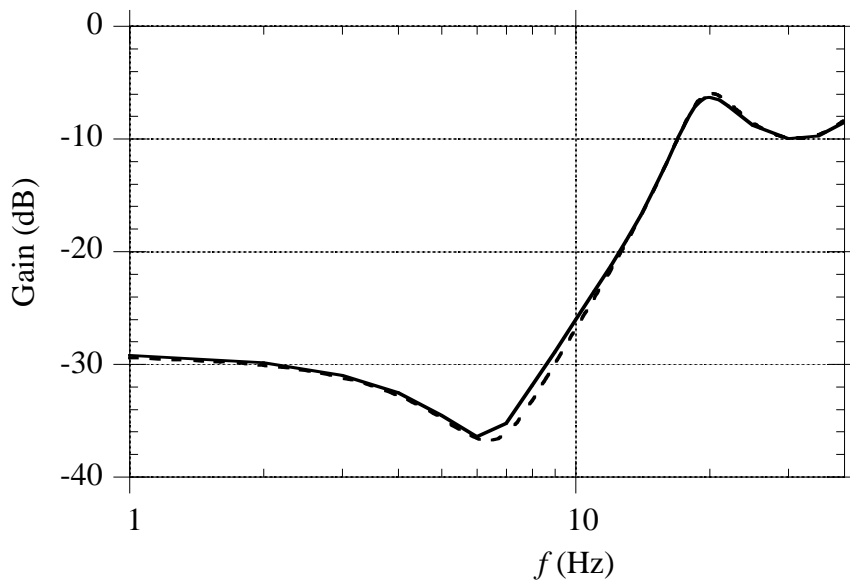
Figure 5.4.   Calculated magnitudes of $\Delta \Omega_m / \Delta U$ with different perturbation magnitudes. The dashed curve represents results obtained using a small perturbation magnitude and the solid one represents results using a large perturbation magnitude.

We have a maximum discrepancy of 10 %, which in this case is visible around the anti-resonance frequency, 7 Hz. Figure 5.5 illustrates the electrodynamical responses to a 7 Hz perturbation in the magnitude of the supply voltage of $\Delta U = 12$ V and $\Delta U = 80$ V. A component at a frequency twice the applied one is clearly visible in Figure 5.6. Neglecting the last term in (5.2) works well in the case where the disturbance is 8 V, but in the second case this term is too large to be neglected.
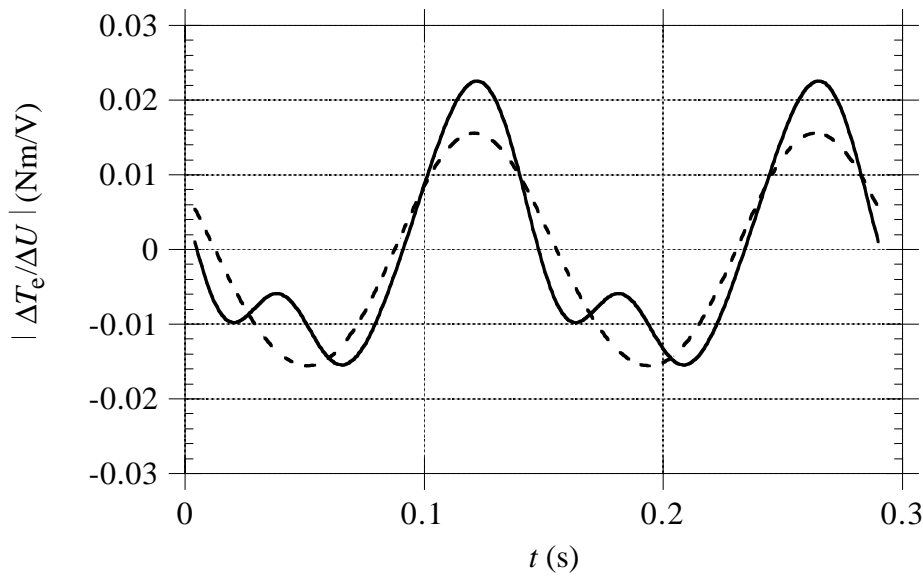
Figure 5.5. Torque response to a small (dashed curve) and a large (solid curve) perturbation in the supply voltage magnitude.

A calculated example is presented in Figure 5.6, in which a large (100 % of rated torque, peak to peak) and a small (10 % of rated torque) shaft torque perturbation are applied on the 15 kW machine operating as motor at rated torque ($U = 400$ V and $f = 50$ Hz). Calculations were also performed using a model linearized at the investigated operating point, but since the results coincided with the results obtained using the small perturbation magnitude, the small-signal analysis result is not presented.
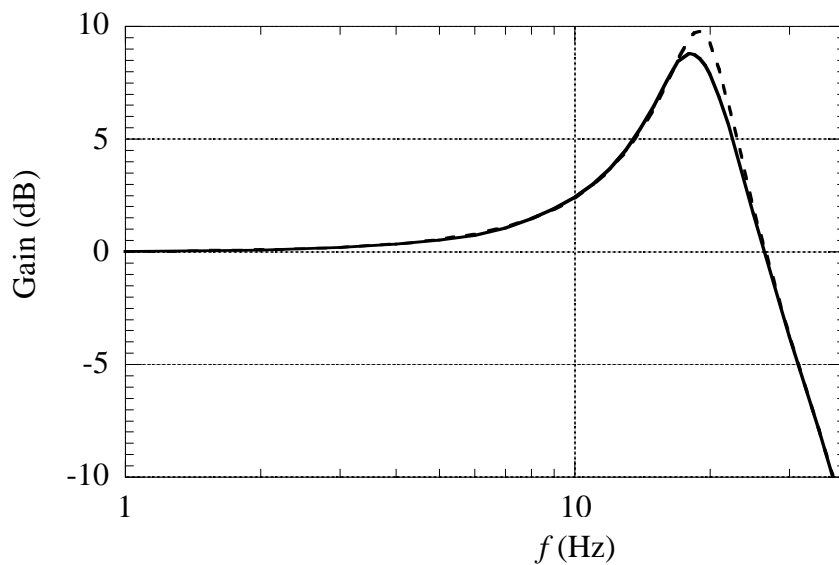
Figure 5.6. Calculated magnitudes of $\Delta T_e / \Delta T_s$ with different perturbation magnitudes. The dashed curve represents results obtained using a small perturbation magnitude and the solid one represents results using a large perturbation magnitude.

79

Although the point (in the steady-state operating region) is reached where the non-linearity of the machine is as most important the difference in the magnitude $\Delta T_e/\Delta T_s$ is detectable only around the dominating eigenfrequency, where it is about 10 %. In generator operation, where the slope of the steady-state torque-speed curve decreases less, the influence is smaller.

The magnitude of a supply frequency perturbation can be up to about 5 Hz before the results differ more than 10 % from the results obtained using small-signal analysis. Sometimes it is of greater interest to define the allowed phase deviation instead of the allowed frequency variation. In order to obtain a result which deviates less than 10 % from the small-signal analysis, the phase perturbation must be below 10°.

5.3 Main flux saturation

As the flux in the machine increases, the value of the magnetizing inductance decreases due to saturation. This is of no importance below rated flux for the investigated 15 kW machine and at rated flux of little importance. The saturation can be taken into account for steady-state purposes by adjusting only the magnetizing inductance. In order to take the dynamic effects of the main flux saturation into consideration, the approach in Section 2.3 can be used.

Figure 5.7 presents the calculated magnitudes of $\Delta T_e/\Delta T_s$ with dynamic saturation effects as well as without saturation effects considered, not even a steady-state correction of the magnetizing inductance. The applied voltage is 276 V and the supply frequency is 30 Hz, which corresponds to a flux increase of 20 % compared to the nominal one (380 V and 50 Hz). The value of the magnetizing inductance is in this case only 65 % of the nominal one.
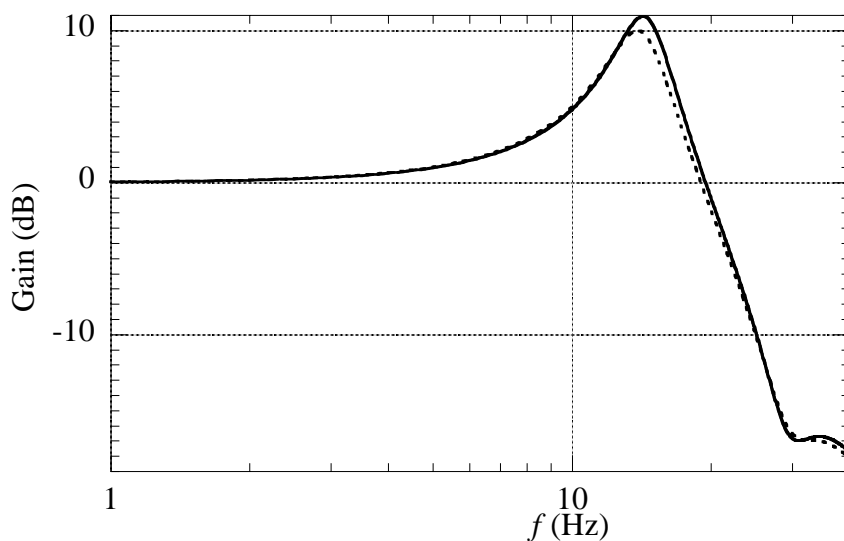
Figure 5.7. Calculated magnitudes of $\Delta T_e/\Delta T_s$ with saturation effects taken into account, dashed curve, and without effects of saturation taken into account, solid curve.

From Figure 5.7 it can be noted that the peak gain of $\Delta T_e/\Delta T_s$ is reduced by about 10 % when the saturation is taken into account. However, if the same magnetizing inductance, i.e. the saturated one, is used in both calculations, the difference between the two calculations is reduced to almost nothing.

Melkebeek (1980, 1983) measured and calculated the rotor speed response to voltage magnitude perturbations at no load, at frequencies around the resonance frequency, and found that the saturation reduced the magnitude of the rotor speed response substantially. For a 2.2 kW machine at a nominal flux level, he found a 50 % reduction of $\Delta\Omega_m/\Delta U$ at the resonance frequency compared to the case where the flux level of the machine was about 50 % of the nominal one. Specially adapted rotors were used in the experiments.

For the 15 kW machine investigated, such an influence of saturation was not found. At nominal flux levels, the calculated rotor speed response was the same with or without saturation taken into account. At a flux level of 20 % higher than the nominal one, the calculated peak magnitude of $\Delta\Omega_m/\Delta U$ was reduced by about 15 % due to saturation effects. If the comparison was made with the same magnetizing inductance, i.e. only the dynamic influence of the main flux saturation was investigated, the difference was reduced to about 3 %.

The strongest dynamic influence of the saturation was detected at very low-frequency responses to voltage magnitude perturbations. (Melkebeek measured the rotor speed response above about 10 Hz.) Figure 5.8 presents the measured and calculated magnitudes of $\Delta T_e/\Delta U$ and $\Delta\Omega_m/\Delta U$ with and without the dynamic effects of saturation taken into account. The same magnetizing inductance is used for both cases. The applied voltage is 276 V and the supply frequency is 30 Hz, i.e, the flux level used is 120 % of the nominal one.

A clear difference caused by the dynamic effect of the main flux saturation is visible in Figure 5.8. At the anti-resonance frequency, the rotor speed and electrodynamical torque responses to voltage magnitude perturbations are three times higher when the dynamic effect of saturation is accounted for compared to the case when only the steady-state effect of the saturation is taken into account. Also the other responses to voltage magnitude perturbations of very low frequencies are affected.
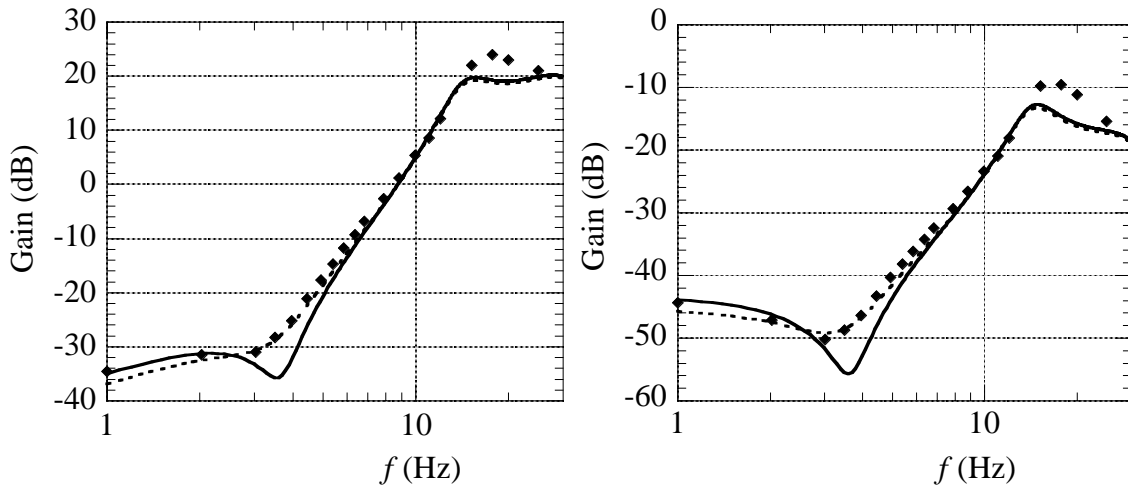
Figure 5.8. Calculated magnitudes of $\Delta T_e/\Delta U$ (left) and $\Delta \Omega_m/\Delta U$ (right) with dynamic effects of saturation taken into account, dashed curve, and without dynamic effects of saturation taken into account, solid curve. Dots are measured values.

5.4 Skin effect

The rotor conductors of a cage induction machine are designed to have a higher resistance increasing with higher rotor frequencies by utilizing the skin effect. Apart from the fact that the starting torque is raised, the damping is also increased. Figure 5.9 presents the magnitudes of $\Delta T_e/\Delta T_s$ with and without skin effect taken into account. The machine is operating at no load and at $U = 400$ V and $f = 50$ Hz
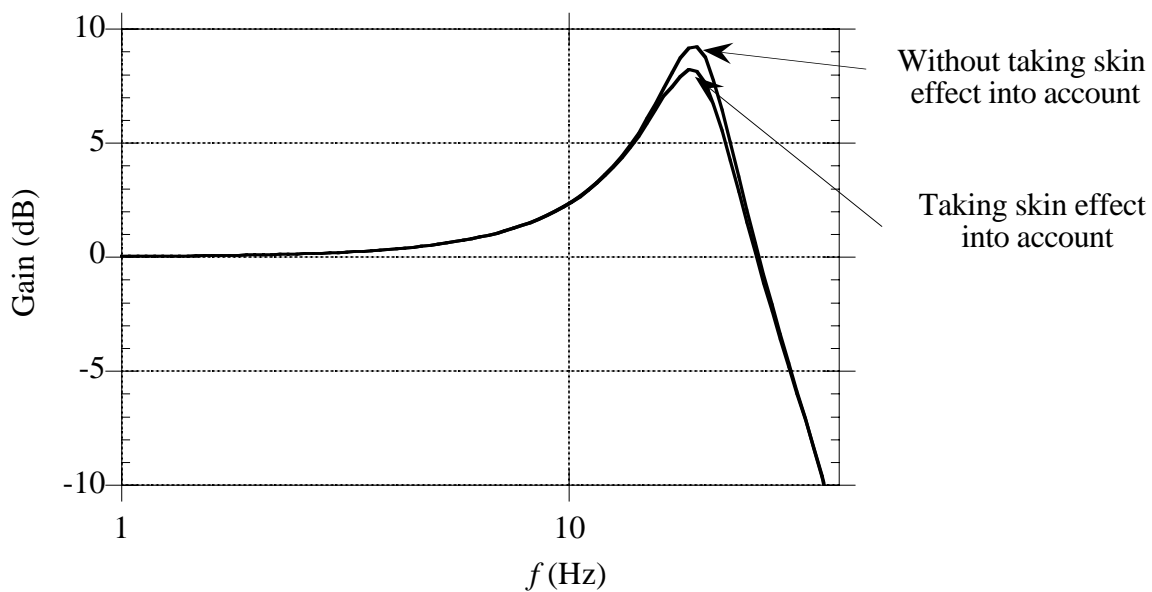
Figure 5.9. Calculated magnitudes of $\Delta T_e/\Delta T_s$ with and without skin effect taken into account.

At 18 Hz, which is the dominating resonance frequency of the 15 kW machine operating at 400 V and 50 Hz, the rotor resistance is increased by 10 %, and consequently the damping is improved by 10 %. In a deep-bar rotor the increase of the rotor resistance will be larger. Meyer (1976) found an increase of the damping by 20 % for a 3.1 MW machine at a rotor frequency of 5 Hz, i.e. at the eigenfrequency of the induction machine investigated.

5.5 Inclusion of iron losses

Usually, the iron losses affect the dynamic behaviour of the machine very little. The only case where the effect of iron losses is clearly visible is the electric power response to very low-frequency perturbations in the voltage magnitude and supply frequency. Figure 5.10 presents the magnitudes of $\Delta P_e/\Delta U$ when the machine is operating as generator driven by a shaft torque of 70 Nm at $U = 288$ V and $f = 43.5$ Hz.

From Figure 5.10 it appears clearly that the iron losses have to be considered in order to determine the magnitude of $\Delta P_e/\Delta U$ for perturbation frequencies below 3 Hz. However, it must be pointed out that the electric power response magnitude is low for these low-frequency perturbations.
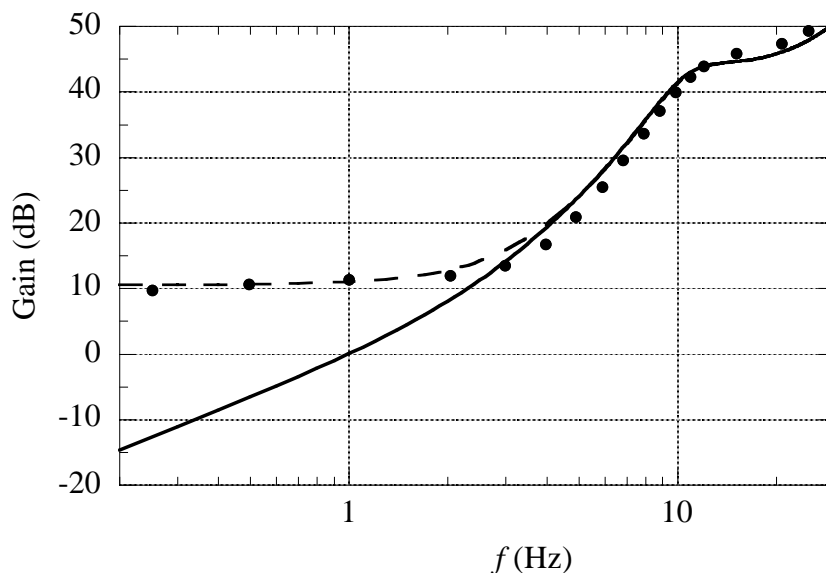
Figure 5.10. Calculated and measured magnitudes of $\Delta P_e/\Delta U$. Dots represent measured values, dashed and solid lines represent calculations taking and not taking the iron losses into account, respectively.

5.6 Flux level

The flux level of the machine is decreased by reducing the magnitude of the supply voltage without lowering the frequency. The purpose of reducing the flux level of the induction machine is that the efficiency can be improved when the steady-state shaft torque is low. Figure 5.11 presents the measured and calculated electrodynamical torque response to shaft torque perturbations. The 15 kW machine is driven by a shaft torque of 70 Nm and operating at a supply frequency of 30 Hz and at two different voltage levels, 240 V (5 % higher than nominal flux) and 200 V (flux reduced by 12 %). The effect of saturation has not been taken into account, since it affects the results only slightly.

From Figure 5.11 it can be observed that a reduction of the flux level increases the damping strongly and it reduces the resonance frequency.
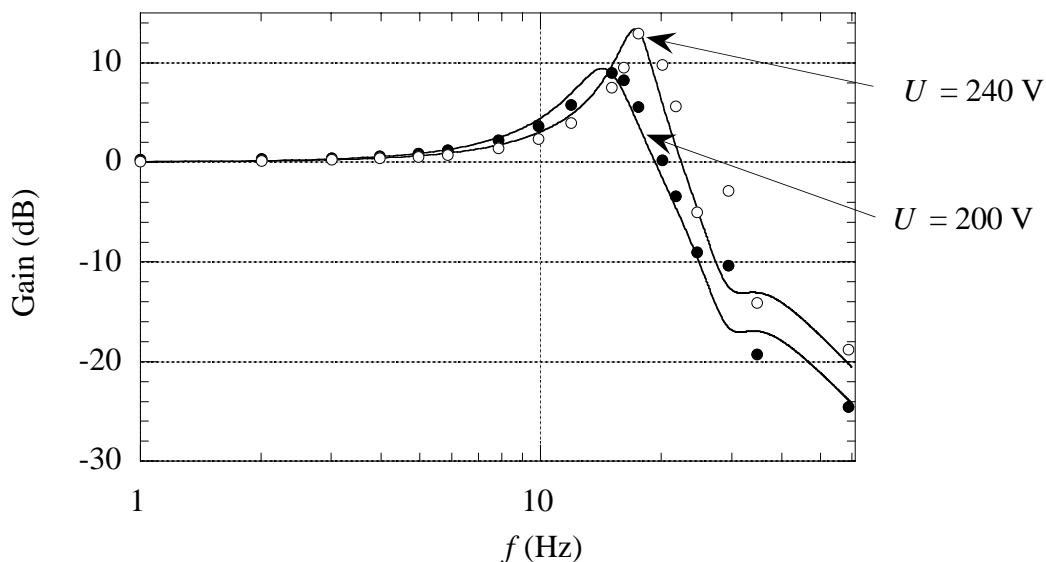
Figure 5.11. Magnitudes of $\Delta T_e/\Delta T_S$. Dots and circles are measured values and lines are calculated values.

5.7 Weak grid

5.7.1 Stator and line resistance

The stator resistance is not included in the NSR-model. At a supply frequency of 50 Hz, this is not of great importance for larger machines with a relatively small stator resistance. For smaller machines, however, the reduction of the damping due to the stator resistance cannot be

neglected. For the investigated 15 kW machine the damping predicted by the NSR-model is 20 % too low at 50 Hz and 400 V.

Even self-excited oscillations have been reported in cases where an extremely high additional stator resistance has been used (Palit 1978, Kron & Lorenzon 1969). A series resistance must accordingly be taken into account when the properties of the machine are determined. In Figure 5.12 the magnitudes of $\Delta T_e/\Delta T_S$ are presented for some stator resistances. The machine is operating as a generator driven by a shaft torque of 70 Nm, the voltage is 288 V and the supply frequency is 43.5 Hz.
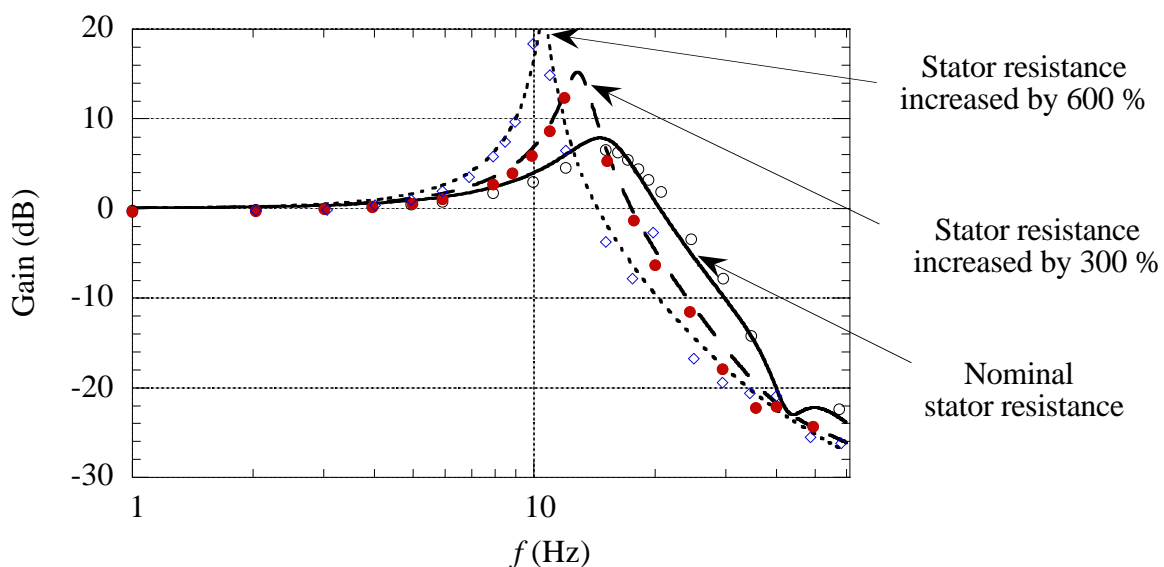
Figure 5.12. Gain of the transfer function $\Delta T_e/\Delta T_S$ with three different stator resistances. The lines are calculated results performed according to the detailed model and the dots, rhombuses and circles are measured values.

When the machine is fed from a converter, the resistance in the power switches, such as transistors or GTOs, must be considered as the dynamic performance of the induction machine is investigated. Another important feature of power switches is that they have a voltage drop, which has the same effects as an additional stator resistance.

Increased stator resistance does not automatically lead to reduced damping. For low supply frequencies the situation is usually the opposite. A growing stator resistance will always finally lead to increased damping. Usually, the induction machine has a certain stator resistance value where the damping reaches a minimum or even becomes negative. As the stator resistance increases above this value, the damping is improved. For the 15 kW machine operating at 50 Hz and 400 V, the damping reaches a minimum for a stator resistance of 4.5 Ω, 25 times the

rated value, with a damping ratio close to zero. At no load the machine will even be unstable. Usually, the damping of the machine is improved as the inertia increases, but if we in this example with a stator resistance of 4.5 Ω connect a load having an inertia equal to the inertia of the machine, the machine will become even more unstable.

5.7.2 Line and leakage inductance

Additional line and stator leakage inductance mainly lead to a lowered resonance frequency. Figure 5.13 shows the measured and calculated magnitudes of $\Delta T_e/\Delta T_s$ for some stator leakage inductances. The machine is operating as a generator driven by a shaft torque of 70 Nm. The supply frequency is 43.5 Hz and the supply voltage is 288 V.
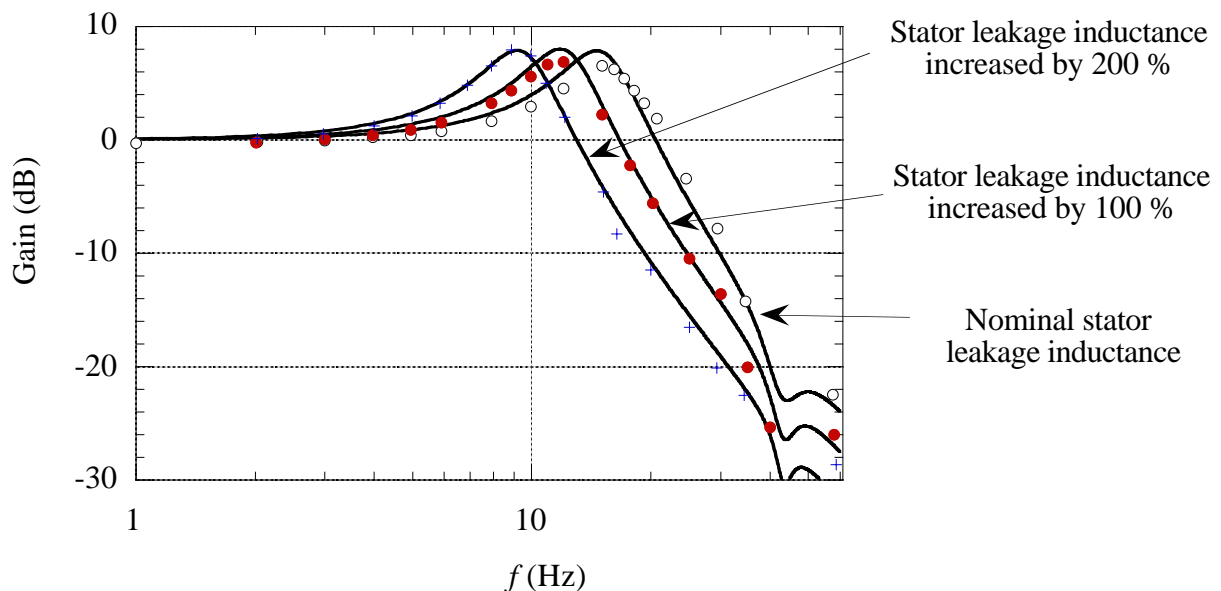
Figure 5.13. Magnitudes of $\Delta T_e/\Delta T_s$ with different stator leakage inductances. The lines are calculated results and the circles, dots and crosses are measured values.

5.8 Variable frequency

When an induction machine is driven in variable-speed operation, the voltage is usually reduced in proportion to the frequency in order to keep a constant flux in the machine. If the proportion between the supply voltage and supply frequency is kept constant, the NSR-model (2.53) does not indicate that the dynamic behaviour should change as the supply frequency varies. Figure 5.14 presents the measured and calculated magnitudes of $\Delta T_e/\Delta T_s$ for three different supply frequencies at the same flux level, 87 % of the nominal one. The machine is operating as generator with a driving shaft torque of 70 Nm.

Figure 5.14 shows that the supply frequency strongly affects the damping of the machine. It is the influence of the stator resistance that leads to different dynamic behaviour as the supply frequency varies. When the supply frequency is lowered, the stator resistance will be relatively larger compared to the reactances of the machine.
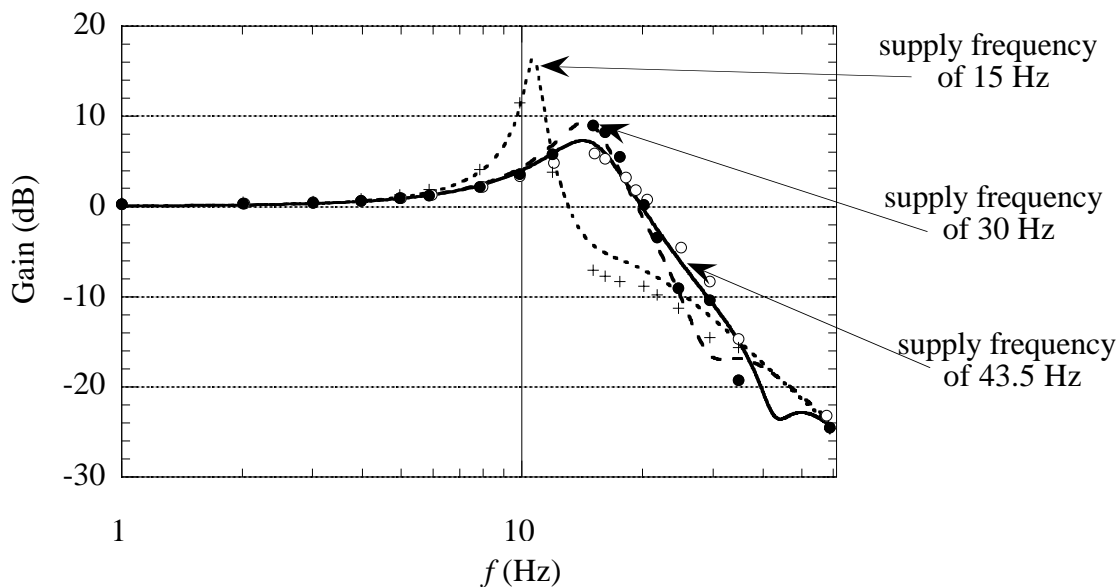
Figure 5.14. Magnitudes of the transfer function $\Delta T_e/\Delta T_S$ for some different supply frequencies. Lines represent calculated values. Crosses, dots and circles show measurements at 15, 30 and 43.5 Hz, respectively.

5.9 Influence of phase-compensating capacitors

To compensate for the reactive power needed by the induction machine, phase-compensating capacitors can be installed at the machine. The low-frequency dynamic influence of the phase-compensating capacitors is rather small. A minor influence can be observed depending on the grid configuration, the capacitance and the static shaft torque of the machines. Generally, it can be said that the damping is somewhat reduced, since the capacitors increase the voltage at the induction machine.

In Figure 5.15 the measured and calculated magnitudes of $\Delta \Omega_m/\Delta T_S$ are presented with and without capacitors of 300 μF per phase connected to the machine. The capacitance was chosen to compensate the power factor to one at no load operation. An additional inductance of 2 mH is also connected between the converter and the machine in both cases. The voltage at the machine will otherwise be governed by the converter only, and the capacitors will have no influence on the dynamic performance of the machine.

87

The machine is operating as generator driven by a shaft torque of 70 Nm, the applied voltage is 288 V and the supply frequency is 43.5 Hz. The machine voltage is 286 V with capacitors and 274 V without. An additional calculation without capacitors was also performed at a higher voltage level of 300 V. The voltage at the machine is in this case the same as when the 300 µF capacitor was connected, i.e. 286 V.

From Figure 5.15 it can be observed that the rotor speed response is similar in the case where capacitors were connected at the machine as when the applied voltage was increased and no capacitors were used. The other responses are affected in a similar way. However, the reactive power response to voltage magnitude perturbations has a more complicated pattern as phase-compensating capacitors are connected, and depends both on the static shaft torque and the capacitance.
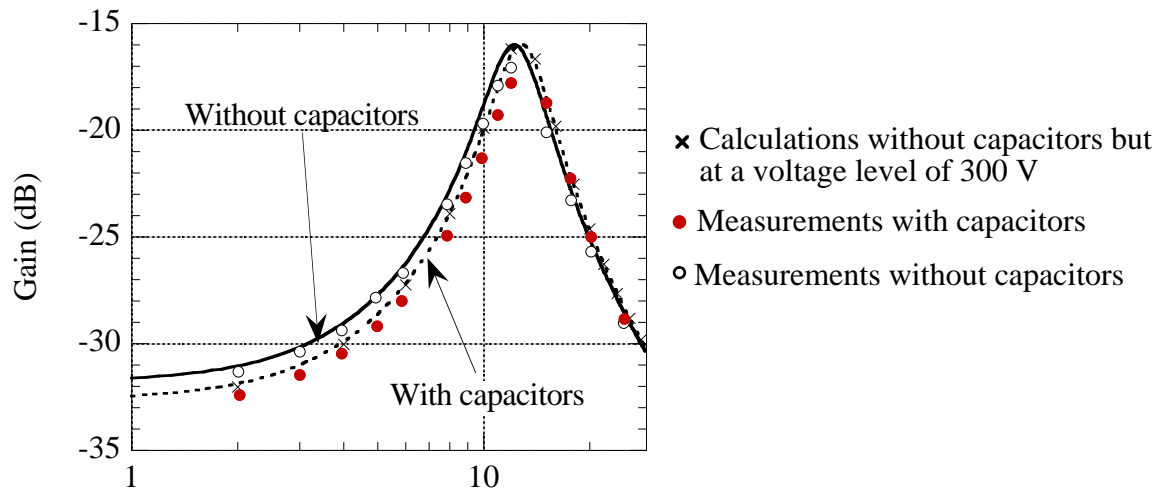
Figure 5.15. Magnitudes of $\Delta\Omega_m/\Delta T_s$. Lines and crosses represent calculated values, and circles and dots show measured values.

5.10 Non-stiff machine shaft

The purpose of deriving linear reduced order models of the induction machine is to simplify the dynamic analysis. By using the LD-model and NSR-model it is possible to analyse a larger system analytically, for instance the drive train of a wind turbine. Constant-speed wind turbines often produce periodic power pulsations. Santjer and Gerdes (1994) report a case where the periodic power pulsations have reached 20 % of the rated power. The origin of these pulsations is the blade rotation. The frequency of the pulsations depends on the number of blades of the turbine and the rotor speed. Usually the frequency of the periodic power pulsations is between 0.7 and 2.2 Hz.

If the NSR-model is used to represent the induction machine together with the soft shaft and wind turbine rotor, a fourth-order linear model is obtained. A mechanical analogy of the wind turbine drive train is presented in Figure 5.16.
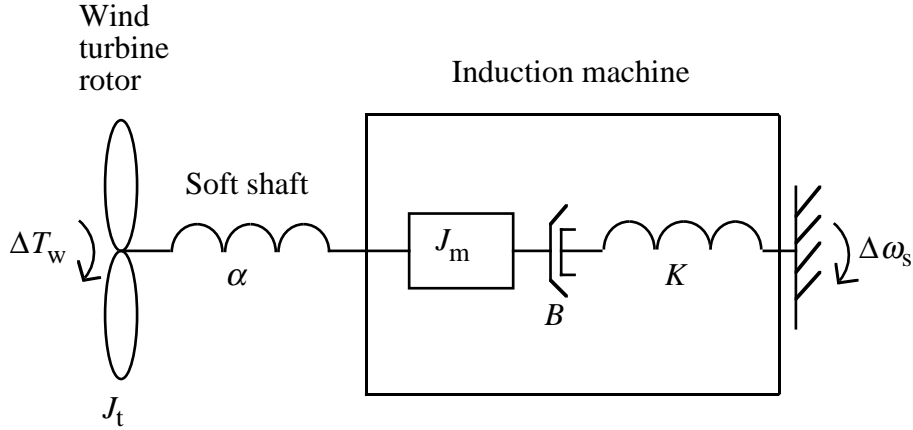
Figure 5.16. NSR-model connected to a wind turbine rotor via a soft shaft.

The linearized analytical transfer function from wind torque to electrodynamical torque can now be derived, yielding

$$\frac{\Delta T_e}{\Delta T_w} = \frac{K}{s^4 \dfrac{J_t J_m}{\alpha} + s^3 \dfrac{J_m J_t K}{B\alpha} + s^2(J_m + J_t(1 + \dfrac{K}{\alpha})) + s\dfrac{KJ_t + KJ_m}{B} + K} \tag{5.4}$$

Wilkie et al. (1990) used a first-order model to represent the induction machine as wind turbine generator. With the wind turbine generator represented by the LD-model, the transfer function from wind torque to electrodynamical torque becomes

$$\frac{\Delta T_e}{\Delta T_w} = \frac{1}{s^3 \dfrac{J_m J_t}{B\alpha} + s^2\dfrac{J_t}{\alpha} + s\dfrac{J_t + J_m}{B} + 1} \tag{5.5}$$

Figure 5.17 presents the magnitudes of $\Delta T_e/\Delta T_w$ for a 225 kW wind turbine predicted by the NSR-based model, by the LD-model and by the seventh-order model presented in Section 2.2. The machine is operating as generator driven by a shaft torque of one quarter of the rated one.
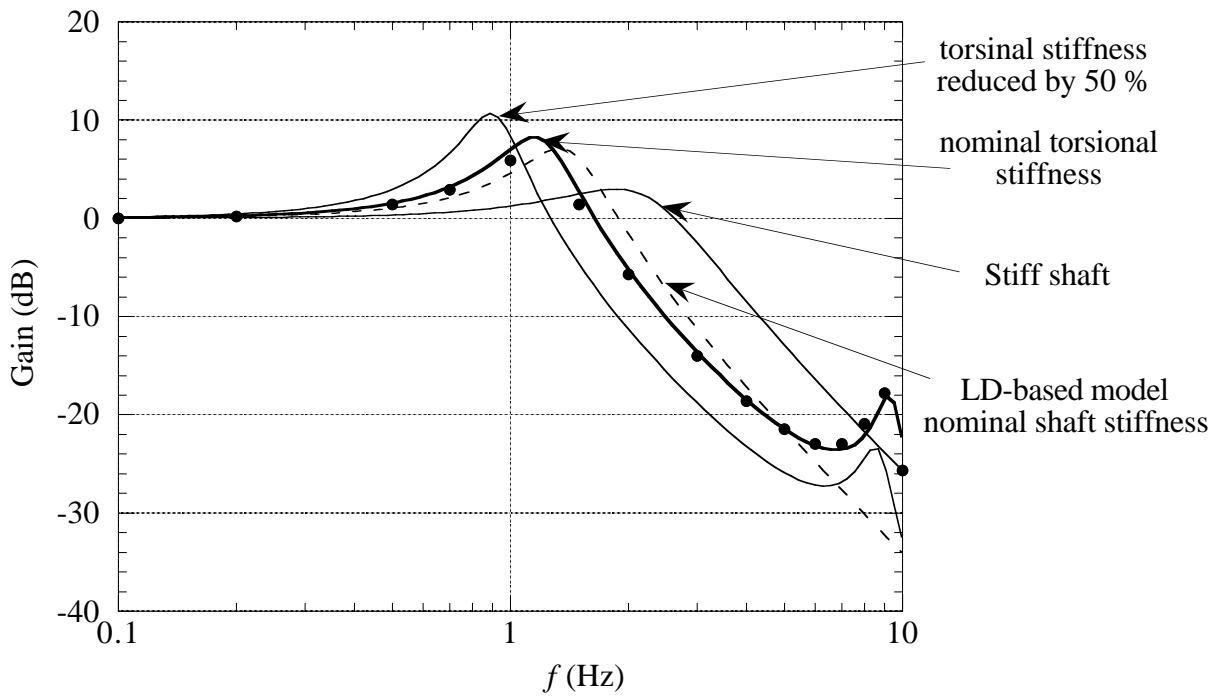
Figure 5.17. The gain of the transfer function $\Delta T_e/\Delta T_w$ with varied shaft torsional stiffness. Solid curves represent values determined by the NSR-based model, dashed curve represent values determined using the LD-based and dots represent values determined by the seventh-order model.

As can be observed in Figure 5.17, the NSR-based model predicts a similar result as the detailed model. The LD-based model is as good as the NSR-based model up to a perturbation frequency of 0.5 Hz. There are two resonance frequencies visible in the figure. The lower oscillation mode is governed by the rotor and shaft stiffness of the wind turbine and the other is basically determined by the induction machine inertia and leakage inductances of the machine, i.e. the dominating eigenfrequency of the induction machine. In many cases, the lower oscillation mode coincides with the blade passage frequency of the wind turbine, which is a reason why periodic power pulsations from wind turbines sometimes are so large.

As the machine is subjected to a higher driving torque, the damping at the lower resonance frequency will increase somewhat, which the two linear models fail to predict.

Also the response to frequency perturbations can be analysed using the NSR-model. For instance, the simplified transfer function from supply frequency perturbation to electrodynamical torque is

$$\frac{\Delta T_e}{\Delta \omega_s} = \frac{s3\dfrac{KJ_t J_m}{\alpha} + sK(J_m + J_t)}{s4\dfrac{J_t J_m}{\alpha} + s3\dfrac{J_m J_t K}{B\alpha} + s2(J_m + J_t(1 + \dfrac{K}{\alpha})) + s\dfrac{KJ_t + KJ_m}{B} + K} \quad (5.6)$$

In Figure 5.18 the magnitude of $\Delta T_e/\Delta \omega_s$ for the wind turbine drive train is compared for a stiff and a soft shaft. The drive train with a soft shaft is modelled using the seventh-order model, the NSR-based model and the LD-based model. The machine is operating as generator driven by a shaft torque of one quarter of the rated one.
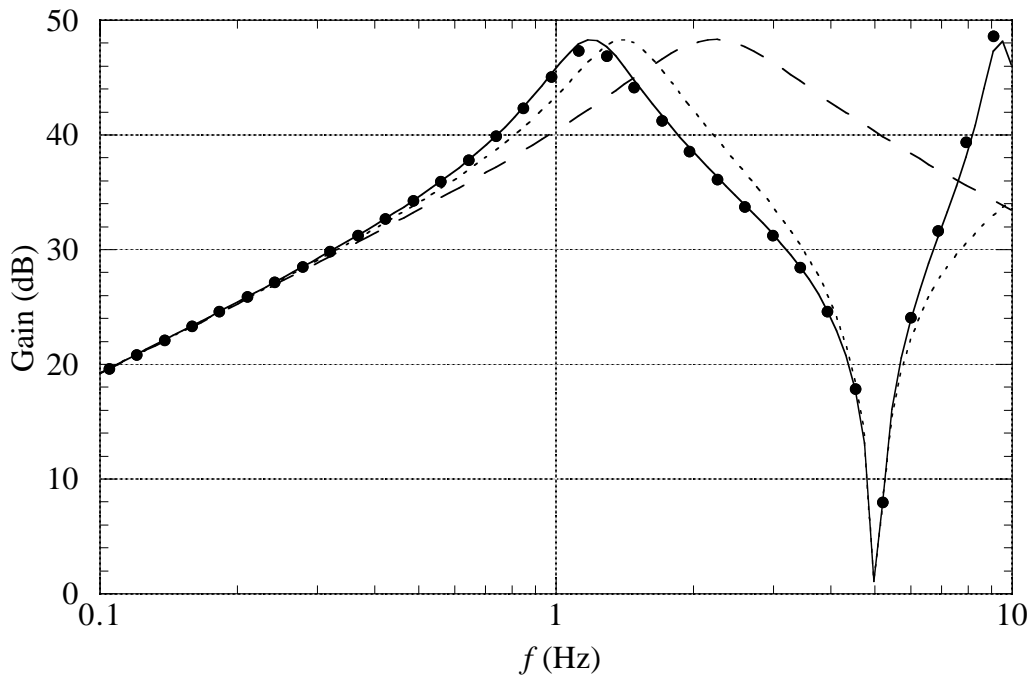
Figure 5.18. The gain of the transfer function $\Delta T_e/\Delta \omega_s$ with a stiff shaft (− − −) and a soft shaft using diffferent models: NSR-based model (——), LD-based model (·········) and dots seventh-order model.

As in the previous case where the response to a torque perturbation was presented, the damping at the lower resonance frequency will increase somewhat, as the machine is subjected to a higher driving torque, which the two linear models fail to predict.

6 EXTRAPOLATION TO OTHER MACHINE SIZES

In Chapter 4 the response of a 15 kW machine was investigated as the machine was subjected to different types of perturbations. In this chapter the responses of a large number of machines are analysed in order to obtain some generally applicable results. Ahmed-Zaid and Taleb (1991) investigated some step responses of eleven machines in order to give some guidelines for the selection of an induction machine model. The results were strongly influenced by the fact that some of the machines had very large rated slips, about 5 %.

The parameters of 31 machines, ranging in size from 2 kW to 4 MW, are presented in Table 6.1. Mainly four-pole machines are investigated but also several six-pole ones. The inductances and resistances of the machines are given in per unit values. The parameters of machines 21-31 were given by Cathey et al. (1973), i.e., the same source as Ahmed-Zaid and Taleb (1991) used. The parameters of the other machines were obtained from manufacturers of induction machines.

If small-signal analysis is applied on the induction machine, the transfer function from shaft torque to electrodynamical torque is found to have three zeros and five poles. The locations of the three zeros are close to the locations of three of the poles, and the transfer function from shaft torque to electrodynamical torque can be simplified to the second order. Providing that the supply frequency is not too low, a useful approximation of the transfer function from shaft torque disturbance to electrodynamical torque is

$$\frac{\Delta T_e}{\Delta T_s} = H(s) = \frac{\omega_0^2}{s^2 + 2\xi\omega_0 s + \omega_0^2} \qquad (6.1)$$

where ξ is the damping ratio and ω_0 the undamped eigenfrequency.

In Figures 6.1 and 6.2 the undamped eigenfrequencies and damping ratios of the machines, determined by small-signal analysis, are presented. The machines are operating as motors loaded by a quarter of rated shaft torque. The machines are not connected to a load, i.e. the total inertia is the machine inertia only. In Figure 6.1 it can be observed that the undamped eigenfrequency of an induction machine is lowered as the machine size increases. A 5 kW machine has a resonance frequency of about 25 Hz and a MW size induction machine has an undamped eigenfrequency of about 5-10 Hz.

Table 6.1. Parameters of the investigated induction machines (at 20 ˚C).

No.	Power (kW)	U (V)	R_s (%)	R_r (%)	L_m (pu)	$L_{s\lambda}$ (pu)	$L_{r\lambda}$ (pu)	f_s (Hz)	p	J_m (kgm²)	Rated slip
1	4	380	1.93	1.76	0.73	0.039	0.039	50	2	0.015	0.043
2	7.5	400	1.41	1.00	0.57	0.039	0.035	50	3	0.082	0.026
3	11	400	1.46	1.01	0.93	0.042	0.047	50	2	0.073	0.024
4	11	400	1.33	1.05	0.61	0.044	0.040	50	3	0.10	0.027
5	15	400	0.99	1.07	0.70	0.053	0.045	50	3	0.22	0.028
6	15	400	1.21	1.1	1.03	0.044	0.051	50	2	0.094	0.027
7	18.5	400	0.95	0.71	0.93	0.042	0.063	50	2	0.16	0.017
8	22	400	0.87	0.71	1.06	0.045	0.070	50	2	0.19	0.017
9	30	400	0.72	0.72	0.98	0.034	0.056	50	3	0.76	0.017
10	45	400	0.63	0.56	1.20	0.049	0.081	50	2	0.41	0.021
11	180	415	0.78	0.72	1.51	0.049	0.051	50	3	4.5	0.017
12	200	380	0.47	0.63	1.75	0.057	0.081	50	2	2.5	0.017
13	200	690	0.41	0.58	1.89	0.052	0.076	50	2	3.0	0.016
14	200	690	0.31	0.37	1.29	0.052	0.061	50	3	6.6	0.010
15	225	400	0.51	0.51	1.30	0.049	0.093	50	3	7.4	0.013
16	400	690	0.3	0.49	1.98	0.046	0.079	50	2	6.6	0.013
17	100	380	0.73	0.65	1.70	0.055	0.096	50	2	1.1	0.019
18	400	380	0.75	0.5	2.11	0.054	0.080	50	2	7.5	0.015
19	630	380	0.6	0.44	2.03	0.051	0.080	50	2	10.8	0.013
20	800	380	0.53	0.44	2.08	0.051	0.083	50	2	13.0	0.013
21	2.23	220	0.95	1.78	0.70	0.020	0.020	60	2	0.045	0.050
22	18.6	460	1.04	2.23	1.12	0.029	0.029	60	2	0.277	0.058
23	37.2	460	0.73	1.89	1.33	0.031	0.031	60	2	0.83	0.053
24	74.5	460	0.52	2.35	1.45	0.031	0.031	60	2	2.22	0.056
25	186	2300	1.14	0.67	1.74	0.050	0.050	60	2	3.5	0.017
26	372	2300	0.88	0.63	2.19	0.049	0.049	60	2	5.6	0.015
27	596	2300	0.70	0.50	2.35	0.047	0.047	60	2	10.7	0.012
28	745	2300	0.75	0.50	4.43	0.049	0.049	60	2	14.9	0.012
29	1117	2300	0.56	0.37	2.42	0.046	0.046	60	2	22.3	0.009
30	1676	2300	0.44	0.33	2.39	0.041	0.041	60	2	31.9	0.008
31	4470	4160	0.27	0.27	3.31	0.045	0.045	60	2	337	0.007
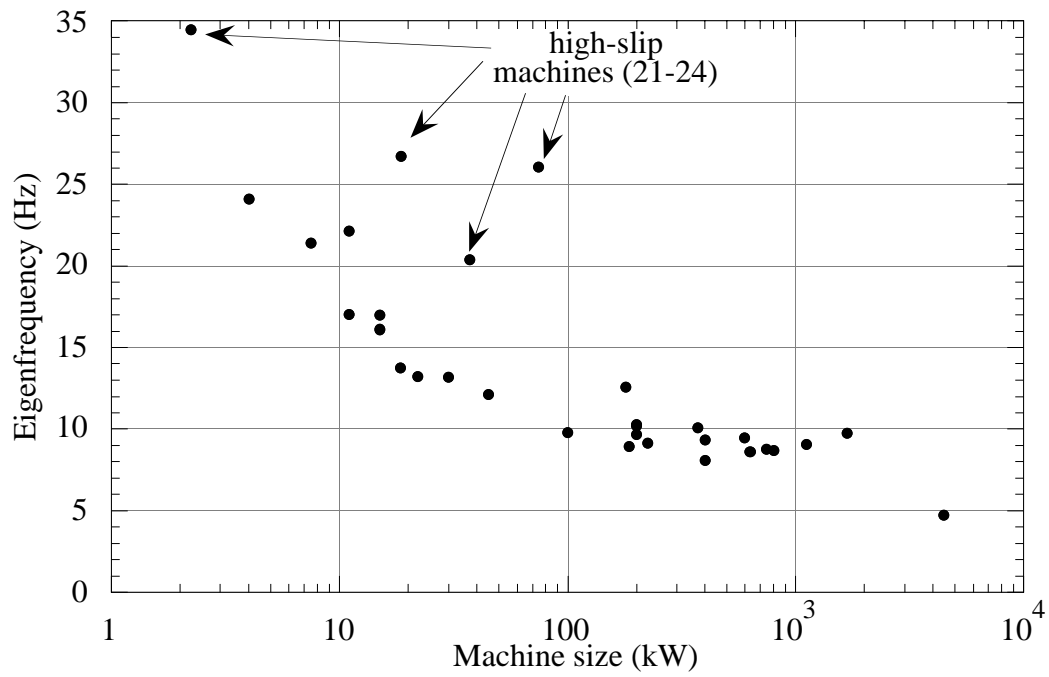
Figure 6.1. Undamped eigenfrequency of the 31 investigated induction machines.
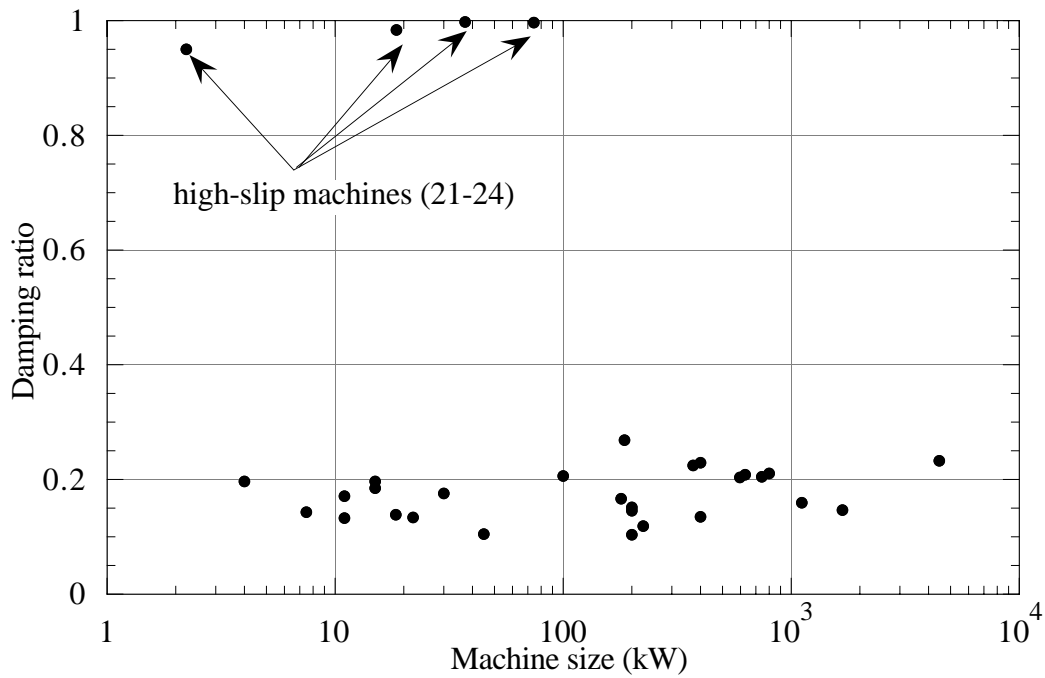
Figure 6.2. Damping ratio of the 31 investigated induction machines.

The result of most of the machines form a general trend. The four high-slip machines 21-24 presented by Cathey et al. (1973) deviate from the trend of the other machines.

From Figure 6.2 it is clear that the four smaller machines described by Cathey et al. (1973) have an extremely high damping ratio, caused by the high rotor resistance, while the damping ratio of the other machines varies between 0.1 and 0.3, independent of the machine size.

The transfer function from shaft torque to electrodynamical torque in which the stator resistance has been neglected, (2.54), can be used to obtain approximate values of the undamped eigenfrequency and damping ratio

$$\omega_{0NSR} = \frac{L_m U}{L_s \omega_s} \sqrt{\frac{p^2}{J_m L'_r}} \qquad (6.2)$$

$$\xi_{NSR} = \frac{R_r}{2} \frac{L_s}{L_m} \frac{\omega_s}{U} \sqrt{\frac{J_m}{p^2 L'_r}} \qquad (6.3)$$

respectively. These equations for estimating the eigenfrequency and damping ratio do not work well when the damping is very high as in the case of machines 21-24. In Figure 6.3 the undamped eigenfrequency obtained using (6.2) is compared with the one obtained using small-signal analysis. Machines 21-24 have been excluded. The prediction of the undamped eigenfrequencies differs less than 1 % for the investigated machines. The prediction of the damping ratio is, however, not as good as the prediction of the eigenfrequency. The error function

$$\varepsilon = \frac{\xi_{NSR} - \xi_{ss}}{\xi_{ss}} \qquad (6.4)$$

is used to determine the error in the prediction of the damping ratio. ξ_{ss} is the damping ratio obtained using small-signal analysis. In Figure 6.4 the error in the prediction of the damping ratio is presented as a function of machine size. Again, machines 21-24 have been excluded.
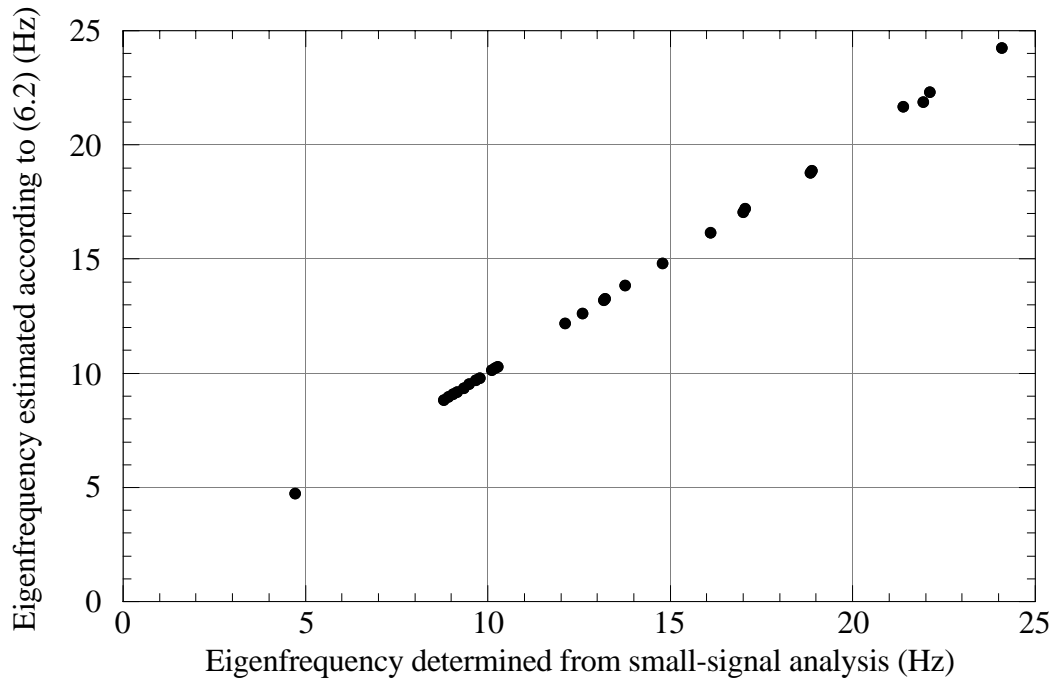
Figure 6.3. Comparison of undamped eigenfrequencies.
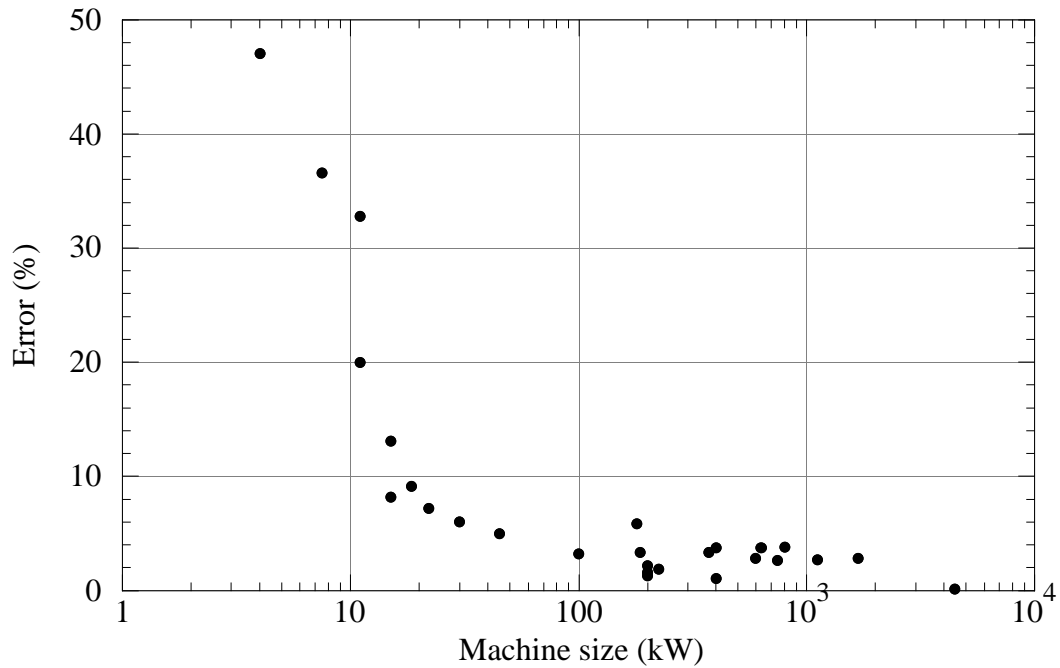
Figure 6.4. ξ error prediction as a function of machine size.

The error is largest for smaller machines, which have relatively high stator resistances compared to the leakage inductances while the error is smaller for the larger machines.

97

In Chapter 4 it was shown that the rotor speed and electrodynamical torque response of the 15 kW machine to shaft torque and supply frequency perturbations could be well predicted using the NSR-model. From Figure 6.4 it can be noted that the NSR-model can even better predict the same responses of larger machines.

The damping ratio strongly influences the performance of the induction machine. The investigated 15 kW machine, operating at 288 V and 43.5 Hz and with an inertia of 0.44 kgm^2, has a damping ratio of 0.28, which means that the rotor speed response at the eigenfrequency is twice the steady-state rotor speed response.

Machine 24, a 100 hp machine with high rated slip, has a damping ratio close to 1. In Figure 6.5 the rotor speed response, calculated using the Park model, NST I-model, LA-model, and ND-model, is presented for the machine. It can be noted that the rotor speed response is not higher than the steady-state response for any perturbation frequency. Further, it can be observed that the values predicted by the NST I and LA-models coincide very with the values predicted by the Park model.

The opposite is the 200 kW machine, number 14, with a damping ratio of 0.11, where the rotor speed response at the eigenfrequency is 20 times (26 dB) the rotor speed response at steady-state. The rotor speed response predicted by the various models of the 200 kW machine is presented in Figure 6.6. Again, the values predicted by the NST I and LA-models coincide very well with the values predicted by the Park model. From Figures 6.5 and 6.6 it is obvious that the first-order model predicts a less erroneous rotor speed response to torque perturbations as the damping ratio increases.

The limit frequencies for the first-order model to determine the rotor speed response to torque perturbations for the investigated machines are presented as a function of the damping ratio in Figure 6.7. The limit frequency is defined as the frequency at which the discrepancy between the investigated model and the Park model exceeds a certain level, in this case 3 dB (41%) and 0.8 dB (10 %).

The four high-slip machines have very high limit frequencies; none of them has an error higher that 3 dB compared to the Park model for perturbation frequencies up to 100 Hz and the machines are thus not visible in Figure 6.7. Two of the high-slip machines have a 0.8 dB limit frequency of 70 % while the other two are not visible in Figure 6.7 since they have an error of less than 0.8 dB for all perturbation frequencies. The limit frequencies for the other machines are between 10 and 40 % depending on the desired accuracy and damping ratio.
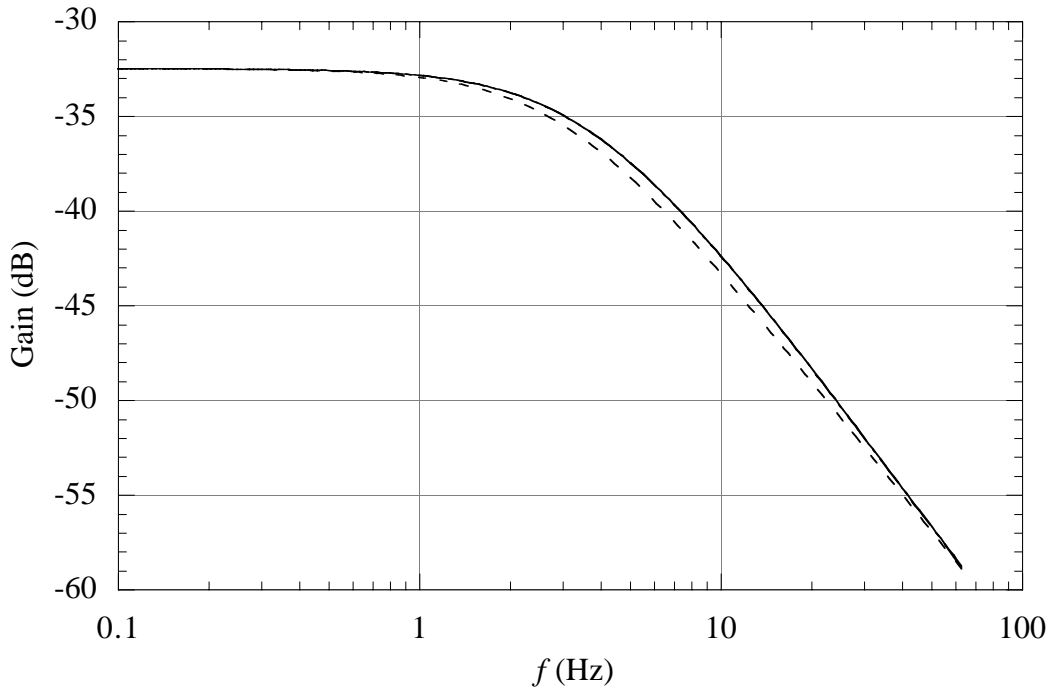
Figure 6.5. Calculated gains of $\Delta\Omega_m/\Delta T_s$ for the 100 hp machine (24). Park model (——),
    NST I(··········), LA(— — —) and ND (- - - - -).
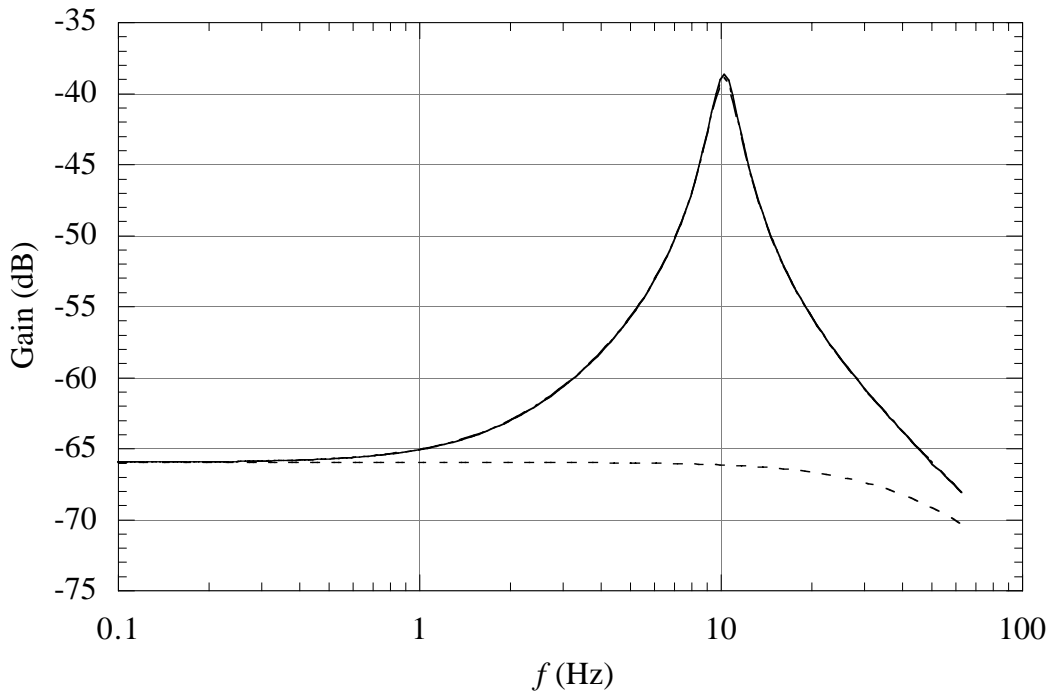
Figure 6.6. Calculated gains of $\Delta\Omega_m/\Delta T_s$ for the 200 kW machine (11). Park model (——),
    NST I(··········), LA(— — —) and ND (- - - - -).
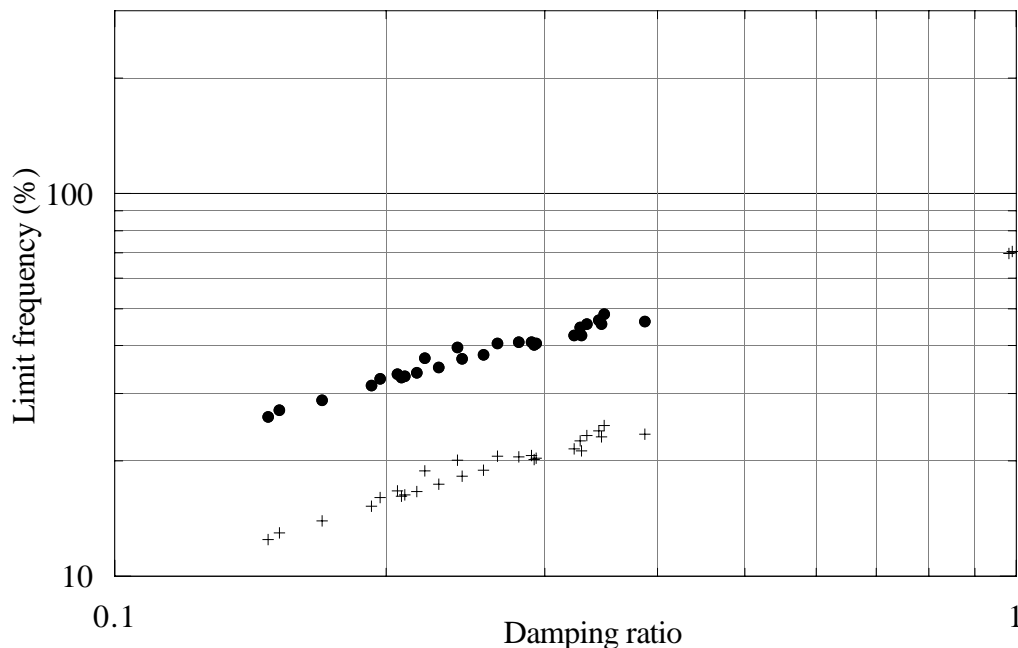
Figure 6.7. Limit frequency for the ND-model to predict the rotor speed response to torque perturbations. Dots are 3 dB error limits and crosses are 0.8 dB error limits. The limit frequencies are expressed as percentage of the eigenfrequencies.

It is important to point out that the damping ratio is of little or no importance for the possibility of using simpler models to predict the other transfer function characteristics.

The 3 dB limit frequencies of the NST-models, LA-model and ND-model were determined for the different transfer functions of the 31 machines. The moments of inertia were twice the values given in Table 6.1, in order to take into account the moments of inertias of load connected to the machines. This means that the damping ratio is increased by 41 % and the eigenfrequency is reduced by 41 % according to (6.3) and (6.2), respectively.

The machines are divided into four groups. Group one consists of the ten smaller machines 1-10, group two consists of machines 11-20, group three of the high-slip machines 21-24, and group four consists of the seven larger machines 25-31 described by Cathey et al. (1973). In Tables 6.2-6.9 the 0.8 dB and 3 dB limit frequencies are presented for the different transfer functions and different models. The machines are operating as motors loaded by rated torque as the limit frequencies of the LA-model is determined and as motor loaded by a one quarter of rated torque as the limit frequencies of the other models are determined. The operating point is in most cases of little importance for the performance of the reduced-order models, except for the LA-model. The limit frequencies of the LA-model are generally lowered as the shaft torque increases, both in motor and generator operation, which is caused by the fact that the damping is

underestimated. Especially erroneous is the prediction of the damping of machines 11-20 in the cases where they are connected to loads having a very low moment of inertia and operating with a shaft torque higher than the rated one.

The limit frequencies are independent of the disturbance magnitude at least up to a voltage magnitude perturbation of 60 % (peak ot peak), a shaft torque perturbation magnitude of 100 % and a supply frequency perturbation magnitude of 10 %. Table 6.2 and 6.3 present the limit frequencies for the ND-model.

Table 6.2. Approximate 0.8 dB limit frequencies for the ND-model.

	1-10	11-20	21-24	25-31	Lowest upper limit for all machines
$\dfrac{\Delta\Omega_m}{\Delta T_s}$	1-4	1	5-99	0.7-1.5	1 *
$\dfrac{\Delta T_e}{\Delta T_s}$	2.5-5	2	15-25	1-2	1 *
$\dfrac{\Delta P}{\Delta T_s}$	2.5-5	2	15-25	1-2	1 *
$\dfrac{\Delta Q}{\Delta T_s}$	0.5-5	1-2	0.5-30	2-5	0.5
$\dfrac{\Delta I_s}{\Delta T_s}$	4-8	2-3	15	1-3	1
$\dfrac{\Delta\Omega_m}{\Delta\omega_s}$	2.5-5	2	7-45	1.2	1 *
$\dfrac{\Delta T_e}{\Delta\omega_s}$	2.5-5	2	7-45	1.2	1 *
$\dfrac{\Delta P}{\Delta\omega_s}$	2.5-5	2	7-40	1-2	1 *
$\dfrac{\Delta Q}{\Delta\omega_s}$	0.1-0.7	0.1	0.3-1.3	0.02-0.3	0.02
$\dfrac{\Delta I_s}{\Delta\omega_s}$	0.07-5	0.004-0.03	0.3-30	0.002-1.3	0.002
$\dfrac{\Delta\Omega_m}{\Delta U}$	0.7-1.5	0.6-0.9	2-3	0.7-1	0.5
$\dfrac{\Delta T_e}{\Delta U}$	0.7-1.5	0.6-0.9	2-3	0.7-1	0.5
$\dfrac{\Delta P}{\Delta U}$	0.03-0.2	0.002-0.02	0.2-4	0.01-1	0.002
$\dfrac{\Delta Q}{\Delta U}$	0.2-1	0.1-0.2	0.9-1.6	0.05-0.2	0.05
$\dfrac{\Delta I_s}{\Delta U}$	0.08-0.5	0.01-0.05	0.2-0.7	0.004-0.1	0.004

* about 30 % of the dominating eigenfrequency for respective machine

Table 6.3. Approximate 3 dB limit frequencies for the ND-model.

	1-10	11-20	21-24	25-31	Lowest upper limit for all machines
$\dfrac{\Delta\Omega_m}{\Delta T_s}$	2-8	2	>100	1.5-3	2 *
$\dfrac{\Delta T_e}{\Delta T_s}$	5-10	4	25-40	2-4	2 *
$\dfrac{\Delta P}{\Delta T_s}$	5-10	4	25-40	2-4	2 *
$\dfrac{\Delta Q}{\Delta T_s}$	1-8	8	1-40	4-9	1
$\dfrac{\Delta I_s}{\Delta T_s}$	5-21	4	25	2-5	2
$\dfrac{\Delta\Omega_m}{\Delta\omega_s}$	4-9	4	40-50	2-4	2 *
$\dfrac{\Delta T_e}{\Delta\omega_s}$	4-9	4	40-50	2-4	2 *
$\dfrac{\Delta P}{\Delta\omega_s}$	4-9	4	40-50	2-4	2 *
$\dfrac{\Delta Q}{\Delta\omega_s}$	0.3-1.5	0.2-0.4	0.5-2.3	0.05-4	0.05
$\dfrac{\Delta I_s}{\Delta\omega_s}$	0.1-7.2	0.01-0.1	15-40	2-5	0.01
$\dfrac{\Delta\Omega_m}{\Delta U}$	1.5-3	1.5	5	1.5-2	1.5
$\dfrac{\Delta T_e}{\Delta U}$	1.5-3	1.5	5	1.5-2	1.5
$\dfrac{\Delta P}{\Delta U}$	0.1-0.6	0.04-3	5	1.5-3	0.01
$\dfrac{\Delta Q}{\Delta U}$	0.5-2.5	0.3-0.4	2-4	0.1-0.5	0.1
$\dfrac{\Delta I_s}{\Delta U}$	0.1-1.2	0.01-0.1	0.5-1.5	0.01-0.2	0.01

* about 55 % of the dominating eigenfrequency for respective machine

The $\Delta\Omega_m$, ΔT_e and ΔP responses to $\Delta\omega_s$ and ΔT_s perturbations predicted by the ND-model could accurately be described for all the machines (except the high-slip machines which have higher limit frequencies) as a percentage of the eigenfrequency. This is not the case with the other combinations of input and output signals. The $\Delta\Omega_m$, ΔT_e and ΔP responses to $\Delta\omega_s$ and ΔT_s perturbations could be determined up to a perturbation frequency of 30 % of the dominating eigenfrequency (i.e. at least up to 2 Hz) before the discrepancy to the Park model reached 10 %.

The $\Delta\Omega_\mathrm{m}$, ΔT_e responses to ΔU perturbations as well as the ΔQ and ΔI_s responses to ΔT_s perturbations can be predicted up to a perturbation frequency of at least 0.5 Hz. The prediction of the other transfer function characteristics is otherwise poor.

The responses predicted by using the ND-model vary strongly between the different induction machine groups. A first-order model of a high-slip machine can better predict the responses of the induction machine while first-order models of other machines have poorer performance. Table 6.4 and 6.5 present the limit frequencies for the LA-model.

Table 6.4. Approximate 0.8 dB limit frequencies for the LA-model.

	1-10	11-20	21-24	25-31	Lowest upper limit for all machines
$\dfrac{\Delta\Omega_\mathrm{m}}{\Delta T_\mathrm{s}}$	3-7	2-3	99	2-4	2
$\dfrac{\Delta T_\mathrm{e}}{\Delta T_\mathrm{s}}$	5-10	3-4	25-55	3-5	3
$\dfrac{\Delta P}{\Delta T_\mathrm{s}}$	5-10	3-4	25-55	3-5	3
$\dfrac{\Delta Q}{\Delta T_\mathrm{s}}$	1-5	1	10-16	1-2	1
$\dfrac{\Delta I_\mathrm{s}}{\Delta T_\mathrm{s}}$	2-7	2	35-50	2-4	2
$\dfrac{\Delta\Omega_\mathrm{m}}{\Delta\omega_\mathrm{s}}$	5-15	3-4	15	4-24	3
$\dfrac{\Delta T_\mathrm{e}}{\Delta\omega_\mathrm{s}}$	5-15	3-4	15	4-24	3
$\dfrac{\Delta P}{\Delta\omega_\mathrm{s}}$	5-15	3-4	15	4-20	3
$\dfrac{\Delta Q}{\Delta\omega_\mathrm{s}}$	0.003-5	0.05-0.1	0.02-0.3	0.02-0.08	0.003
$\dfrac{\Delta I_\mathrm{s}}{\Delta\omega_\mathrm{s}}$	0.1-0.4	0.1-0.2	15	0.3-2.6	0.1
$\dfrac{\Delta\Omega_\mathrm{m}}{\Delta U}$	1-3	1	4	1	1
$\dfrac{\Delta T_\mathrm{e}}{\Delta U}$	1-3	1	4	1	1
$\dfrac{\Delta P}{\Delta U}$	0.1-0.2	0.1	4	0.1-1.5	0.1
$\dfrac{\Delta Q}{\Delta U}$	0.1-1	0.1	0.5-1	0.1	0.1
$\dfrac{\Delta I_\mathrm{s}}{\Delta U}$	0.3-1	0.6-3	0.3-0.9	1-3	0.3

Table 6.5. Approximate 3 dB limit frequencies for the LA-model.

	1-10	11-20	21-24	25-31	Lowest upper limit for all machines
$\dfrac{\Delta\Omega_m}{\Delta T_s}$	6-99	4-6	>100	>100	4
$\dfrac{\Delta T_e}{\Delta T_s}$	6-47	4-6	50-60	50-60	4
$\dfrac{\Delta P}{\Delta T_s}$	6-47	5	50-60	55-60	4
$\dfrac{\Delta Q}{\Delta T_s}$	2-11	2-3	20-50	2-4	2
$\dfrac{\Delta I_s}{\Delta T_s}$	6-40	4-5	45-55	50-60	4
$\dfrac{\Delta\Omega_m}{\Delta\omega_s}$	6-30	5-6	25	40	5
$\dfrac{\Delta T_e}{\Delta\omega_s}$	6-30	5-6	25	40	5
$\dfrac{\Delta P}{\Delta\omega_s}$	6-25	5-6	25	30-35	5
$\dfrac{\Delta Q}{\Delta\omega_s}$	0.02-7.7	0.1-0.3	0.6-10	0.1-0.7	0.02
$\dfrac{\Delta I_s}{\Delta\omega_s}$	0.5-30	4-5	25	35	0.5
$\dfrac{\Delta\Omega_m}{\Delta U}$	1.5-5	1.5	8	1.5-2.5	1.5
$\dfrac{\Delta T_e}{\Delta U}$	1.5-5	1.5	8	1.5-2.5	1.5
$\dfrac{\Delta P}{\Delta U}$	0.3-8	2	8	1.5-3	0.3
$\dfrac{\Delta Q}{\Delta U}$	0.2-2	0.01-0.1	1.5-3	0.01-0.2	0.01
$\dfrac{\Delta I_s}{\Delta U}$	0.5-6	4	1-13	3-9	0.5

The LA-model predicts the ΔT_e, $\Delta\Omega_m$ and ΔP responses to ΔT_s and $\Delta\omega_s$ perturbations up to a perturbation frequency of at least 3 Hz before the discrepancy to the Park model reaches 10 %. The transfer functions $\Delta Q/\Delta T_s$, $\Delta I_s\Delta T_s$, $\Delta\Omega_m/\Delta U$ as well as $\Delta T_e/\Delta U$ can be predicted up to a perturbation frequency of 1.5 Hz. The prediction of the other transfer functions is limited to extremely low-frequency perturbations. The high-slip machines are more successfully modelled by a second-order model than the other machines.

In Table 6.6 and 6.7 the limit frequencies for the NST I-model are presented.

Table 6.6. Approximate 0.8 dB limit frequencies for the NST I-model.

	1-10	11-20	21-24	25-31	Lowest upper limit for all machines
$\dfrac{\Delta\Omega_\mathrm{m}}{\Delta T_\mathrm{s}}$	15-99	>100	>100	>100	15
$\dfrac{\Delta T_\mathrm{e}}{\Delta T_\mathrm{s}}$	15-45	50	50	50	15
$\dfrac{\Delta P}{\Delta T_\mathrm{s}}$	15-45	50	50	50	15
$\dfrac{\Delta Q}{\Delta T_\mathrm{s}}$	10-25	15-20	15-20	15	10
$\dfrac{\Delta I_\mathrm{s}}{\Delta T_\mathrm{s}}$	20-35	40	35-45	35	20
$\dfrac{\Delta\Omega_\mathrm{m}}{\Delta\omega_\mathrm{s}}$	10-15	15	15	18	10
$\dfrac{\Delta T_\mathrm{e}}{\Delta\omega_\mathrm{s}}$	10-15	15	15	18	10
$\dfrac{\Delta P}{\Delta\omega_\mathrm{s}}$	10-15	15	15	18	10
$\dfrac{\Delta Q}{\Delta\omega_\mathrm{s}}$	10-15	15	10-16	18	10
$\dfrac{\Delta I_\mathrm{s}}{\Delta\omega_\mathrm{s}}$	5-15	15	15	18	5
$\dfrac{\Delta\Omega_\mathrm{m}}{\Delta U}$	1-2	1	3	1-1.5	1
$\dfrac{\Delta T_\mathrm{e}}{\Delta U}$	1-2	1	3	1-1.5	1
$\dfrac{\Delta P}{\Delta U}$	0.05-0.4	0.003-0.04	3	0.01-2	0.003
$\dfrac{\Delta Q}{\Delta U}$	10-15	15	15	18	10
$\dfrac{\Delta I_\mathrm{s}}{\Delta U}$	7-17	5	15	3-15	3

Table 6.7. Approximate 3 dB limit frequencies for the NST I-model.

	1-10	11-20	21-24	25-31	Lowest upper limit for all machines
$\dfrac{\Delta\Omega_{\mathrm{m}}}{\Delta T_{\mathrm{s}}}$	>100	>100	>100	>100	>100
$\dfrac{\Delta T_{\mathrm{e}}}{\Delta T_{\mathrm{s}}}$	40-50	50	50-55	55	40
$\dfrac{\Delta P}{\Delta T_{\mathrm{s}}}$	40-50	50	50-55	55	40
$\dfrac{\Delta Q}{\Delta T_{\mathrm{s}}}$	20-25	25	30	25	20
$\dfrac{\Delta I_{\mathrm{s}}}{\Delta T_{\mathrm{s}}}$	20-40	45	40-50	50-60	20
$\dfrac{\Delta\Omega_{\mathrm{m}}}{\Delta\omega_{\mathrm{s}}}$	25-30	25	30	32	25
$\dfrac{\Delta T_{\mathrm{e}}}{\Delta\omega_{\mathrm{s}}}$	25-30	25	30	32	25
$\dfrac{\Delta P}{\Delta\omega_{\mathrm{s}}}$	25	25	30	32	25
$\dfrac{\Delta Q}{\Delta\omega_{\mathrm{s}}}$	25	25	30	32	25
$\dfrac{\Delta I_{\mathrm{s}}}{\Delta\omega_{\mathrm{s}}}$	10-30	25	30	33	10
$\dfrac{\Delta\Omega_{\mathrm{m}}}{\Delta U}$	2-4	2	4-5	2	2
$\dfrac{\Delta T_{\mathrm{e}}}{\Delta U}$	2-4	2	4-5	2	2
$\dfrac{\Delta P}{\Delta U}$	4-7	2-6	5	2-3	2
$\dfrac{\Delta Q}{\Delta U}$	20-30	28	30	33	20
$\dfrac{\Delta I_{\mathrm{s}}}{\Delta U}$	25	25	30	25	25

Again, the samme pattern can be observed: The high-slip machines are best suited to be modelled by the NST I-model. The NST I-model can predict with a 10 % accuracy the responses to ΔT_{s} and $\Delta\omega_{\mathrm{s}}$ perturbations up to at least 10 Hz (20 Hz with a 3 dB accuracy) except for the prediction of $\Delta I_{\mathrm{s}}/\Delta\omega_{\mathrm{s}}$, which is limited to 5 Hz (10 Hz with a 3 dB accuracy). The 10 % error frequency limit for $\Delta\Omega_{\mathrm{m}}/\Delta U$ and $\Delta T_{\mathrm{e}}/\Delta U$ is about 1 Hz, for $\Delta Q/\Delta U$ 10 Hz and for $\Delta I_{\mathrm{s}}/\Delta U$ 5 Hz. The ΔP response to ΔU perturbations has an extremely low limit frequency for a 10 % accuracy, for a 3dB accuracy the limit frequency is about 2 Hz.

In Table 6.8 and 6.9 the limit frequencies for the NST III-model are presented.

Table 6.8. Approximate 0.8 dB limit frequencies for the NST III-model.

	1-10	11-20	21-24	25-31	Lowest upper limit for all machines
$\dfrac{\Delta\Omega_\mathrm{m}}{\Delta T_\mathrm{s}}$	>100	>100	>100	>100	>100
$\dfrac{\Delta T_\mathrm{e}}{\Delta T_\mathrm{s}}$	30-40	50	45-55	50	30
$\dfrac{\Delta P}{\Delta T_\mathrm{s}}$	30-40	50	45-55	50	30
$\dfrac{\Delta Q}{\Delta T_\mathrm{s}}$	13-22	15	20	15	15
$\dfrac{\Delta I_\mathrm{s}}{\Delta T_\mathrm{s}}$	15-35	40	30-40	35-50	15
$\dfrac{\Delta\Omega_\mathrm{m}}{\Delta\omega_\mathrm{s}}$	30	28	30	35	30
$\dfrac{\Delta T_\mathrm{e}}{\Delta\omega_\mathrm{s}}$	15-21	16	20	20	15
$\dfrac{\Delta P}{\Delta\omega_\mathrm{s}}$	0.5-20	16	20	20	15
$\dfrac{\Delta Q}{\Delta\omega_\mathrm{s}}$	2-15	16	1	20	1
$\dfrac{\Delta I_\mathrm{s}}{\Delta\omega_\mathrm{s}}$	4-20	16	15-30	20	4
$\dfrac{\Delta\Omega_\mathrm{m}}{\Delta U}$	5-15	15	7	15	5
$\dfrac{\Delta T_\mathrm{e}}{\Delta U}$	0	0	0	0	0
$\dfrac{\Delta P}{\Delta U}$	0.08-2	0.001-0.8	0.002-0.04	0.001-0.3	0.0003
$\dfrac{\Delta Q}{\Delta U}$	15-20	16	25	18	15
$\dfrac{\Delta I_\mathrm{s}}{\Delta U}$	10-15	6-12	0.7-13	0.5-12	0.5

Table 6.9. Approximate 3 dB limit frequencies for the NST III-model.

	1-10	11-20	21-24	25-31	Lowest upper limit for all machines
$\dfrac{\Delta\Omega_m}{\Delta T_s}$	>100	>100	>100	>100	>100
$\dfrac{\Delta T_e}{\Delta T_s}$	40-50	50	50	55	40
$\dfrac{\Delta P}{\Delta T_s}$	40-50	50	50	55	40
$\dfrac{\Delta Q}{\Delta T_s}$	20-30	25	30	25	25
$\dfrac{\Delta I_s}{\Delta T_s}$	25-45	45	40-50	50-60	25
$\dfrac{\Delta\Omega_m}{\Delta\omega_s}$	40-60	40	45	45	40
$\dfrac{\Delta T_e}{\Delta\omega_s}$	30-35	30	35	35	30
$\dfrac{\Delta P}{\Delta\omega_s}$	30	25	35	35	25
$\dfrac{\Delta Q}{\Delta\omega_s}$	30	25	30-35	35	25
$\dfrac{\Delta I_s}{\Delta\omega_s}$	6-30	28	35	35	6
$\dfrac{\Delta\Omega_m}{\Delta U}$	25	27	7-30	35	25
$\dfrac{\Delta T_e}{\Delta U}$	0	0	0-2	0	0
$\dfrac{\Delta P}{\Delta U}$	1-4	0.04-1.5	0.007-0.1	0.003-2	0.0006
$\dfrac{\Delta Q}{\Delta U}$	28-34	28	35	35	30
$\dfrac{\Delta I_s}{\Delta U}$	25-30	25	20-35	20-30	20

The NST III-model has generally somewhat higher limit frequencies than the NST I-model. However, the prediction of $\Delta Q/\Delta\omega_s$, $\Delta I_s/\Delta\omega_s$, $\Delta T_e/\Delta U$, $\Delta P/\Delta U$, $\Delta Q/\Delta U$ and $\Delta I_s/\Delta U$ using the NST III-model is limited to lower frequencies compared to using the NST I-model.

For power system analysis, the most interesting quantities are the active and reactive power responses to voltage and frequency disturbances. It can be observed that first- and second-order models are not well suited for this task. Further, it can be observed that the NST III-model is less suited than the NST I-model for this assignment. The NST I-model can predict the reactive power response up to at least 10 Hz with an error less than 10 %. The active power response predicted by a third-order model is less accurate. However, the magnitude of the active power response to frequency and voltage perturbations is low as long as the disturbances are limited to a few Hz and is thus not as important to model correctly as the reactive power response. The other responses are of minor importance for power system analysis.

It is possible to use either a first-order or second-order model to model the induction machine as a wind turbine generator. This is providing that it is the mechanical system that is studied, rather than the electrical impact of the wind turbine on the grid. The dominating eigenfrequency of a 225 kW wind turbine is about 1.5 Hz and a MW-size wind turbine has a dominating eigenfrequency of about 0.8 Hz. Below 30 % of the dominating eigenfrequency, a first-order model predicts results with an error less than 10 %. At higher perturbation frequencies, a second-order model is a more suitable choice.

7. CONCLUSIONS

The Park model very well predicts the rotor speed, electrodynamical torque, active power, reactive power and stator current responses to perturbations in the shaft torque, supply frequency and voltage magnitude. The predicted electric power and stator current responses to very low-frequency perturbations in the voltage magnitude are improved if the iron losses are taken into account.

The performance of the reduced-order models, i.e. the models of lower order than the Park model, depends on the type of induction machine investigated. High-slip machines as well as machines that have a low ratio between the stator resistance and leakage reactances are best suited to be represented by reduced-order models. Small machines and machines having a rated voltage that is lower than "the normal rated voltage for a machine of that size" are more difficult to represent by reduced-order models.

The first-order model, ND-model, of the induction machine can be used to predict the rotor speed, electrodynamical torque and active power responses to torque and frequency perturbations up to a perturbation frequency of 30 % of the eigenfrequency if an error of 10 % is acceptable, i.e., 10 % discrepancy between the results predicted by the ND-model and the Park model. MW-size machines have an eigenfrequency of about 5-10 Hz and machines with a rating of a few kW have an eigenfrequency of about 25 Hz. The damping ratio of induction machines varies strongly but is usually not important in determining the frequency region in which a reduced-order model can be used.

The ND-model can also be used to predict the rotor speed and electrodynamical torque responses to voltage magnitude perturbations up to a perturbation frequency of 0.5 - 5 Hz depending on the accuracy desired as well as machine investigated. A high ratio between the stator resistance and leakage reactances leads to a lower value while a high-slip machine has a higher value.

The LA-model, a non-linear second-order model, predicts the rotor speed, electrodynamical torque and electric power responses to torque and frequency perturbations up to a perturbation frequency of at least 3 Hz, if an error of 10 % is acceptable. The discrepancy between the results obtained using the LA-model and the Park model depends strongly on the static shaft torque. At no-load, the LA-model can be used to determine the responses to higher perturbation frequencies. In predicting the responses to voltage magnitude perturbations, the LA-model is approximately as useful as a first-order model.

The simpler third-order model, the NST I-model, predicts well all the responses to torque and frequency perturbations up to at least 10 Hz if an error of 10 % is acceptable. In predicting the rotor speed, electrodynamical torque and electric power responses to voltage magnitude perturbations, the NST I-model is as useful as a first- or second-order model. Stator current and reactive power responses can, however, be predicted much better than by an LA- or ND-model, up to a perturbation frequency of at least 10 Hz for the reactive power response and at least 3 Hz for the stator current response.

The more advanced third-order model, the NST III-model, generally predicts better responses than the NST I-model. However, the stator current and reactive power responses to frequency and voltage perturbations are predicted less accurately and the electrodynamical torque response to voltage perturbations is inaccurate also for extremely low-frequency perturbations.

The conclusion drawn here is that for power system analysis it is suitable to use the NST I-model if the computational effort is a problem, otherwise a Park model is, of course, the best choice. The advantage of the NST I-model is that the reactive power response to supply frequency and voltage magnitude perturbations is well predicted up to at least 10 Hz.

Two reduced-order linear models were investigated: a first-order model, the LD-model and a second-order model, the NSR-model. These models are not suited to determine the electrical impact of induction machines. Instead, the field of application for these models is to represent the induction machine in mechanical systems, for instance, in a wind turbine or a reciprocating compressor drive. An example was demonstrated where the drive-train of a wind turbine was modelled using the LD-model and the NSR-model to represent the induction generator. The ND-model is suitable to use if the upper perturbation frequency is about 0.5 Hz while the NSR-model can handle perturbation frequencies up to at least 10 Hz. The rotor speed and electrodynamical torque responses of these models are very similar to those predicted by non-linear models of the same orders. The difference is that the linear models do not predict a correct steady-state response.

The responses to supply frequency and torque perturbations depend only slightly on the static shaft torque if temperature changes are not taken into account. Since the damping of the machine is mainly governed by the rotor resistance, the damping is improved substantially as the machine gets warmer; the damping ratio can be increased by 100 % for the investigated 15 kW machine compared to the case where the machine is cold. The

response to voltage magnitude perturbations, on the other hand, depends strongly on the static shaft torque, even if temperature changes are not taken into account.

In the steady-state operating region, the skin effect in the rotor winding is of minor importance for the investigated 15 kW machine; the damping was improved by about 10 %. At nominal flux levels or below nominal flux levels, the main flux saturation only slightly affected the responses of the investigated machine. At a flux level of 120 % of the nominal one, the very low-frequency rotor speed and electrodynamical torque responses were influenced by the main flux saturation.

The induction machine characteristics are strongly influenced by the steady-state supply frequency even if the flux in the machine is kept constant. As the supply frequency is lowered, the damping ratio is reduced as well. For the 15 kW machine, the damping ratio was reduced to about one third as the supply frequency was lowered from 43.5 to 15 Hz.

REFERENCES

Adkins, B., Harley, R., 1975. "*The general theory of alternating current machines: application to practical problems*", Chapman and Hall, London

Ahmed-Zaid, S., Taleb, M., 1991. "Structural modeling of small and large induction machines using integral manifolds", *IEEE Transactions on Energy Conversion*, vol. 6, no. 3, pp. 529-535

Al-Bahrani, A.H., Mohamadein, A.L., Al-Ohaly, A.A., 1988. "Dynamic response of a group of induction motors operating in parallel", *Electric Machines and Power Systems,* vol.15, pp. 269-281

Cathey, J.J., Cavin, R.K., Ayoub, A.K., 1973. "Transient load model of an induction motor", *IEEE Transactions on Power Apparatus and Systems*, vol. 92, no. 4, pp. 1399-1406

Crow, M.L., 1994. "Dynamics of voltage instability and collapse", *International Journal of Electric Power and Energy Systems*, vol. 16, no. 4, pp. 235-241

de Mello, F.P., Hannett, L.N., 1981. "Large scale induction generators for power systems", *IEEE Transactions on Power Apparatus and Systems*, vol. 100, no. 5, pp. 2610-2618

Deleroi,W., 1970. "Berücksichtigung der Eisensättigung für dynamische Betriebs-zustände", *Archiv für Elektrotechnik*, vol. 54, pp. 31-42

Dell'Aquila, A., Salvatore, L., Savino, M., 1984. "Analysis and development of detailed inverter-fed induction machine equivalent circuits from standstill frequency response and on-line harmonic impedance measurements", *in Conference Proceedings of the International Conference on Electrical Machines (ICEM'84)*, Lausanne, Switzerland, 18-21 September 1984, pp. 376-379

Derbel, N., Kamoun, M.B.A., Poloujadoff, M., 1995. "On the order reduction of induction machine during start-up", *IEEE Transactions on Energy Conversion*, vol. 10, no. 4, pp. 655-660

Ertem, S., Baghzouz, Y., 1988. "A fast recursive solution for induction motor transients", *IEEE Transactions on Industry Applications*, vol. 24, no. 5, pp. 758-764

Ertem, S., Baghzouz, Y., 1989. "A variable-order model of induction machines", *International Journal of Modelling and Simulation*, vol. 9, no. 2, pp. 44-48

Estanqueiro, A.I., Aguiar, R., Saraiva, J.G., Castro, R.M.G., Ferriera de Jesus, J.M., 1993. "The development and application of a model for power output fluctuations in a wind park", *Proceedings of 1993 European Community Wind Energy Conference (ECWEC'93)*, Lübeck-Travemünde, Germany, 8-12 March 1993, pp. 798-801

Freise, W., Jordan, H., Nacke, H., 1964. "Experimentelle Ermittlung der erzwungenen Pendelungen von Drehstrom-Asynchronmaschinen", *ETZ-A* vol. 85, no. 12, pp. 370-372

Hakim, M.M.A., Berg, G.J., 1976. "Dynamic single-unit representation of induction motor groups", *IEEE Transactions on Power Apparatus and Systems*, vol. 95, no. 1, pp. 155-161

Hallenius, K.E., 1982. "Contributions to the theory of saturated electrical machines", Doctoral Thesis, Technical Report no. 122, Chalmers University of Technology, Göteborg, Sweden

Healey, R.C., Williamson, S., Smith, A.C., 1995. "Improved cage rotor models for vector controlled induction motors", *IEEE Transactions on Industry Applications*, vol. 31, no. 4, pp. 812-822

Hinrichsen, E.N., Nolan, P.J., 1982. "Dynamics and stability of wind turbine generators", *IEEE Transactions on Power Apparatus and Systems*, vol. 101, no. 8, pp. 2640-2648

Iliceto, F., Capasso, A., 1974. "Dynamic equivalents of asynchronous motor loads in system stability studies", *IEEE Transactions on Power Apparatus and Systems*, vol. 93, no. 5, pp. 1650-1659

Khalil, N.A., Tan, O.T., Baran, I.U., 1982. "Reduced order models for double-cage induction motors", *IEEE Transactions on Power Apparatus and Systems*, vol. 101, no. 9, pp. 3135-3140

Kovacs, P.K., 1984. "*Transient phenomena in electrical machines*", Elsevier, Budapest

Krause, P.C., Rodriguez, F.D., Wasynchuk, O., Mojica, D.A., 1987. "Neglecting stator transients when representing isolated operation of induction machines", *IEEE Transactions on Power Systems*, vol. 2, no. 1, pp. 183-188

Kron, A.W., Lorenzon, H.W., 1969. "Die selbsterregten Pendelungen von Drehstrom-Asynchronmaschinen", *ETZ-A*, vol. 90, no. 9, pp. 200-205

Kylander, G., 1995. "Thermal modelling of small cage induction motors", Doctoral Thesis, Technical Report no. 265, Chalmers University of Technology, Göteborg, Sweden

Leonhard, A., 1966. "Die Asynchronmaschine bei periodischen und sprungartigen Belastungsänderungen", *Elektrotechnik und Maschinenbau*, vol. 83, no. 6, pp. 357-359

Lorenzen, H.W., 1967. "Der Einfluβ der Stromverdrängung auf die erzwungenen Pendelungen von Asynchronmaschinen", *ETZ-A*, vol. 88, no. 18, pp. 445-451

Mayeda, T., Komukai, T., Uemura, Y., Satoh, S., 1985. "Some considerations on oscillation modes of power systems including induction motors", *Electrical Engineering in Japan*, vol. 105, no. 3, pp. 113-122, USA

Melkebeek, J.A.A., 1980. "Stabiliteitsonderzoek van de Spanningsgevoede Induktie-motor", Doctoral thesis, Gent State University, Gent, Belgium

Melkebeek, J.A.A., 1983. "Magnetising-field saturation and dynamic behaviour of induction machines. Part 1: Improved calculation method for induction-machine dynamics", *IEE Proceedings B*, vol. 130, no. 1, pp. 1-9

Meyer, A., 1976. "Einfluss der Stromverdrängung auf den stationären Betrieb und die erzwungenen Pendelungen von Asynchronmaschinenen", *Brown Boveri Mitteilungen*, vol. 63, no. 8, pp. 500-507

Mohamadein, A.L., 1978. "Generalised chart, load angle, and stability limit in induction motors", *Electric Machines and Electromechanics*, vol. 3, no. 1, pp. 65-74

Mohamadein, A.L., Al-Bahrani , A.H., Al-Ohaly, A., 1986. "Dynamic performance of a group of induction motors using load-angle approach", *in Conference Proceedings of the International Conference on Electrical Machines (ICEM'86)*, München, Germany, 8-10 September 1986, pp. 959-962

Nacke, H., 1962. "Schwingungsverhalten des Asynchronmotors", *ETZ-A*, vol. 83, no. 24, pp. 793-797

Ohtsuki, H., Yokoyama, A., Sekine, Y., 1991. "Reverse action of on-load tap changer in association with voltage collapse", *IEEE Transactions on Power Systems*, vol. 6, no. 1, pp. 300-306

Ojo, O.J., Consoli, A., Lipo, T.A., 1990. "An improved model of saturated induction machines", *IEEE Transactions on Industry Applications*, vol. 26, no. 2, pp. 212-221

Palit, B.B., 1978. "Eigenwertuntersuchungen an einer Drehstrom-Asynchronmachine bei selbsterregten Drehschwingungen", *Bull. SEV/VSE*, vol. 69, no. 8, pp. 371-376

Peterson, B., 1991. "*Oscillations in inverter fed induction motor drives*", Licentiate thesis, Lund Institute of Technology, Lund, Sweden

Proakis, J.G., Manolakis, D.G., 1988. "*Introduction to digital signal processing*", Macmillan Publishing Company, New York

Rahim, A., Laldin, A.R., 1987. "Aggregation of induction motor loads for transient stability studies", *IEEE Transactions on Energy Conversion*, vol. 2, no. 1, pp. 55-61

Richards, G.G., Tan, O.T., 1981. "Simplified models for induction machine transients under balanced and unbalanced conditions", *IEEE Transactions on Industry Applications*, vol. 17, no. 1, pp. 15-21

Richards, G.G., Tan, O.T., 1986. "Decomposed, reduced order model for double-cage induction machines", *IEEE Transactions on Energy Conversion*, vol. 1, no. 3, pp. 87-93

Richards, G.G., 1989. "Reduced order models for an induction motor group during bus transfer", *IEEE Transactions on Power Systems*, vol. 4, no. 2, pp. 494-498

Rodriguez, F.D., Wasynczuk, O., 1987. "A refined method of deriving reduced order models of induction machines", *IEEE Transactions on Energy Conversion*, vol. 2, no. 1, pp. 31-37

Sheinman, Y., Rosen, A., 1991. "A dynamic model for performance calculations of grid-connected horizontal axis wind turbines", *Wind Engineering*, vol.15, no.4, pp.211-239

Santjer, F., Gerdes, G., 1994. "Netzrückwirkungen, verursacht durch den Betrieb von Windkraftanlagen am Netz", *DEWI Magazin,* no.5, pp. 35-41

Sekine, Y., Ohtsuki, H., 1990. "Cascaded voltage collapse", *IEEE Transactions on Power Systems*, vol. 5, no. 1, pp. 250-256

Ueda, R., Takata, S., 1981. "Effects of induction machine load on power system", *IEEE Transactions on Power Apparatus and Systems*, vol. 100, no. 5, pp. 2555-2562

Wasynczuk, O., Diao, Y-M., Krause, P.C., 1985. "Theory and comparison of reduced order models of induction machines", *IEEE Transactions on Power Apparatus and Systems*, vol. 104, no. 3, pp. 598-606

Wilkie, J., Leithead, W.E., Anderson, C., 1990. "Modelling of wind turbines by simple models", *Wind Engineering*, vol. 14, no. 4, pp. 247-274

APPENDIX A. DETERMINATION OF THE INDUCTION MACHINE PARAMETERS

In this Appendix the parameters of the investigated 15 kW machine are determined. The parameters given by the manufacturer of the 15 kW induction machine investigated are presented together with the measured values in Table A.1. The equivalent circuit of the induction machine with the iron loss equivalent is presented in Figure A.1.

Table A.1. Measured values and values given by the manufacturer of the investigated 15 kW machine. (Resistances referred to 20 °C)

Parameter		Value given by the manufacturer	Measured/used values
R_s	stator resistance	0.18 Ω	0.184 Ω
R_r	rotor resistance	0.19 Ω	0.175 Ω
L_m	magnetizing inductance	42.6 mH	27 - 43 mH
$L_{s\lambda}$	stator leakage inductance	2.55 mH	2.55 mH
$L_{r\lambda}$	rotor leakage inductance	2.07 mH	2.00 mH
J	moment of inertia	0.205 kgm^2 (*) 0.45 kgm^2 (**)	0.45 kgm2
R_m	iron loss equivalent resistance	166 Ω (50 Hz)	135 Ω (43.5 Hz) 97-48 Ω (30 Hz)
U	voltage	380 V	288 V
f	frequency	50 Hz	43.5 Hz

(*) induction machine inertia only.

(**) inertia of induction machine, dc-machine (0.22 kgm^2) and the two torque transducer couplings (2 times 0.0125 kgm^2).
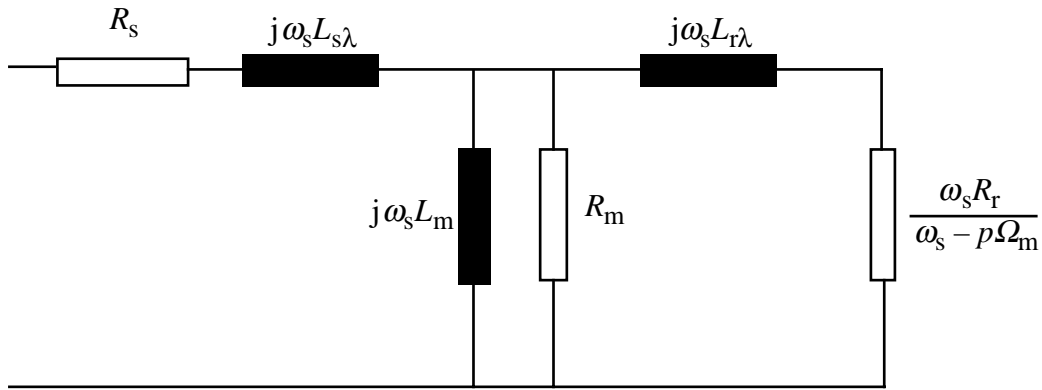
Figure A.1. The equivalent circuit with an iron loss equivalent resistance added in parallel with the magnetizing inductance.

Determining resistance and leakage inductance of the stator

Since no suitable method of separating the stator and rotor leakage inductances was available, the stator leakage inductance is assumed to be 2.55 mH, which is the value provided by the manufacturer. Anyway, the separation of the leakage inductances to the rotor and stator is of little importance for the dynamic performance of the machine, as long as the total leakage inductance is correct (Grantham 1985, Akbaba et al. 1995). The stator resistance was measured to be 0.184 Ω at 20 °C.

Determination of magnetizing inductance

The magnetizing inductance, L_m, was determined in the conventional way by means of a no load test performed at different voltage levels. The magnetizing inductance was also determined as a function of the temperature for a given flux level. In Figures A.2 and A.3 the measured magnetizing inductance is presented as a function of the magnetizing current, i_m, and rotor temperature together with linear function approximations. The machine is operating at no load.
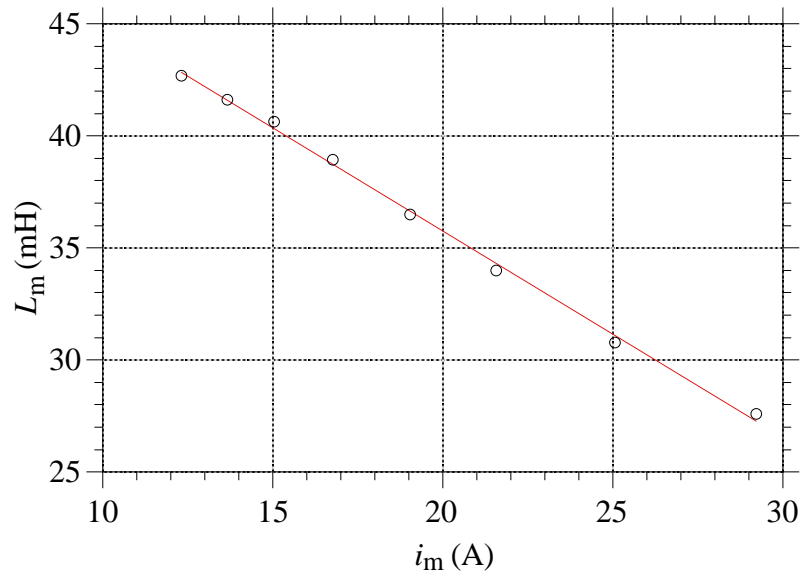
Figure A.2. Measured magnetizing inductance as a function of the magnetizing current. Rotor temperature 40 ℃.
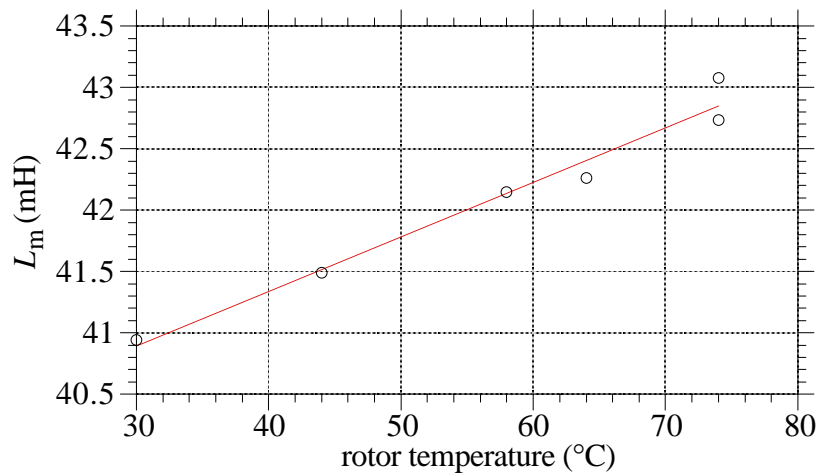
Figure A.3. Measured magnetizing inductance as a function of the rotor temperature. U = 288 V, f = 43.5 Hz.

The magnetizing inductance may be represented as a linear function of the magnetizing current and rotor temperature T:

$$L_m = k_1 - k_2 i_m + k_3 T \qquad \text{(A.1)}$$

where

$$k_1 = 14.64 \text{ H} \qquad \text{(A.2)}$$

$$k_2 = 0.921 \text{ H/A} \tag{A.3}$$

$$k_3 = 0.04471 \text{H/°C} \tag{A.4}$$

for 12 A $< I_\mathrm{m} <$ 29 A and 30 °C $< T <$ 80 °C

Determination of iron loss equivalent resistance

The iron loss equivalent resistance R_m was determined in the conventional way from a no load test performed at various voltages and at some different frequencies. At 43.5 Hz, R_m was found to be 135 Ω and at 50 Hz R_m was found to be 160 Ω, which is very close to the value given by the manufacturer, 166 Ω. At 30 Hz R_m was found to be 97 Ω.

Determination of rotor leakage inductance

The rotor leakage inductance was determined from a locked-rotor test performed at a supply frequency of 10 Hz in order to avoid the influence of the skin effect in the rotor winding. The stator current used was varied between 10 and 40 A in order to determine at which current level saturation of the leakage inductances becomes important. The rated rotor current (referred to the stator winding) is 22 A. Up to a rotor current of 30 A the leakage inductance was constant and at a rotor current of 38 A, the leakage inductance had been lowered by 2 %. In order to determine the rotor leakage inductance, the equivalent circuit presented in Figure A.1 was used. Apart from the rotor leakage inductance, the rotor resistance had not yet been determined. However, the rotor resistance value affected the determination of the rotor leakage inductance only slightly, so the rotor resistance was assumed to be 0.19 Ω according to the manufacturer data. The rotor leakage inductance was found to be 2.03 mH, somewhat less than the value given by the manufacturer.

Determination of rotor resistance

The rotor resistance, R_r, was not determined from the locked rotor test since the accuracy of the rotor resistance value may be better by determining the rotor resistance from a load test. The shaft torque was varied from about rated torque at motor operation to about rated torque at generator operation at a voltage of 288 V and at a supply frequency of 43.5 Hz. The measured power-slip, torque-slip and reactive power-slip curves are presented together with curves calculated using two different rotor resistances in Figures A.4-A.6
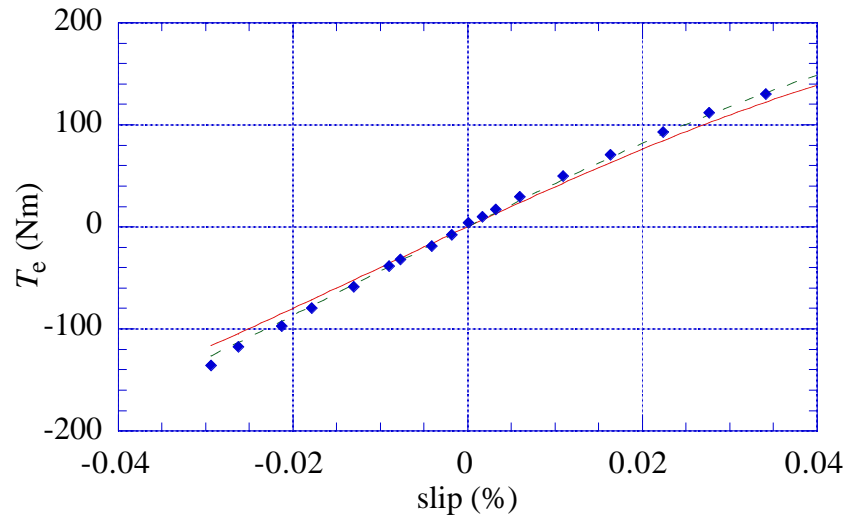
Figure A.4. Measured and calculated torque-slip curves. Dots represent measured values and lines show calculated ones. Solid line with R_r = 0.19 Ω and dashed line with R_r = 0.175 Ω (at 20 °C).
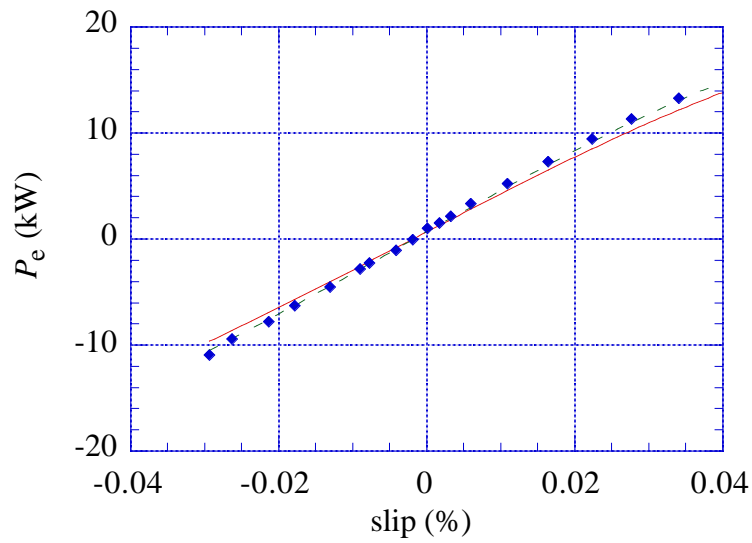
Figure A.5. Measured and calculated electric power-slip curves. Dots represent measured values and lines show calculated ones. Solid line with R_r = 0.19 Ω and dashed line with R_r = 0.175 Ω (at 20 °C).
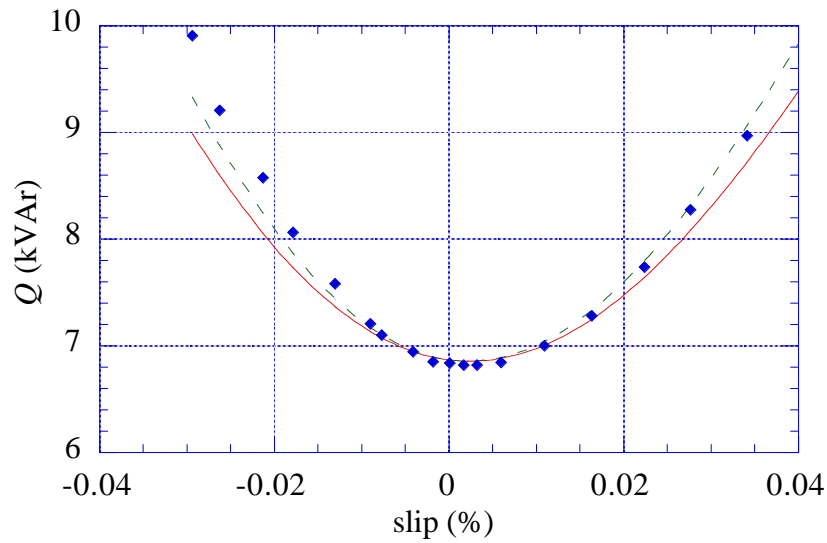
Figure A.6. Measured and calculated reactive power-slip curves. Dots represent measured values and lines show calculated ones. Solid line with $R_r = 0.19$ Ω and dashed line with $R_r = 0.175$ Ω (at 20 ℃).

As can be noted from Figures A.4-A.6, a rotor resistance of 0.175 Ω predicts the static behaviour of the induction machine better than the value of 0.19 Ω given by the manufacturer.

Locked rotor test at variable frequency

The purpose of the variable-frequency locked-rotor test is to determine the rotor cage characteristics. From the measured characteristics a multiple-cage rotor configuration can be adapted.

The locked rotor test was performed at different voltage levels and at different supply frequencies. Throughout the locked rotor measurements, the machine temperature was kept constant. In order to obtain a voltage with a low harmonic content, a synchronous generator was used for feeding the machine. The voltages, currents, frequency and power factor were measured by means of a digital power meter and the torque was measured by a torque transducer. The locked-rotor torque was determined as the average torque over one cogging period. The current levels were kept below the rated current in order not to saturate the machine.

Knowing the magnetizing inductance, the stator leakage inductance and the stator resistance, the resistance and leakage inductance of the rotor were determined using the equivalent circuit presented in Figure A.1. Compared to usual locked rotor tests, the

difference here is that the locked rotor torque is measured. This makes a more accurate determination of the rotor resistance possible.

The rotor resistance is usually determined from the locked-rotor resistance

$$R_k \approx R_s + (\frac{L_m}{L_m + L_{r\lambda}})^2 R_r + R_{cl} \tag{A.5}$$

where R_{cl} is an equivalent resistance representing the core losses and additional losses. R_{cl} is usually not taken into account, which means that the rotor resistance value becomes somewhat too high. With the knowledge of the locked-rotor torque, it is possible to separate R_{cl} from R_r.

The rotor leakage inductance and rotor resistance measured by the locked rotor test are presented in Figure A.7 and Figure A.8, respectively. The measured rotor winding characteristics were then used to determine the parameters of the double-cage rotor winding.
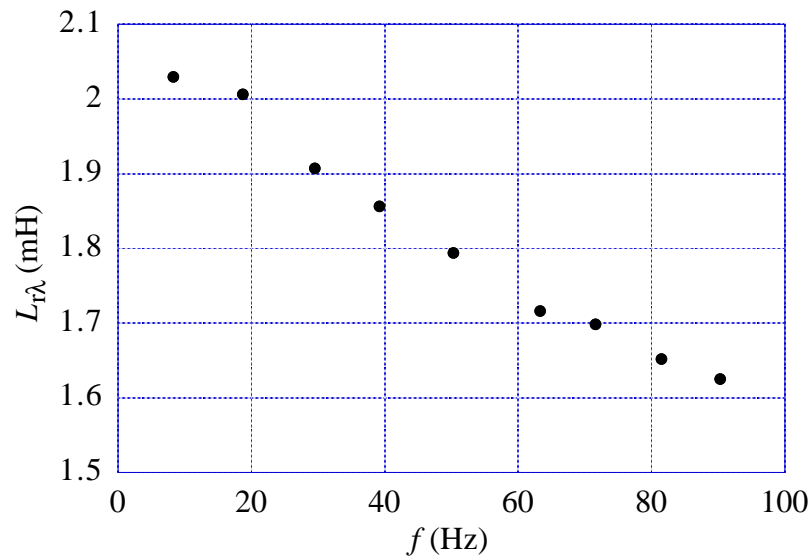
Figure A.7. Measured rotor leakage inductance.

127
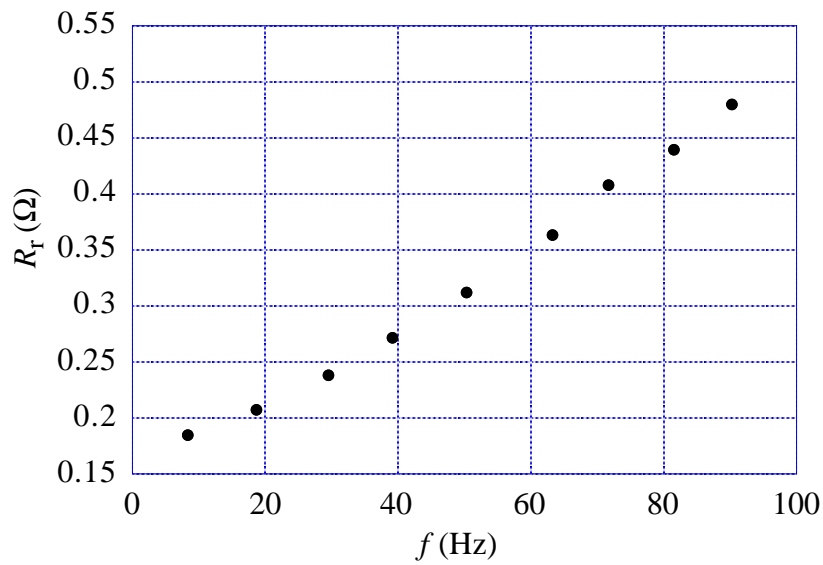
Figure A.8. Measured rotor resistance.

References

Akbaba, M., Taleb, M., Rumeli, A., 1995. "Improved estimation of induction machine parameters", *Electric Power Systems Research*, 34, p. 65-73

Grantham, C., 1985, "Determination of induction motor parameter variations from a variable frequency standstill test". *Electric Machines and power systems*, 10:239-248

APPENDIX B. PROCEDURE TO DERIVE THE NST I MODEL

The procedure to derive the NST-models have been presented by, for example, Rodriguez and Wasynczuk (1987). In this Appendix only the NST I-model will be derived.

The cage induction machine equations can be expressed as

$$p\Psi_{qds} = \mathbf{W}_0\Psi_{qds} + \mathbf{Y}_0\Psi_{qdr} + \mathbf{B}_{s0}\mathbf{u}_{qds} \tag{B.1}$$

$$p\Psi_{qdr} = \mathbf{Q}_0\Psi_{qds} + \mathbf{S}_{l0}\Psi_{qdr} + \Omega_m\mathbf{S}_{nl0}\Psi_{qdr} \tag{B.2}$$

$$p\,\Omega_m = \frac{1}{J_m}\,[\Psi_{qds}{}^t\mathbf{T}_{sr}\,\Psi_{qdr} - T_l] \tag{B.3}$$

where

$$p = \frac{d}{dt} \tag{B.4}$$

$$\Psi_{qds} = [\,\Psi_{qs}\ \Psi_{ds}]^t \tag{B.5}$$

$$\Psi_{qdr} = [\,\Psi_{qr}\ \Psi_{dr}]^t \tag{B.6}$$

$$\mathbf{u}_{qds} = [u_{qs}\ u_{ds}]^t \tag{B.7}$$

and

$$\mathbf{W}_0 = \begin{bmatrix} \frac{-R_s}{L_s{}'} & -\omega_s \\ \omega_s & \frac{-R_s}{L_s{}'} \end{bmatrix},\ \mathbf{Q}_0 = \begin{bmatrix} \frac{k_sR_r}{L_r{}'} & 0 \\ 0 & \frac{k_sR_r}{L_r{}'} \end{bmatrix},$$

$$\mathbf{Y}_0 = \begin{bmatrix} \frac{k_rR_s}{L_s{}'} & 0 \\ 0 & \frac{k_rR_s}{L_s{}'} \end{bmatrix},\ \mathbf{S}_{l0} = \begin{bmatrix} \frac{-R_r}{L_r{}'} & -\omega_s \\ \omega_s & \frac{-R_r}{L_{r\text{-}}{}'} \end{bmatrix},$$

$$\mathbf{S}_{nl0} = \begin{bmatrix} 0 & p \\ -p & 0 \end{bmatrix},\ \mathbf{B}_{s0} = \begin{bmatrix} 1 & 0 \\ 0 & 1 \end{bmatrix},\ \mathbf{T}_{sr} = \begin{bmatrix} 0 & \frac{pk_r}{L_s{}'} \\ \frac{-pk_r}{L_s{}'} & 0 \end{bmatrix}$$

The output signals are determined by

$$\mathbf{Y} = \mathbf{N}\Psi_{qds} + \mathbf{M}\Psi_{qdr} \tag{B.8}$$

The output signals of $\mathbf{Y}$ may be the currents, flux linkages, rotor speed, electrodynamical torque as well as active and reactive powers. If $\mathbf{Y} = [\ i_{qs}\ i_{ds}]^t$ then

$$\mathbf{N} = \begin{bmatrix} \dfrac{L_r}{L_rL_s - L_mL_m} & 0 \\ 0 & \dfrac{L_r}{L_rL_s - L_mL_m} \end{bmatrix} \text{ and } \mathbf{M} = \begin{bmatrix} \dfrac{-L_m}{L_rL_s - L_mL_m} & 0 \\ 0 & \dfrac{-L_m}{L_rL_s - L_mL_m} \end{bmatrix}$$

By neglecting the effect of stator transients, i.e, the term $p\Psi_{qds}$, the solution of (B.1) is

$$\Psi_{qds}{}^* = -\ \mathbf{W}_0^{-1}\mathbf{Y}_0\Psi_{qdr} - \mathbf{W}_0^{-1}\mathbf{B}_{s0}\mathbf{u}_{qds} \tag{B.9}$$

This term differs from the actual flux linkage Ψ_{qds} and, in essence, represents its slow component. Equations (B.2)-(B.3) with $p\Psi_{qds}$ neglected, after some algebraic manipulation, may be expressed as

$$p\Psi_{qdr} = [\mathbf{S}_{l0} - \mathbf{Q}_0\mathbf{W}_0^{-1}\mathbf{Y}_0]\Psi_{qdr} + \varOmega_m\mathbf{S}_{nl0}\Psi_{qdr} - \mathbf{Q}_0\mathbf{W}_0^{-1}\mathbf{B}_{s0}\mathbf{u}_{qds} \tag{B.10}$$

$$p\varOmega_m = \frac{1}{J_m}\{\Psi_{qdr}{}^t[-\mathbf{W}_0^{-1}\mathbf{Y}_0]^t\mathbf{T}_{sr}\Psi_{qdr} + \mathbf{u}_{qds}{}^t[-\mathbf{W}_0^{-1}\mathbf{B}_{s0}]^t\mathbf{T}_{sr}\Psi_{qdr} - T_l\ \} \tag{B.11}$$

Equations (B.10)-(B.11) represent the standard reduced order model of the induction machine, the NST I-model. An expression for the output signals in terms of the state variables in (B.10)-(B.11) can be derived by substituting $\Psi_{qds}{}^*$, defined by (B.9) in (B.8) and rearranging. This gives

$$\mathbf{Y} = [\mathbf{M} - \mathbf{N}\mathbf{W}_0^{-1}\mathbf{Y}_0]\ \Psi_{qdr} - \mathbf{N}\mathbf{W}_0^{-1}\mathbf{B}_{s0}\mathbf{u}_{qds} \tag{B.12}$$

References

Rodriguez, F.D., Wasynczuk, O., 1987. "A refined method of deriving reduced order models of induction machines", *IEEE Transactions on Energy Conversion*, vol. 2, no. 1, pp. 31-37